Title

Olefin and sulfur oxidations as probes of cytochrome P450 mechanism and active site binding

Permalink

https://escholarship.org/uc/item/23n088r1

Author

Fruetel, Julia A

Publication Date

1992

Peer reviewed|Thesis/dissertation

OLEFIN AND SULFUR OXIDATIONS AS PROBES OF CYTOCHROME P450

MECHANISM AND ACTIVE SITE BINDING

by

Julia A. Fruetel

DISSERTATION

Submitted in partial satisfaction of the requirements for the degree of

DOCTOR OF PHILOSOPHY

in

PHARMACEUTICAL CHEMISTRY

in the

GRADUATE DIVISION

of the

UNIVERSITY OF CALIFORNIA

San Francisco

ACKNOWLEDGEMENTS

To Andy, with love

ABSTRACT

OLEFIN AND SULFUR OXIDATIONS AS PROBES OF CYTOCHROME P450 MECHANISM AND ACTIVE SITE BINDING

Julia A. Fruetel

Cytochrome P450 enzymes oxidize lipophilic substrates stereo- and regioselectively. The factors which determine how substrates bind and are consequently oxidized are unknown for a majority of P450 enzymes, as three-dimensional structures are not currently available for most of the enzymes. A detailed study of the oxidation of prochiral olefins and sulfides by cytochrome P450101 (P450$_{cam}$), a bacterial enzyme whose crystal structure is known (Poulos, T.L., Finzel, B.C. and Howard, A.J. (1987) *J. Mol. Biol.* **195**, 687), was thus undertaken to define substrate-protein interactions which determine the reaction chemistry and stereospecificity within the confines of a known active site.

The mechanism of olefin oxidation was explored using *trans*-1-phenyl-2-vinylcyclopropane as a trap for radical intermediates. Oxidation by cytochrome P450$_{cam}$ yielded the corresponding epoxide, (*trans*-2-phenylcyclopropyl)acetaldehyde and *trans*-5-phenyl-2-penten-1,5-diol. The finding that the latter two products derive from acid-catalyzed ring-opening of the epoxide at neutral pH obscures detection of the these compounds as direct enzyme metabolites. The lack of detection of the ring-opened product *trans*-5-phenyl-2-penten-1-ol implies that the lifetime of a radical intermediate would be too short for it to be considered a discrete entity on the reaction pathway.

The oxidation of a series of substituted styrenes and thioanisoles was investigated with P450$_{cam}$ and three active site mutants, F87A, F87W and Y96F. The results indicate that these compounds are oxidized stereoselectively, although with significant uncoupling of the oxidative reaction to form hydrogen peroxide. Modeling of the reactions by molecular dynamics suggests that hydrophobic interactions strongly determine substrate binding and thus the stereochemical outcome of the reaction. *para*-Substitution causes a marked change in the reaction stereochemistry, implying steric and possibly hydrogen-bonding interactions occur between the *para*-substituent and active site residues. The reaction stereochemistry is also sensitive to mutation of active site residues Phe 87 and Tyr 96, and suggests that active site residues move in response to the mutations.

The oxidation of the same substrates was studied with three other cytochrome P450 enzymes. Cytochrome P450$_{terp}$, a bacterial enzyme which oxidizes α-terpineol to 7-hydroxyterpineol, showed extremely high stereoselectivity with these substrates, consistent with a restrictive binding pocket. Cytochrome P450$_{BM-3}$, a bacterial enzyme which oxidizes long-chain fatty acids, showed very high turnover but very low stereoselectivity, in agreement with a spacious active site cavity. Cytochrome P4502B1, a microsomal enzyme induced by phenobarbital in rats, showed intermediate stereoselectivity, suggesting a large binding pocket that has limited access to the heme center.

TABLE OF CONTENTS

LIST OF FIGURES

LIST OF TABLES

xix

LIST OF ABBREVIATIONS

BSTFA	*bis*(Trimethylsilyl)trifluoroacetamide
CI	Chemical ionization
DLPC	*l*-3-Phosphatidyl choline dilauroyl
DTPA	Diethylenetriaminepentaacetic acid
DTT	Dithiothreitol
E. coli	*Escherichia coli*
EDTA	Ethylenediaminetetraacetic acid
EI	Electron impact
GLC	Gas-liquid chromatography
HPLC	High-performance liquid chromatography
MD	Molecular dynamics
MOPS	(3-[N-Morpholino]propane)sulfonic acid
MS	Mass spectrometry
NADH	Nicotinamide adenine dinucleotide (reduced)
NAD+	Nicotinamide adenine dinucleotide (oxidized)
NADPH	Nicotinamide adenine dinucleotide phosphate (reduced)
NADP+	Nicotinamide adenine dinucleotide phosphate (oxidized)
NMR	Nuclear magnetic resonance
P. putida	*Pseudomonas putida*
P450	Cytochrome P450
PAGE	Polyacrylamide gel electrophoresis
PMSF	α-Toluenesulfonyl fluoride

RNase	Ribonuclease
SDS	Sodium dodecyl sulfate
THF	Tetrahydrofuran
TLC	Thin layer chromatography
TMS	Trimethylsilyl
UCSF	University of California, San Francisco
UV	Ultraviolet
vis	visible

1.0 INTRODUCTION

1.1 Cytochrome P450 Enzymes

Cytochromes P450 are some of the most powerful *in vivo* oxidizing agents known. These enzymes catalyze the oxidation of unactivated carbon-hydrogen bonds, as well as epoxidations and heteroatom oxidations, often in a stereo- and regioselective manner. Their unusual reactivity is ascribed to a heme prosthetic group which has a cysteine thiolate anion as the fifth iron ligand. This unusual thiolate ligand also imparts to the enzyme its characteristic spectral properties, first recognized in 1958 when the enzymes were described as novel "liver pigments" (Klingenberg, 1958; Garfinkel, 1958). It wasn't until 1964 that P450 enzymes were determined to be hemoproteins (Omura and Sato, 1964).

Cytochromes P450 are found in a wide variety of species and tissues. Mammals, bacteria and plants have all exploited the oxidizing ability of P450 enzymes for a variety of purposes. In bacteria, for example, these enzymes are water-soluble, and are involved in such diverse functions as the hydroxylation of steroids, fatty acids, and the breakdown of carbon sources for food. Mammalian P450s are membrane-bound, localized to either the mitochondria, as in the case of the steroidogenic P450s, or the endoplasmic reticulum, where the microsomal P450s are located. This latter group of P450s oxidizes both endogenous compounds, such as prostaglandins and fatty acids, and foreign compounds such as drugs and environmental pollutants.

Since their initial discovery in the 1950s more than 150 different P450 isozymes have been identified, with sequences varying from 15 to 98% in

identity (Nelson and Strobel, 1987). In order to keep track of the growing number of isozymes in a way which identifies each with those of similar structure, a new nomenclature was proposed by Daniel Nebert and others which is based on divergent evolution as determined by structural homology (Nebert *et al.*, 1991).

Using this method, each P450 family (determined as those enzymes with $\geq 40\%$ identity) is given a number, and each subfamily (those with >55% identity) is given a capital letter. Individual isozymes within the subfamily are then given a number. This system generates 27 gene families, 10 of which exist in mammals. Table 1.1 lists the standardized nomenclature for a variety of P450 enzymes, including those discussed in this thesis.

Table 1.1: *Standardized nomenclature for various cytochrome P450 enzymes (from Nebert et al., 1991).*

Standardized Nomenclature	Trivial Names	Source, Induction
P4501A1	P450c, β-NF-B	rat, 3-methylcholanthrene
P4504A1	P450$_{LA\omega}$	rat, chlofibrate
P45011A1	P450$_{scc}$	human
P45021A1	P450C21	human
P4502B1	P450$_b$, PB-4, PB-B	rat, phenobarbital
P4502B2	P450$_e$, PB-5, PB-D	rat, phenobarbital
P4502E1	P450j	human, ethanol
P450101	P450$_{cam}$	*P. putida*, camphor
P450103	P450$_{BM-3}$	*B. megaterium*, pentobarbital
P450108	P450$_{terp}$	*Pseudomonas*, α-terpineol

The large number of P450 enzymes available makes it possible to study the properties of this enzyme family using a variety of sources. Indeed, studies of bacterial enzymes have greatly facilitated both mechanistic

and structural understanding, as these P450s are soluble, readily available, and in some cases, crystallizable.

The physiological role of P450 enzymes is of great importance in both the initiation and treatment of disease. Although P450 enzymes generally facilitate elimination of drugs and other foreign compounds by making them more hydrophilic, they can also activate compounds to more toxic species, thus playing a role in the initiation of diseases such as cancer. Administration of certain drugs can increase the levels of particular P450 enzymes, and thus if the toxicity or the protection against toxicity is associated with one particular inducible isozyme, administration of the appropriate inducer could significantly modulate the toxicity. Hence an understanding of the chemistry of these enzymes and their functioning in the body is critical to understanding the underlying causes of diseases.

The role of P450 enzymes in the treatment of disease is significant due to the fact that these enzymes constitute the major drug-metabolizing enzymes in the body. Indeed, for some drugs the active compound is a P450 metabolite. The importance of these enzymes not only in drug metabolism but also other critical processes in the body suggest inhibiting these enzymes may be of therapeutic interest. The use of aminoglutethimide, a P45019 inhibitor, to treat hormone-dependent metastatic breast carcinoma, and miconazole, a P45051 inhibitor, as an antifungal agent, represent the successful use of P450 inhibitors as drugs. However, specificity is crucial in designing such inhibitors, due to both the large number of P450 isozymes and the fact that many P450s, particularly the drug-metabolizing isozymes, have overlapping specificities. Hence, an understanding of the active site features which determine substrate specificity for a given isozyme is critical to rational drug design attempts.

3

1.2 Cytochrome P450$_{cam}$

1.2.1 Structure and Function in *P. putida*

Much of the insight gained into the mechanism and structure of P450 enzymes has come from studies performed with the bacterial monooxygenase cytochrome P450101 (P450$_{cam}$). This water-soluble P450 comes from *Pseudomonas putida*, a soil bacterium capable of utilizing *d*-camphor as its sole carbon source (Bradshaw *et al.*, 1959). This enzyme initiates the breakdown of camphor to citric acid cycle components by hydroxylating camphor specifically at the 5-*exo* position (Hedegaard and Gunsalus, 1965; see Figure 1.1). The first three enzymes along this pathway are all induced by camphor, consistent with the discovery that the genes for these enzymes are clustered together on the same operon (Rheinwald *et al.*, 1973).
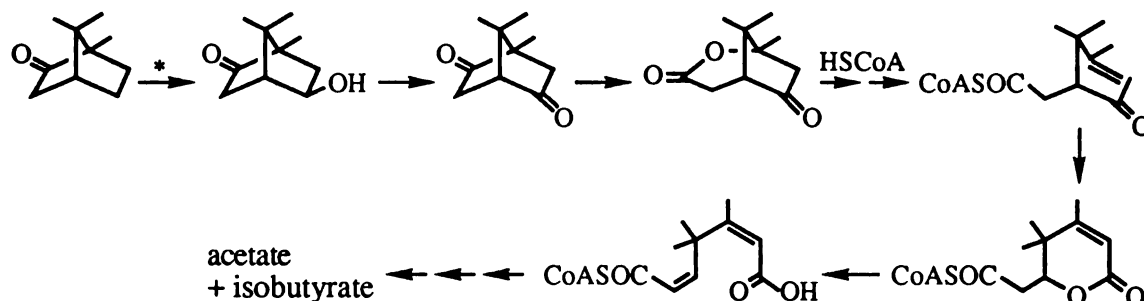
Figure 1.1: P450$_{cam}$ catalyzes the first step (denoted by an asterisk) in the metabolic degradation of camphor by Pseudomonas putida (adapted from Sligar and Murray, 1986).

For activity, P450$_{cam}$ requires the help of two additional proteins, putidaredoxin, a 2Fe-2S protein, and putidaredoxin reductase, an FAD-containing enzyme which binds NADH. These proteins supply the electrons

needed to generate the activated iron-oxo species which is the ultimate oxidant in P450 enzymes. The electrons originate with NADH and are extracted in one step by the reductase, then shuttled in two one-electron steps, via putidaredoxin, to $P450_{cam}$ (Peterson and Prough, 1986; see Figure 1.2). All three of these enzymes have been expressed and purified from both *P. putida* and *E. coli* in high yields (Gunsalus and Wagner, 1978; Cushman *et al.*, 1967; Katagiri *et al.*, 1968; Unger *et al.*, 1986; Peterson *et al.*, 1990).

$$
\begin{array}{ccccccc}
& 2\,e\text{-} & & 1\,e\text{-} & & 1\,e\text{-} & \\
\text{NADH} & & \text{Redt} & & \text{2Fe-2S} & & \text{P-450} \\
& & \text{(ox)} & & \text{(red)} & & \text{(ox)} \\
\text{NAD}^+ & & \text{Redt} & & \text{2Fe-2S} & & \text{P-450} \\
& & \text{(red)} & & \text{(ox)} & & \text{(red)}
\end{array}
$$
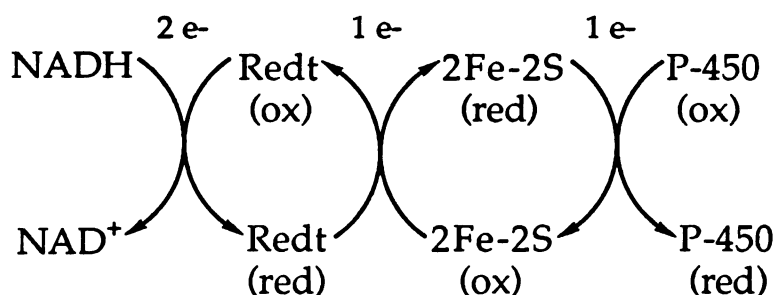
Figure 1.2: *Electron-shuttling pathway for* $P450_{cam}$. *The electrons are abstracted from NADH by the reductase, which then shuttles them one at a time via the iron-sulfur protein putidaredoxin to* $P450_{cam}$.

The finding that $P450_{cam}$ is soluble, crystallizable, and can be obtained in large amounts due to high expression in either *P. putida* or *E. coli* (~3 and 10% of the soluble protein, respectively; Gunsalus and Wagner, 1978; Sligar and Murray, 1986) enabled it to be the first P450 for which a crystal structure was possible. The first structure of the camphor-bound protein was determined at 2.6 Å resolution in 1985 by Thomas Poulos and coworkers and has since been followed by a higher resolution structure (1.63 Å; Poulos *et al.*, 1987), and structures of the camphor-free enzyme (Poulos *et al.*, 1986), the enzyme bound with various ligands (Poulos and Howard, 1987; Raag and Poulos, 1989a, 1989b, and 1991), the enzyme modified by phenyldiazene (Raag *et al.*, 1990), and the active site mutant T252A (Raag *et al.*, 1991).

The x-ray crystal structures of P450$_{cam}$ reveal this 45,000-Da enzyme to be roughly triangular in shape, with a maximum dimension of ~60 Å and a minimum of ~30 Å (see Figure 1.3). Twelve helical segments, labeled A through L, account for ~40% of the structure, while antiparallel β-pairs account for ~10%. Although a majority of the helical structure is on the right side of the molecule as shown in Figure 1.3, the protein does not fold into N- and C-terminal domains as do many other proteins.

A	37–46	β1	52–66
B	67–77	β2	226–233
B′	89–96	β3	295–301
C	106–126		315–323
D	127–145	β4	305–312
E	149–169	β5	382–405
F	173–185		146–150
G	192–214		
H	218–225		
I	234–267		
J	267–276		
K	280–292		
L	359–378		
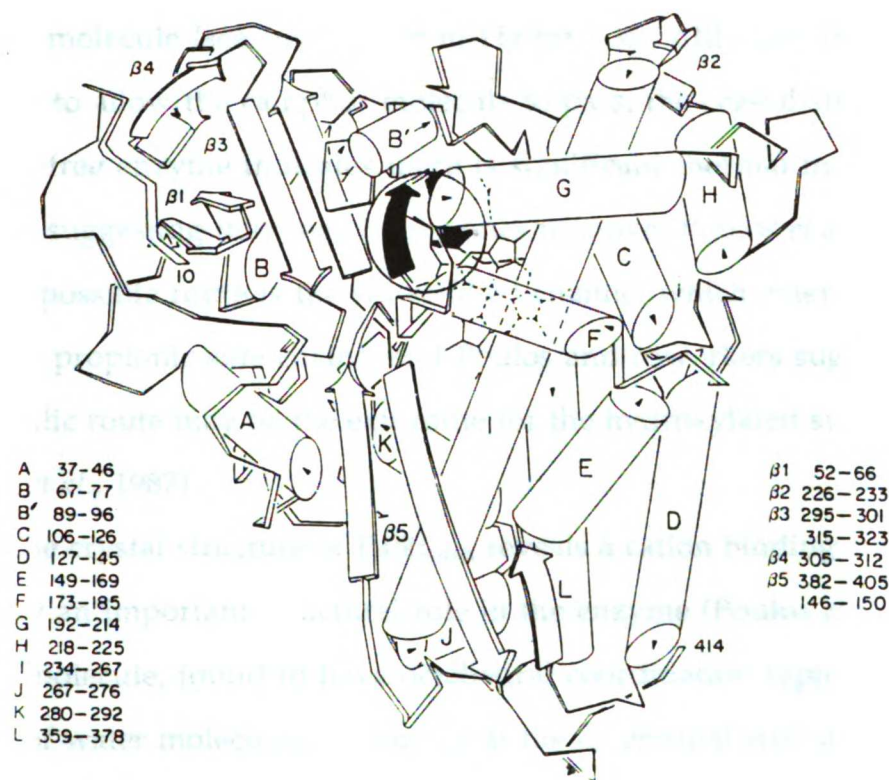
Figure 1.3: *A schematic diagram of the P450$_{cam}$ crystal structure. Cylinders represent α-helices and flat arrows denote β-pair structures. The numbers list residues in helical (A-L) and anti-parallel β-conformations. The circle indicates a possible substrate access channel (from Poulos et al., 1985).*

The heme group is buried in the protein, sandwiched between helices I and L. Helix L supplies the protein ligand to the heme, Cys 357, and thus is

referred to as the proximal helix. Helix I is called the distal helix and forms part of the camphor (and presumably oxygen) binding pocket.

As the heme is buried in the enzyme, unexposed to solvent, so is the camphor binding pocket. No route is apparent from the surface of the protein to the enzyme active site for the camphor molecule, and thus protein residues must move significantly for the substrate to enter the protein. The most probable opening occurs where residues 88, 185, and 395 are juxtaposed to form a distinct depression and small opening above the camphor molecule (see small circle in Figure 1.3). Although this opening is too small to allow the camphor molecule to pass, the crystal structure of the camphor-free enzyme indicates there is significant thermal motion in these residues, suggesting they may be the ones to move (Poulos et al., 1986). Another possible route is the water-filled channel which extends between the heme propionic side chains, and Poulos and coworkers suggest this more hydrophilic route may be the exit route for the hydroxylated substrate (Poulos et al., 1987).

The crystal structure of $P450_{cam}$ reveals a cation binding site which may play an important structural role in the enzyme (Poulos et al., 1987). A solvent molecule, found to have octahedral coordination typical of cations but not of water molecules, is situated at the C-terminal end of a short helical segment containing residues 89-96, holding these residues in a unfavorable conformation. This unfavorable conformation allows the side chains of Tyr 96 and Phe 98 to point into the active site pocket, contacting each other and the bound camphor molecule. The finding that $P450_{cam}$ is more stable in the presence of cations (Hui Bon Hoa and Marden, 1982) and binds camphor ~8-fold more tightly in the presence of cations (Peterson,

7

1971), supports the important structural role proposed for this cation binding site in stabilizing the active site pocket.

Where putidaredoxin binds to $P450_{cam}$ is not obvious from the crystal structure, and this is complicated by the fact that no crystal structure has yet been determined for putidaredoxin. Some structural information has been obtained for putidaredoxin using NMR spectroscopy, which suggests that the protein contains predominantly β-sheet secondary structure and predicts a folding topology for putidaredoxin which is similar to adrenodoxin, the iron-sulfur protein utilized by P45011A1, even though these proteins differ significantly in their amino acid sequences (Pochapsky and Ye, 1991). Which residues interact with $P450_{cam}$ were not identified by this study, although a hydrophobic patch which appears to be on the outside of the protein was implicated as a possible binding surface. Studies of the C-terminal tryptophan of this protein indicate it is important for putidaredoxin activity (Davies *et al.*, 1990), and the finding that it is exposed to solvent (Stayton and Sligar, 1991; Ye *et al.* 1992) suggests it is involved in electron transfer between the two proteins, and thus is likely to be situated at the binding surface between them.

Studies of cytochrome b_5 association with $P450_{cam}$ suggested possible ionic interactions which could be involved. Computer modeling of $P450_{cam}$ and cytochrome b_5, which is also able to reduce $P450_{cam}$, led to the conclusion that probable contacts could be made between the conserved carboxylate residues in cytochrome b_5 and the basic amino acid groups Arg 72, Arg 112, Arg 364, and Lys 344 in $P450_{cam}$ (Stayton *et al.*, 1988). These residues in $P450_{cam}$ are on the surface of the protein nearest to Cys 357, the thiolate ligand to the heme iron. The finding that putidaredoxin competitively inhibits cytochrome b_5 association with $P450_{cam}$ (Stayton *et al.*,

1989), and that mutation of the basic residues to either neutralize or reverse the charge results in diminished K_m values for putidaredoxin (Stayton and Sligar, 1990), suggests that putidaredoxin also interacts with P450$_{cam}$ at this site.

1.2.2 Catalytic Mechanism

Cytochromes P450 oxidize substrates by incorporating one atom of oxygen into the substrate molecule, utilizing a heme cofactor, molecular oxygen and two electrons derived from either NADH or NADPH, according to the overall equation 1.1.

$$RH + O_2 + 2H^+ + NAD(P)H \rightarrow ROH + H_2O + NAD(P)^+ \tag{1.1}$$

How the electrons and molecular oxygen are harnessed to oxidize unactivated carbon, sulfur, and nitrogen centers is outlined in the P450 reaction cycle in Figure 1.4, and is discussed below. The steps required, in the order they occur, are (1) binding of substrate, (2) reduction of the ferric heme iron to the ferrous state, (3) binding of molecular oxygen, (4) reduction of the iron-dioxygen complex, (5) oxygen-oxygen bond cleavage to yield water and an activated iron-oxo species, (6) incorporation of the iron-bound oxygen into substrate, and (7) release of substrate from the binding pocket.

Binding of Camphor

When substrates bind to P450 enzymes, the strong heme absorbance centered around 416 nm (called the Soret absorbance) shifts to either higher or lower wavelengths. For the binding of camphor to cytochrome P450$_{cam}$

9
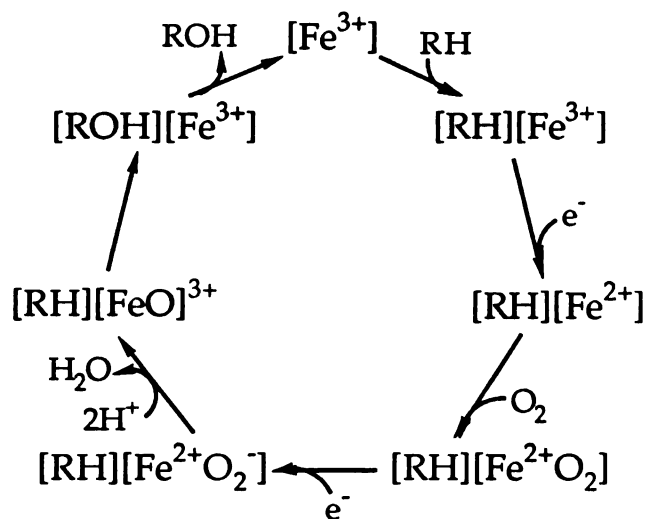
Figure 1.4: The P450 reaction cycle. RH and ROH refer to the substrate and the product, respectively.

the absorbance shifts to 391 nm, and represents a change in the spin state of the iron from low spin (S = 1/2) to high spin (S = 5/2) as detected by Mossbauer (Sharrock *et al.*, 1973 and 1976; Champion *et al.*, 1975) and electron spin resonance studies (Tsai *et al.*, 1970).

Studies using heme models found that high spin complexes were generally penta-coordinate, while low spin complexes were hexa-coordinate (Gibson and Tamburini, 1984). The fact that in P450 enzymes the heme nitrogens and the cysteine thiolate ligand make up five ligands to the iron suggested that when the protein is in its low-spin resting state there is an iron ligand in the protein active site, but when the substrate is bound this ligand is displaced. Spectroscopic studies of P450$_{cam}$ complexes with various ligands suggested that the coordinating atom was an oxygen (Dawson *et al.*, 1982; Philson *et al.*, 1979; Griffin and Peterson, 1975), but whether the oxygen is part of an amino acid side chain or a solvent molecule remained unclear.

The latter of these possibilities was confirmed when the crystal structures of the camphor-bound and camphor-free complexes of P450$_{cam}$ were determined by Thomas Poulos and coworkers (Poulos *et al.*, 1985, 1986, and 1987). In the camphor-bound complex, camphor completely fills the active site pocket, having close contacts on all sides with either protein residues or the heme surface (Poulos *et al.*, 1987; see Figure 1.5). No electron density is observed axial to the heme iron, suggesting no sixth ligand is positioned near the heme iron. This is presumably due to the close proximity of the C-5 carbon of the camphor molecule, which is the carbon hydroxylated by the enzyme.
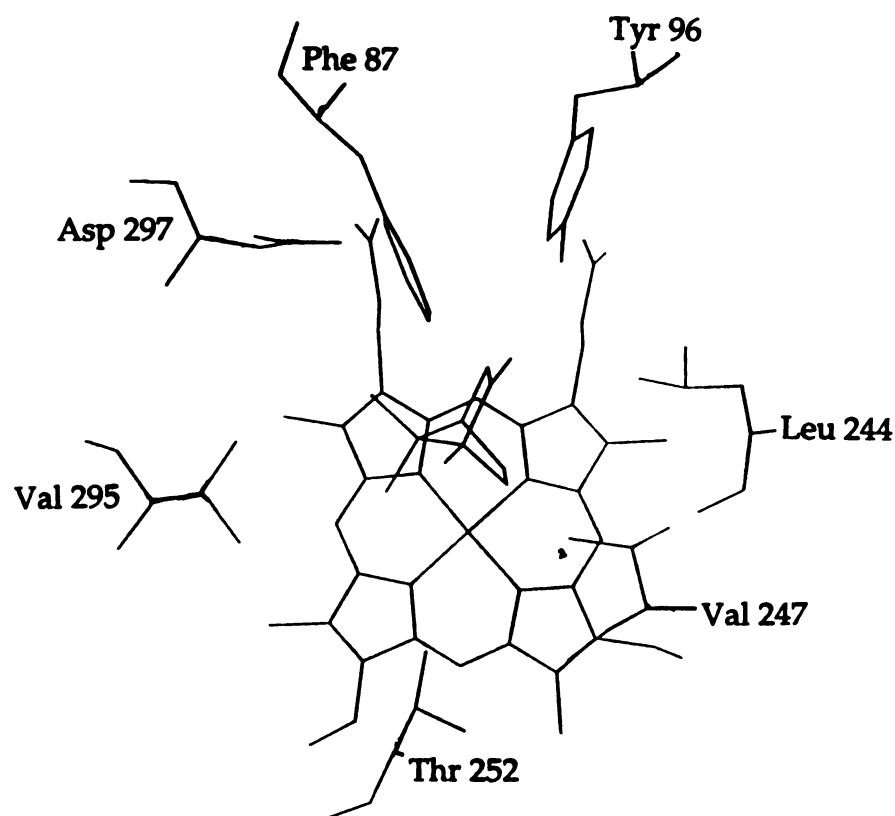
Figure 1.5: *View of the active site residues in camphor-bound cytochrome* P450$_{cam}$ *(from Poulos* et al., *1987).*

11

Comparison of the camphor-bound and camphor-free structures indicates that no significant movement of protein groups into the enzyme active site occurs when camphor is not present, thus ruling out the possibility of an amino acid side chain coordinating to the iron (Poulos *et al.*, 1986). The electron density axial to the heme iron is thus ascribed to a water or hydroxide ion coordinated to the iron, and the rest of the space in the active site can be modeled with six water molecules.

Not all substrates behave like camphor and are able to displace the ligand to the heme iron. Crystal structures of norcamphor and camphane bound in the $P450_{cam}$ active site reveal the presence of an aqua ligand to the heme iron even when the substrate is present (Raag and Poulos, 1989a, 1991). The persistence of this ligand may explain why norcamphor and camphane are unable to fully convert the enzyme to the high spin form (Table 1.2), since a sixth ligand to the heme iron would presumably require the enzyme to be at least part of the time in the low spin state. However, the crystal structure of adamantane bound in the active site of $P450_{cam}$ also shows a sixth ligand to the heme iron (Raag and Poulos, 1991), yet this substrate is able to convert $P450_{cam}$ almost exclusively to the high spin state (Table 1.2).

To explain how the enzyme could shift to the high spin state while remaining hexacoordinate, Raag and Poulos have proposed that the pK of the aqua ligand changes upon binding of substrate (Raag and Poulos, 1989a). In the substrate-free complex, the iron ligand is a strong field hydroxide ion (OH^-), forming a low spin complex which is stabilized by the high dielectric environment of the water-filled active site pocket (see Figure 1.6a). When substrate binds and displaces this ligand, the heme becomes pentacoordinate and shifts to high spin, as discussed previously (Figure 1.6b). If substrate binds and the ligand is not displaced, the removal of the other waters in the

12

active site decreases the hydrophilicity of the active site, affecting the pK of the aqua ligand. Now protonation to form the weak field water ligand (H_2O) is favored, thereby shifting the equilibrium towards the high spin state (Figure 1.6c). These arguments are supported by pH studies which indicate that lowering the pH shifts the spin equilibrium towards the high spin form (Sligar and Gunsalus, 1979).
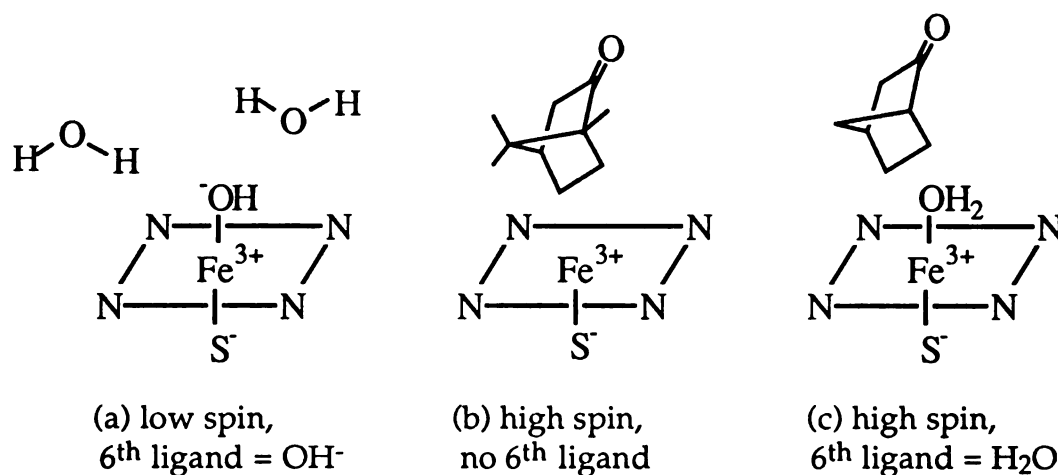
Figure 1.6: Proposed iron-ligand geometries for $P450_{cam}$ in the three spin states: (a) low spin, substrate-free, (b) high spin with sixth ligand displaced (eg, camphor bound), and (c) high spin with sixth ligand intact (eg, norcamphor bound) states (adapted from Poulos and Raag, 1992).

Reduction by Putidaredoxin

In addition to changing the spin state of the heme iron, substrate binding also raises the redox potential of the P450 enzyme, enabling it to be reduced by its electron-shuttling partner. For $P450_{cam}$, the potential changes from -300 mV to -173 mV when camphor binds, making its reduction by putidaredoxin (redox potential = -196 mV) thermodynamically favorable (Sligar and Gunsalus, 1976). The requirement for substrate to bind in order

for the enzyme to be reduced is catalytically expedient, as consequently enzyme turnover only occurs when substrate is present.

A study of the interactions of camphor analogs with P450$_{cam}$ indicate that substrates which are unable to fully convert the enzyme to the high spin state are also unable to completely shift the redox potential (Fisher and Sligar, 1985). A linear correlation was found between the spin state equilibrium and the redox potential for several P450$_{cam}$ substrates, indicating that the two properties are integrally related (see Table 1.2). Interestingly, the binding constant of the substrate is not related to either of these parameters.

The close relationship between spin state and redox potential suggests the nature of the sixth ligand to the heme iron affects the redox potential. The finding that the redox potential of P450$_{cam}$ is sensitive to pH (is increased by lowering the pH; Sligar and Gunsalus, 1979) also supports the proposed change in protonation state between low-spin hydroxide-liganded iron to high-spin water-liganded iron. Protonation of the hydroxide ligand removes a negative charge from the heme complex, and consequently would be expected to favor an increase in the redox potential of the enzyme.

Table 1.2: Comparison of the ability of different substrates to convert P450$_{cam}$ to the high spin form and the redox potential of the substrate-bound enzyme (from Fisher and Sligar, 1985 and Gould et al., 1981).

Substrate	% High Spin	E (mV)	K$_D$ (µM)
d-camphor	97	-170	0.8
adamantanone	96	-175	1.3
d-3-bromocamphor	75	-197	48
d-fenchone	57	-208	17
norcamphor	46	-206	150
no substrate	7	-303	---

Binding of Molecular Oxygen

Once the heme iron is reduced to the ferrous state, it can bind molecular oxygen. How the oxygen molecule fits into the $P450_{cam}$ active site with camphor present is not absolutely known, as no crystal structure is available for the camphor-O_2-$P450_{cam}$ complex. Analysis of the camphor-bound crystal structure suggests there is very little room for the oxygen to bind without movement of either the substrate or protein residues (Poulos *et al.*, 1987).

Analysis of the camphor-bound structure does, however, indicate a probable pocket for oxygen to bind. Part of the active site pocket is composed of an α-helix, called the I helix, which runs parallel to the surface of the heme and extends over the B ring of the heme (see Figure 1.7). At the point
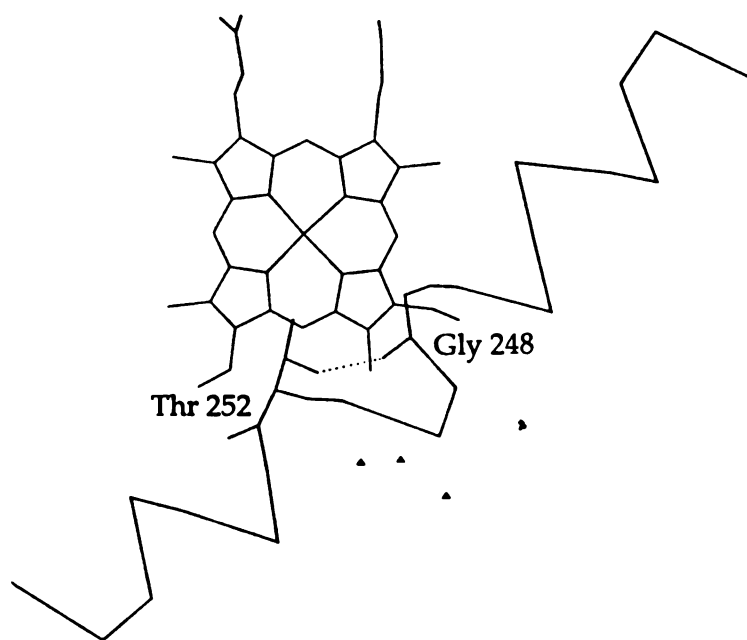
Figure 1.7: Overhead view of the $P450_{cam}$ active site showing the kink in the I helix near the heme center caused by a disruption in the normal helical hydrogen-bonding pattern at Gly 248 and Thr 252. The hydrogen bond between Gly 248 and Thr 252 is shown by a dotted line, and triangles denote bound water molecules.

closest to the heme center there is a kink in the helix, caused by an unusual hydrogen-bonding pattern between Thr 252 and Gly 248. Poulos and coworkers have proposed that the kink in the helix provides a groove for oxygen to bind in, with the residue at the center of the groove, Thr 252, available to serve as a possible proton donor in the oxygen-oxygen bond-breaking step (Poulos *et al.*, 1987).

The proposed importance of the function of this residue and its surrounding residues in the P450 reaction cycle is supported by the fact that these residues are some of the most highly conserved among all P450 enzymes, with Thr 252 absolutely conserved (see Section 1.3.1).

As a model for the camphor-O_2-P450$_{cam}$ complex, the crystal structure of the camphor-CO-P450$_{cam}$ complex was solved (Raag and Poulos, 1989b). In this structure, the carbon monoxide molecule was found coordinated to the heme iron with an Fe-C-O bond angle of 166°, indicating that the CO is bent from the heme normal. This is similar to the binding angles observed for CO in hemoglobin and myoglobin, where steric hindrance from neighboring protein residues prevents the ligand from binding along the heme normal (Baldwin, 1980; Shaanan, 1983).

As proposed for the O_2 complex, the oxygen atom of the CO molecule is nestled in the groove of the I helix centered at Thr 252 (see Figure 1.8). The camphor molecule, in order to accomodate the CO molecule, binds further away from the I helix by about 0.8 Å, but remains in nonbonded contact with the CO molecule. Also it was found that the C-5 carbon of the camphor molecule (the carbon hydroxylated by P450$_{cam}$), its 5-*exo* hydrogen, and the carbon atom of the CO molecule are all colinear, important for the proposed mechanism of the reaction, as is discussed later.

In sum, the binding of the CO molecule in the camphor-CO-P450$_{cam}$ complex is similar to that proposed for O_2, and is consistent with the proposed mechanism for the reaction. Also, it supports the proposed importance of Gly 248 and Thr 252 in the reaction mechanism, suggesting a common role for these residues in all P450 enzymes.
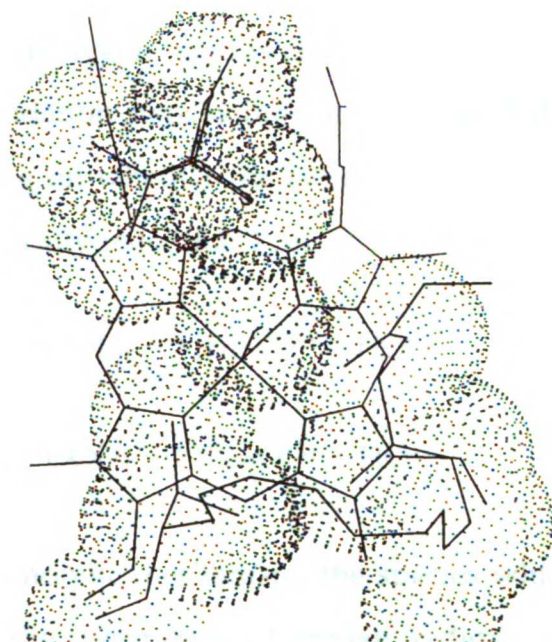
Figure 1.8: *View of the active site pocket of P450$_{cam}$ with both camphor and carbon monoxide bound. Van der Waals surfaces indicate the snug fit of the CO molecule between the camphor molecule and the I helix (from Raag and Poulos, 1989b).*

Cleavage of the Dioxygen Bond and Oxidation of Camphor

The next step in the P450 reaction cycle after molecular oxygen binding is the reduction of the complex by one electron to iron-peroxy status, followed by oxygen-oxygen bond cleavage to form the activated iron-oxo species and water. It is this iron-oxo species which then is capable of

hydroxylating unactivated carbon-hydrogen bonds, a feat very few chemical oxidizing agents can match. The mechanism of this reaction is proposed to involve abstraction of a hydrogen atom from the substrate, followed by collapse of the substrate radical with the iron-oxo species to form the hydroxylated product (see Section 2.1.1 for more on the hydroxylation mechanism). In the case of camphor, the product of the reaction is exclusively 5-*exo*-hydroxycamphor.

How the dioxygen bond is cleaved is important to the mechanism of the substrate oxidation step, as the nature of the hydrogen abstracting species varies depending on whether the bond is cleaved homolytically (equation 1.2) or heterolytically (equation 1.3).

$$[Fe^{2+}OOH] \longrightarrow [Fe=O]^{2+} + HO^{\bullet} \tag{1.2}$$

$$[Fe^{2+}OOH] \longrightarrow [Fe=O]^{3+} + HO^{-} \tag{1.3}$$
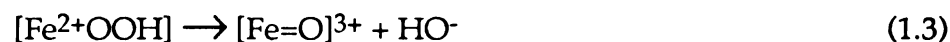
In the homolytic mechanism, the species which abstracts the hydrogen from the substrate is a hydroxyl radical. The iron-oxo species $[Fe=O]^{2+}$ then recombines with the substrate radical, together with a proton, to yield the hydroxylated substrate. Support for this mechanism comes from studies which show that in the $P450_{cam}$-mediated hydroxylation of camphor, either the 5-*endo* or 5-*exo* hydrogen can be abstracted, but only the 5-*exo*-hydroxylated product is formed (Gelb *et al.*, 1982). This indicates that the specificities of the two steps of the reaction are different and suggests that the hydrogen abstracting species and the oxygenation species are different. The fact that the oxygenation species is more constrained (i.e., only delivers oxygen to the *exo* face) is consistent with that species being an iron-bound oxygen species such as $[Fe=O]^{2+}$.

Several lines of evidence argue against a homolytic mechanism, however, and these stem from studies done using artificial oxidants with either P450 enzymes or heme model systems. The utility of artificial oxidants such as iodosobenzene and hydrogen peroxide as substitutes for the NAD(P)H/O$_2$/reductase/(redoxin) system was explored initially because the reaction steps following reduction of P450 by the second electron (see the P450 reaction cycle, Figure 1.4) occur too quickly to observe the intermediates. By using artificial oxidants, intermediates in the reaction pathway have been detected spectroscopically.

The ability of P450 enzymes to utilize hydrogen peroxide, hydroperoxides and peracids to support aromatic and aliphatic hydroxylation (Rahimtula and O'Brien, 1974; Hrycay et al., 1975; Ellin and Orrenius, 1975), N-demethylation (Kadlubar et al., 1973) and O-dealkylation (Rahimtula and O'Brien, 1975) reactions suggest that P450s behave like peroxidases and generate the Compound I species [Fe=O]$^{3+}$. This species has been extensively characterized in peroxidases, and contains either a porphyrin-centered radical cation as in horseradish peroxidase, or a protein-centered radical as in cytochrome c peroxidase (Marnett et al., 1986; see Figure 1.9).
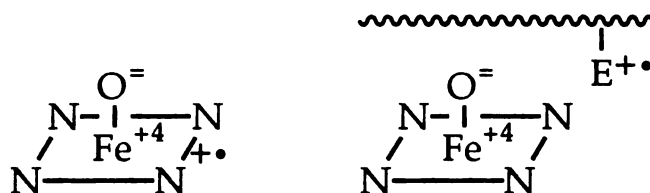
Figure 1.9: The electron distribution of Compound I in (a) horseradish peroxidase (contains a porphyrin-centered radical-cation) and (b) cytochrome c peroxidase (contains a protein-centered radical) (adapted from Ortiz de Montellano, 1986).

Attempts to identify such an intermediate in P450s using peroxy compounds have failed, however, as these compounds yield intermediates whose spectra depend on the structure of the peroxy compound used (Blake and Coon, 1979). Consequently, they cannot be single oxygen-bound intermediates, but rather more likely represent the precursor, $[Fe^{2+}OOR]$. Also, the finding that metabolic profiles obtained using peroxides do not always match those obtained using the $NADPH/O_2$ system suggests side reactions occur with these oxidants which obscure the P450 mechanism (Ortiz de Montellano, 1986).

The finding that P450 enzymes plus hydroperoxides can catalyze olefin epoxidations suggests that alkoxyl or hydroxyl radicals are not involved, as electron abstraction from the π-bond by an alkoxyl or hydroxyl radical would be highly unfavorable (Marnett et al., 1986). Such a mechanism would also not be likely to show the retention of olefin stereochemistry characteristic of P450-catalyzed epoxidations (Ortiz de Montellano et al., 1983).

Stronger evidence for heterolytic oxygen cleavage comes from studies of P450 and iodosobenzene. This oxidant delivers only one oxygen to the heme iron, generating an iron-oxo species whose spectra is independent of the structure of the original iodosobenzene and is similar to that of Compound I in peroxidases (Blake and Coon, 1989). The finding that this oxidant is capable of hydroxylation in microsomal suspensions (Lichtenberger et al., 1976; Gustafsson et al., 1979) and epoxidations with model heme systems (Groves et al., 1980; McMurry and Groves, 1986) indicates that the iron-bound oxygen species formed is capable of both hydrogen (or electron) abstraction *and* oxygen recombination, consistent with the heterolytic mechanism proposed for P450 enzymes.

A few inconsistencies between the iodosobenzene and NAD(P)H/O_2-derived products indicate that the reaction may not be as simple as hoped, however. Comparison of the metabolites from the two reactions reveals the regioselectivities are not always the same between the two systems (Berg *et al.*, 1979), and suggests that some part of the iodosobenzene structure may be present in the active site during hydroxylation. Also, the oxygen atom in the product from the iodosobenzene reaction derives from water, unlike in the NAD(P)H/O_2 reaction (Heimbrook and Sligar, 1981; Macdonald *et al.*, 1982; White and McCarthy, 1984). The finding that the iodosobenzene oxygen does not exchange with water in the absence of P450 suggests the oxygen exchange is occurring *after* the formation of the iron-oxygen complex, and thus the iron-oxo species in the iodosobenzene and O_2/NADPH-catalyzed reactions can not be the same. One possible explanation to reconcile this discrepancy is that P450 catalyzes the oxygen exchange with water prior to oxygen transfer to the iron (Ortiz de Montellano, 1986).

In sum, there are arguments for both sides of the heterolytic *vs.* homolytic oxygen bond cleavage debate, with some favoritism for the heterolytic mechanism. The studies utilizing peroxy compounds as oxygen donors indicate that under those conditions homolytic bond cleavage is possible, although how much of that reflects the natural P450 reaction mechanism is unclear. The question of the different specificities in the hydrogen abstraction and oxygen recombination steps in the P450$_{cam}$-catalyzed hydroxylation of camphor was addressed by Raag and Poulos, who noted that in the crystal structure of the camphor-CO-P450$_{cam}$ complex the camphor molecule is bound more loosely than in the complex without the CO molecule present, suggesting that greater mobility of camphor in the oxygen-bound state could enable both the *exo-* and *endo-*hydrogens to be

21

presented to the iron-oxo species for abstraction (Raag and Poulos, 1989). Why oxygen recombination with the *endo* face of the radical does not occur even to a small extent, however, is still not clear.

A second question of interest in the oxygen-oxygen bond cleavage mechanism is what supplies the catalytic push for bond cleavage? In peroxidases, oxygen-oxygen bond cleavage is facilitated by nearby arginine and histidine residues in the active site, which can assist in the transfer of protons and can stabilize charge separation in the activated complex (Poulos and Kraut, 1980). In P450$_{cam}$, however, the active site is predominantly hydrophobic, lacking any acidic or basic residues which might act in a similar fashion. Consequently, it is argued that the cysteine ligand to the iron provides the chemistry needed for bond cleavage, as it should bind to the heme iron as the negatively-charged thiolate anion, thus providing greater electron donating ability than can histidine, the iron ligand in peroxidases (Dawson *et al.*, 1976).

The lack of polar groups in the active site pocket, combined with the lack of waters present when camphor is bound, raises the question of where do the protons come from? Analysis of the crystal structure indicates the presence of three crystallographically-defined water molecules which link Thr 252 in the oxygen binding pocket with another highly conserved residue, Glu 366 (Raag and Poulos, 1991). Such an unusual internal solvent channel could serve as the source of protons required for oxygen activation.

1.2.3   Uncoupling Reactions

The cytochrome P450 reaction cycle describes an enzyme able to bring together a variety of cofactors and proteins to form a powerful oxidizing

machine. Only for a handful of isozymes and substrates, however, are these enzymes 100% efficient. $P450_{cam}$, with its natural substrate camphor, is one of the best, utilizing >95% of the NADH and O_2 equivalents to produce hydroxylated camphor (Atkins and Sligar, 1987a; Fruetel *et al.*, 1992). The other 3% or so is released as hydrogen peroxide, one of the possible products formed when the enzyme uncouples and discharges an iron-oxygen intermediate onto an unproductive pathway (equation 1.4). The other two possible uncoupling products are superoxide (usually detected as hydrogen peroxide; equation 1.5) and water (equation 1.6).

$$[Fe^{2+}O_2] \xrightarrow{e^-} [Fe^{2+}O_2^-] \leftrightarrow [Fe^{3+}O_2^=] \rightarrow [Fe^{3+}] + O_2^= \xrightarrow{2H^+} H_2O_2 \qquad (1.4)$$

$$[Fe^{2+}O_2] \leftrightarrow [Fe^{3+}O_2^-] \rightarrow [Fe^{3+}] + O_2^{-\cdot} \xrightarrow{e^-, 2H^+} H_2O_2 \qquad (1.5)$$

$$[FeO]^{3+} \xrightarrow{2e^-, 2H^+} H_2O \qquad (1.6)$$
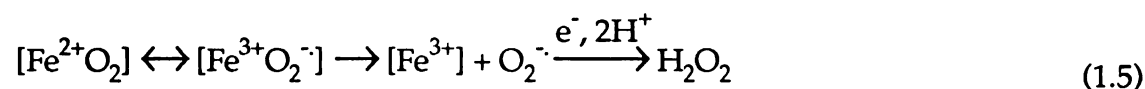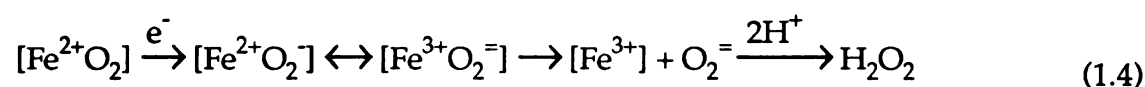
Substrate-Induced Uncoupling

Studies of $P450_{cam}$ turnover of camphor analogs such as norcamphor and camphane indicate that not only are these substrates unable to fully convert the enzyme to high spin, but they are also not hydroxylated with full efficiency. A comparison of the amount of hydroxylated product formed versus NADH consumed indicates that only 12 and 8 % of the NADH used went towards product formation with norcamphor and camphane, respectively (Atkins and Sligar, 1988; 1989).

This inefficiency has been observed with microsomal P450s as well, and the discrepancy between NADPH and product rates can be accounted for

by the production of hydrogen peroxide (Nordblom and Coon, 1977). Whether the hydrogen peroxide is released directly from the enzyme or results from superoxide release is difficult to distinguish, as superoxide production has been measured for both $P450_{cam}$ and microsomal P450s (Sligar *et al.*, 1974; Kuthan *et al.*, 1978).

In the case of norcamphor and $P450_{cam}$, hydrogen peroxide formation does not account for all the NADH consumed. Comparison of NADH and oxygen consumption with product and hydrogen peroxide formation reveals a "striking unaccountability" of electrons deriving from NADH (Atkins and Sligar, 1987a; see Table 1.3).

Table 1.3: *Comparison of the amounts of NADH and oxygen consumed with product and hydrogen peroxide formed by $P450_{cam}$ in the presence of camphor and norcamphor. The discrepancy between NADH consumption and the products produced with norcamphor is attributed to the formation of "excess" water (from Atkins and Sligar, 1987a).*

| Substrate | nmoles consumed | | nmoles produced | | |
	NADH	O_2	ROH	H_2O_2	xs H_2O
camphor	313 ± 8	290 ± 8	290 ± 2	20 ± 12	0
norcamphor	577 ± 8	365 ± 5	88 ± 12	88 ± 22	189

Given that the normal stoichiometry between NADH and O_2 consumed *vs.* alcohol or hydrogen peroxide produced is 1: 1: 1 (see equations 1.7 and 1.8), this suggests that some reaction must be occurring which requires NADH but not O_2 and forms neither hydroxylated product nor

$$NADH + O_2 + RH \xrightarrow{2H^+} ROH + H_2O + NAD^+ \qquad (1.7)$$

$$NADH + O_2 \xrightarrow{2H^+} H_2O_2 + NAD^+ \qquad (1.8)$$
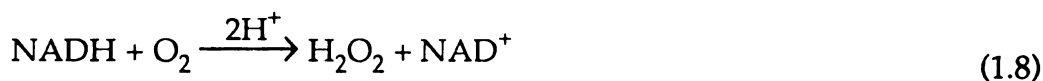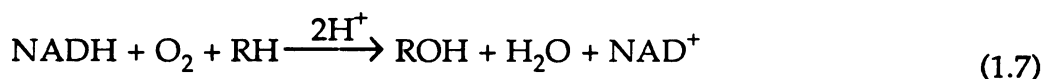
hydrogen peroxide. This reaction, they argue, is the two electron reduction of the activated iron-oxo intermediate, $[Fe=O]^{3+}$, to form water (equation 1.9).

$$NADH + [Fe=O]^{3+} \xrightarrow{2H^+} H_2O + NAD^+$$

(1.9)

Support for this mechanism comes from measurements of the deuterium isotope effects on NADH consumption (0.77), O_2 consumption (1.24) and hydrogen peroxide formation (1.25) with specifically deuterated norcamphors (Atkins and Sligar, 1988). The finding that the isotope effect on NADH consumption is inverse and different from the O_2 and H_2O_2 isotope effects indicates there is a route for NADH utilization that is kinetically independent from O_2 uptake, H_2O_2 formation, and product formation. Since the only isotopically sensitive step of the P450 reaction cycle is the hydrogen abstraction step, this suggests the iron-oxo intermediate $[Fe=O]^{3+}$ partitions between hydrogen abstraction and further reduction to form water.

Given that P450 enzymes can uncouple to generate hydrogen peroxide, superoxide or excess water, what determines whether or not the enzyme will do this? Why does P450$_{cam}$, for example, uncouple in the presence of norcamphor and camphane, but not with camphor or thiocamphor?

A look at the x-ray crystal structures of P450$_{cam}$ complexed with these four substrates suggests the presence of water molecules in the active site is linked to the susceptibility of the enzyme to uncouple (Raag and Poulos, 1989a; 1991). Both norcamphor and camphane are small enough to permit water molecules to be present near the heme iron while they are bound;

25

camphor and thiocamphor, on the other hand, completely fill the active site, and can squeeze out even a sixth ligand to the heme iron. Because, in the case of camphor which is tightly coupled, all proton sources are sequestered in the protein and thus access to them is tightly controlled by the protein, Raag and Poulos argue that "uncontrolled access" of water to the iron-bound oxygen species will cause it to discharge. Indeed, model studies have shown that protic environments can destabilize iron-dioxygen complexes, and may be likely to destabilize iron-oxo complexes as well (Brinigar et al., 1974).

Uncoupling Induced by Mutation of Thr 252

Uncoupling of $P450_{cam}$ can occur not only with substrates which are small enough to allow extra waters to be present during the catalytic reaction, but also when the enzyme is mutated at a critical residue near the oxygen binding pocket. Thr 252, one of the most highly conserved residues among P450 enzymes, plays a critical role in creating the oxygen-binding pocket in $P450_{cam}$ by forming an unusual hydrogen bond between the threonine hydroxyl and the carbonyl oxygen of Gly 248, thus disrupting the normal α-helical hydrogen-bonding pattern and creating a groove for the oxygen molecule to bind (see Figure 1.7; Poulos et al., 1987). The fact that this residue is also one of the few hydrophilic residues in the $P450_{cam}$ active site suggests that its hydrogen-bonding capacity may be important in the activation and stabilization of heme-bound oxygen, and may help relay the protons needed for dioxygen bond cleavage and for oxygen incorporation into the substrate. Hence, mutation of this residue to something without hydrogen-bonding capability may be expected to have dire consequences on the ability of the enzyme to efficiently hydroxylate the substrate.

Indeed, two groups independently found that mutation of this residue to alanine, valine or even serine causes the enzyme to uncouple in the presence of camphor (Imai *et al.*, 1989; Martinis *et al.*, 1989). The alanine and valine mutants produced much greater uncoupling towards hydrogen peroxide than did the serine mutant (see Table 1.4), indicating the importance of the side-chain hydroxyl group in controlling enzyme efficiency. The finding that excess water is also formed, as measured with the alanine mutant (Martinis *et al.*, 1989), indicates the side-chain hydroxyl is important in stabilizing both the iron-dioxo and the activated iron-oxo complexes.

Table 1.4: *Comparison of the amounts of product ROH (5-exo-hydroxy-camphor) and hydrogen peroxide produced by* P450$_{cam}$ *and three Thr 252 mutants (from Imai et al., 1989).*

Residue at 252	% ROH[a]	% H$_2$O$_2$[a]
Thr (wild type enzyme)	96	5
Ala	6	83
Val	22	45
Ser	81	15

[a] expressed as % O$_2$ consumed.

Which iron-dioxo species is involved in hydrogen peroxide formation was addressed by Imai and coworkers, who concluded that the hydrogen peroxide formed with the alanine and valine mutants came from the reduced ferrous-peroxy complex (equation 1.2), as (1) no superoxide was detected, and (2) spectral measurements of the ferrous-dioxygen complex found that it decayed much too slowly for it to be the hydrogen peroxide source. The finding that the ferrous-dioxygen complex in the two mutants

decayed faster than the wild-type, however, suggests that the presence of the hydroxyl group stabilizes the dioxygen complex.

Whether the increased uncoupling measured in the Thr 252 mutants is due to changes in the I helix structure near the oxygen binding pocket, or whether it is due to increased exposure of the iron-oxygen species to water-- or both--was addressed by the crystal structure of the Thr 252 to Ala mutant determined by Raag and coworkers (1991).

In this structure, the local distortion in the I helix near the heme center between Gly 248 and Thr 252 becomes even more severe, with the Ala 252 side chain situated even further away from the dioxygen binding groove than the wild-type Thr 252 (Figure 1.10). In this new space a water molecule
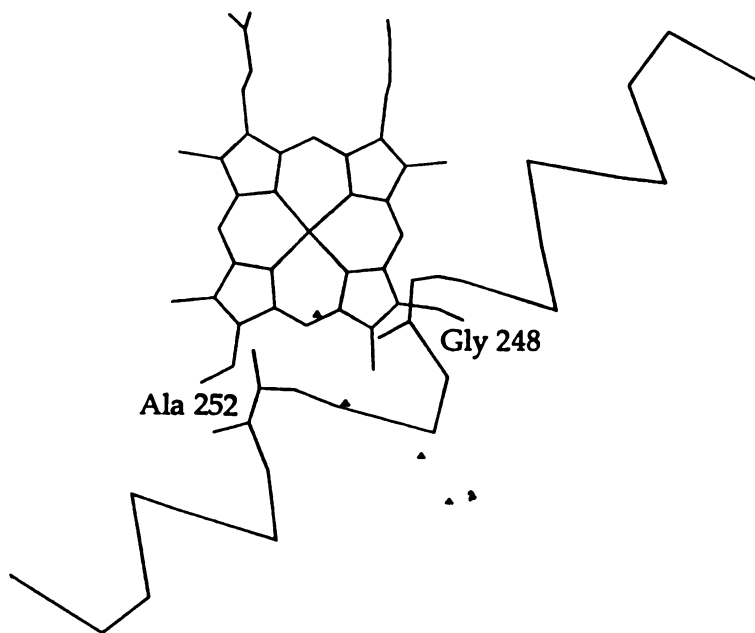
Figure 1.10: Overhead view of the T252A mutant active site showing the kink in the I helix. The kink in the helix is greater in the mutant than in the wild-type enzyme (Figure 1.7), allowing enough room for a water molecule (denoted by a triangle) to bind (from Raag et al., 1991).

28

is bound which is not present in the wild-type enzyme and serves as the hydrogen bond donor necessary to retain the kink in the helix.

The close proximity of the new molecule to the oxygen binding position confirms the hypothesis proposed from the norcamphor and camphane studies that it is the accessibility of the bound oxygen to water that promotes uncoupling. The close proximity of the bound water molecule in the mutant structure suggests that this molecule could destabilize the iron-bound oxygen complexes in at least two ways: by sterically interfering with preferential binding of the oxygen, or by serving as a proton source (Raag *et al.*, 1991). The fact that any proton source supplied by the wild-type protein is sequestered in the protein structure when camphor is present suggests that the protein tightly controls access of protons during the normal catalytic cycle. It is thus the introduction of a new access route to protons that uncouples the enzyme and diverts the iron-bound oxygens onto unproductive pathways.

1.2.4 Factors Controlling Reaction Stereo- and Regiospecificity
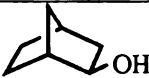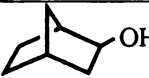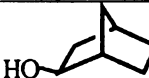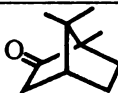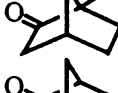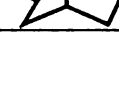
Studies with Camphor Analogs

The crystal structure of camphor bound in the active site of $P450_{cam}$ reveals that this substrate fits like a key in a lock. It is closely surrounded on all sides by hydrophobic surfaces which contour to the shape of the camphor molecule and which, together with the strategic positioning of a hydrogen bond donor to interact with the camphor carbonyl oxygen, appear to allow the substrate to bind in only the orientation that leads to the observed product, 5-*exo*-hydroxycamphor.

29

Analysis of the crystal structure suggests that specific residues are important in determining this particular orientation for camphor (see Figure 1.5). The hydrogen bond donor, Tyr 96, appears to play a critical role in orienting the carbonyl oxygen of camphor away from the heme surface. The side chain methyls of Val 295 intercalate with the *gem*-dimethyls (C8 and C9) of camphor, suggesting a unique binding pocket for these substituents. And a hydrophobic cleft formed by Val 247 and Leu 244 may serve as a recognition site for the third methyl substituent (C10) as well as for the rest of the hydrocarbon ring.

Metabolism studies of camphor analogs in which the carbonyl oxygen, the dimethyls, or the dimethyls and the C10 methyl are missing support the importance of these substituents in orienting the camphor molecule in the active site pocket. As shown in Table 1.5, the regioselectivity of hydroxylation by P450$_{cam}$ decreases in the absence of one or more of these substituents. Removal of the carbonyl oxygen (camphane) causes a 10% decrease in the preference for 5-*exo* hydroxylation, while loss of the *gem-*

Table 1.5: The regioselectivity of hydroxylation of various camphor analogs by P450$_{cam}$ (from Atkins and Sligar, 1988; 1989).

Substrate	5-*exo*	6-*exo*	3-*exo*
	100		
	90	10	
	82	15	3
	45	47	8

dimethyl substituents (1-methylnorcamphor) gives an even greater loss in regioselectivity. Removal of *gem*-dimethyl and the C10 methyl substituents (norcamphor) abolishes the preference for 5-*exo* hydroxylation, as now the amount of 5-*exo* and 6-*exo* products are about the same.

The finding that small amounts of 3-*exo*-hydroxycamphor are observed for norcamphor and 1-methylnorcamphor suggests that these substrates are now small enough to move significantly about the active site. This mobility is consistent with the increased temperature factors measured for norcamphor in the crystal structure of the norcamphor-bound enzyme, suggesting that this substrate binds more loosely than does camphor (Raag and Poulos, 1989a).

Although the crystal structure shows only one orientation for norcamphor binding (would give 5-*exo* hydroxylation), theoretical calculations of norcamphor bound in the $P450_{cam}$ active site predicted that both 5-*exo* and 6-*exo* hydroxylation would occur (Collins and Loew, 1988; Bass *et al.*, 1992). The small amount of 3-*exo* hydroxylation formed was postulated to arise from rotation of the molecule by ~130° about its carbonyl group--a rotation which is allowable due to the lack of interactions of the substrate with Phe 87, Val 295, and Val 247.

In sum, it seems that the smaller substrates such as norcamphor are able to move about the active site in a fairly unrestricted manner, as evidenced by low hydroxylation regiospecificity, uncoupling, and the inability to convert the enzyme fully to high spin. Camphor cannot be bound too tightly in the active site, however, as some movement is required to permit oxygen to bind. Also, when the 5-*endo* and 5-*exo* hydrogens of camphor are replaced by fluorine atoms, thus rendering those positions unreactive to hydroxylation, $P450_{cam}$ hydroxylates camphor at the C9

31

position (Eble and Dawson, 1984), indicating that the camphor molecule has a fair degree of mobility within the active site.
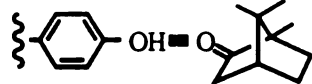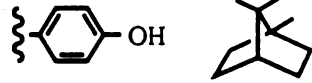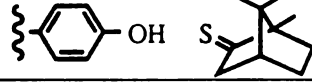
Mutagenesis Studies

The other way to test for the importance of substrate interactions with specific residues in the active site is to mutate those residues to either lessen or increase interactions with the substrate. The role of the hydrogen bond between the camphor carbonyl oxygen and the hydroxyl group of Tyr 96 in determining the regiospecificity of the reaction was tested in this way by mutating the tyrosine to a phenylalanine.

Comparison of the regioselectivity of camphor hydroxylation by this mutant with wild-type hydroxylation of camphor, camphane and thiocamphor--the latter two substrates cannot hydrogen-bond--indicates that the absolute regioselectivity of the reaction is lost with removal of the hydrogen-bond, although not by much (Atkins and Sligar, 1988; see Table 1.6). The finding that camphane generates less high spin enzyme and binds significantly more poorly than camphor or thiocamphor suggests that the substrate carbonyl plays a steric role in addition to a hydrogen bonding role. Residues other than Tyr 96 which contact the carbonyl, such as Phe 87 and Leu 244, may serve to anchor the substrate through nonhydrogen bonding interactions. These interactions would be intact in the Y96F-camphor and wild-type-thiocamphor complexes, yet lacking in the camphane complex (Atkins and Sligar, 1988).

To test the importance of interactions between Val 295 with the camphor *gem*-dimethyls and Val 247 with the camphor C10 methyl group, two mutants were made, V295I and V247A, and the effect on the

Table 1.6: *The effect of the hydrogen bond between Tyr 96 and the camphor carbonyl on the regioselectivity of hydroxylation by P450$_{cam}$ and the active-site mutant Y96F with a variety of camphor analogs (from Atkins and Sligar, 1988).*
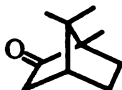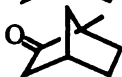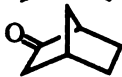
Substrate	hydroxylated products			% high spin	K$_D$ (μM)
	5-*exo*	6-*exo*	3-*exo*[a]		
(structure) OH■O	100			95	1.6
(structure) O	92	2	6	59	3.3
(structure) OH	90	10		46	46
(structure) OH S	64	34	2	65	3.0

[a] includes all other hydroxylated products

regioselectivity of hydroxylation on camphor, 1-methylnorcamphor and camphor were determined (Atkins and Sligar, 1989). Although the increased bulk at residue 295 in the V295I mutant might be expected to disfavor 5-*exo* hydroxylation, very little effect was seen on the patterns of hydroxylation (see Table 1.7). This may be due to the ability of the protein to accommodate such a small change, and/or the fact that the other orientations were equally disfavored.

The decrease in bulk at residue 247 in the V247A mutant however, had a significant effect on the hydroxylation patterns (Table 1.7). For both 1-methylnorcamphor and norcamphor--substrates lacking the *gem*-dimethyl substituents--the amount of 3-*exo* hydroxylation increased significantly to where it was more favored than 6-*exo* hydroxylation. This suggests that a decrease in bulk near the C10 carbon greatly facilitates rotation of these smaller substrates around the carbonyl bond.

Table 1.7: *The regioselectivity of hydroxylation by the active site mutants V295I and V247A with camphor analogs (from Atkins and Sligar, 1989).*

	Hydroxylated products								
	Wild-type			V295I			V247A		
Substrate	5-exo	6-exo	3-exo[a]	5-exo	6-exo	3-exo[a]	5-exo	6-exo	3-exo[a]
	100			100			97		3
	82	15	3	90	10		72	7	21
	45	47	8	46	48	6	40	20	40

[a] includes all other hydroxylated products

In sum, mutagenesis studies have shown that although the hydrogen bond to Tyr 96 and the interactions with Vals 247 and 295 are important, they are by no means solely determining in the high regio- and stereoselectivity observed for camphor hydroxylation by P450$_{cam}$. It appears that a combination of factors are involved which determine how the substrate binds in the active site, and that mutation of active site residues may be compensated for by the enzyme in a manner we do not fully understand in order to retain the regio- and stereochemical integrity of the reaction.

1.3 Mammalian Cytochromes P450

The mammalian cytochromes P450 constitute a class of enzymes of extreme interest to biologists, pharmacologists and toxicologists (as well as chemists!) due to their importance in humans and animals. Knowledge of substrate specificities, reaction stereo- or regioselectivities, and mechanisms of action are directly relevant to *in vivo* effects of drugs and carcinogens, and

thus a great deal of effort has gone into characterizing these systems. Unfortunately, for none of the mammalian enzymes has a crystal structure been obtained, due to the inherent difficulty in crystallizing membrane-bound proteins. Thus, such detailed knowledge of specific substrate-protein interactions as is known for $P450_{cam}$ is not available for the mammalian enzymes. More indirect methods have thus been typically employed to study the active site natures of these enzymes.

The mammalian P450 enzymes generally fall into two groups based on their localization and function in the body. Those which are found in the mitochondria are involved in the oxidation of endogenous compounds such as steroids. These enzymes are similar to the bacterial enzymes such as $P450_{cam}$ in that they require an iron-sulfur redoxin protein, an FAD-containing reductase and the cofactor NADH for activity. An example of a P450 in this group is P45011A1, which requires as helper enzymes adrenodoxin and adrenodoxin reductase to catalyze the side-chain cleavage of cholesterol.

The second group of mammalian P450 enzymes are localized in the endoplasmic reticulum and have as substrates either endogenous or exogenous compounds. The P450s involved in the oxidation of prostaglandins, leukotrienes and some sterols are examples of members of the first class of enzymes, while the drug-metabolizing enzymes constitute the second class. Both classes of P450s require only one helper protein, an FAD/FMN-containing reductase, and the cofactor NADPH for activity. Electrons are shuttled similarly to the $P450_{cam}$ system in that two electrons are abstracted from NADPH by the reductase, which then relays them one at a time to the P450 (see Figure 1.11).

NADPH, NADP+, Redt(ox), Redt(red), P-450(red), P-450(ox) diagram with 2 e- and 1 e-
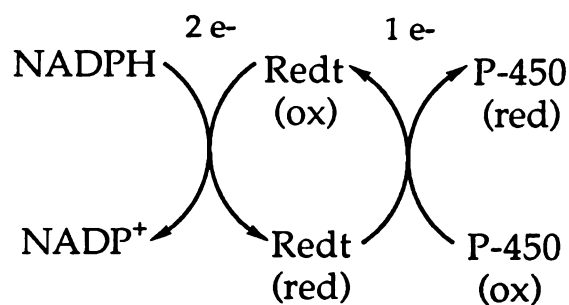
Figure 1.11: *Electron-shuttling pathway for P450 enzymes utilizing a single NADPH-binding reductase.*

1.3.1 Common Structural Elements Among P450s

The fact that P450 enzymes have been found in almost every kind of organism from bacteria to plants to mammals suggests that these enzymes may be quite diverse in their amino acid sequences due to their widely varying substrate requirements and cellular locations. While this is true between certain families of P450s, comparison of all the amino acid sequences known for P450 enzymes to date reveals regions of very high sequence identity, suggesting structural features which may be common to all P450 enzymes.

Heme Binding Pocket

The identification of a cysteine thiolate anion as the protein ligand to the heme iron (Cramer *et al.*, 1978; Champion *et al.*, 1982) suggests that this amino acid should be 100% conserved among all P450s. Initial sequence alignments of P450 enzymes found three highly conserved cysteines which could serve the role; however, only one of them (the one corresponding to Cys 357 in P450$_{cam}$) is in a region of the sequence that is highly conserved among all P450s (Black and Coon, 1986). This role for Cys 357 was confirmed

by the crystal structure of P450$_{cam}$ (Poulos *et al.*, 1985), and by mutagenesis studies of P4501A2, which suggest that the corresponding cysteine in mammalian P450s also serves as the heme ligand (Shimizu *et al.*, 1988).

Although Cys 357 is not part of a helix (it sits at the N-terminal end of the L-helix), the high conservation of residues surrounding this ligand suggests that these residues serve a functional and structural role in P450 enzymes (see Table 1.8). In P450$_{cam}$ the two residues bracketing Cys 357--Phe 350 and Leu 358--form hydrophobic contacts with the heme and, together with Gln 360, form a pocket for the thiolate ligand (Poulos *et al.*, 1985). The fact that Phe 350 is invariant among P450s and that Leu 358 is always a small aliphatic residue suggests similar interactions are occurring in all P450 enzymes. The conservation of Gly 353, which initiates a turn, and Gly 359, which ends the L helix, also suggests a common structural motif in all P450s (Poulos *et al.*, 1985).

The conservation of a charged residue at position 355 suggests a significant role as well. In the crystal structure of P450$_{cam}$, His 355 interacts

Table 1.8: *Alignment of various P450 amino acid sequences in the region surrounding Cys 357 in P450$_{cam}$ (from Nelson and Strobel, 1987).*

P450$_{cam}$	T	F	G	H	G	S	H	L	C$_{357}$	L	G	Q	H	L	A	R
P4501A1 (rat)	L	F	G	L	G	K	R	K	C	I	G	E	T	I	G	R
P4501A2 (rat)	L	F	G	L	G	K	R	R	C	I	G	E	I	P	A	K
P4502B1 (rat)	P	F	S	T	G	K	R	I	C	L	G	E	G	I	A	R
P4504A1 (rat)	P	F	S	G	G	A	R	N	C	I	G	K	Q	F	A	M
P4502E1 (human)	P	F	S	T	G	K	R	V	C	A	G	E	G	L	A	R
P45011A1 (human)	G	F	G	W	G	V	R	Q	C	L	G	R	R	I	A	E
P45021A1 (human)	A	F	G	C	G	A	R	V	C	L	G	E	P	L	A	R

with the heme propionic groups, suggesting that the corresponding arginine in mammalian P450s acts in a similar fashion. Indeed, mutagenesis studies have confirmed this possibility (Shimizu *et al.*, 1988).

Oxygen Binding Pocket

The second region of high sequence identity among P450 enzymes corresponds to the distal helix (helix I) in P450$_{cam}$ (see Table 1.9). This helix runs across the B ring of the heme, and helps to hold the heme in place by sandwiching it with helix L (see Figure 1.3). The proposed importance and function of the kink in this helix centered at Thr 252, caused by an interruption of the normal hydrogen-bonding pattern of α-helices, is to form the binding pocket for molecular oxygen that is implicated as a proton source, as discussed in Sections 1.2.2 and 1.2.3.

Sequence alignments indicate that Thr 252, the residue that is closest to the heme center and is implicated in both forming the kink in the helix and as a proton shuttler, is invariant among P450s, suggesting that it is a common requirement of P450 enzymes (see Table 1.9). Mutation of this threonine to histidine in P4502C2 and P4502C14 generates enzymes which look spectrally normal but which are inactive towards hydroxylation (Imai and Nakamura, 1988). Mutation of this threonine to alanine in P4501A2 produces an enzyme which has different substrate specificity and regioselectivity, indicating that the threonine plays an important role not only in the ability of the enzyme to turn over, but also in the active site topology (Furuya *et al.*, 1989a; 1989b). Note that in none of these studies was

Table 1.9: *Alignment of various P450 amino acid sequences in the region surrounding Thr 252 in P450$_{cam}$ (from Nelson and Strobel, 1988, 1987).*

P450$_{cam}$	L	L	L	V	G	G	L	D	T$_{252}$	V	V	N	F	L	S	F
P4501A1 (rat)	D	L	F	G	A	G	F	D	T	I	T	T	A	I	S	W
P4501A2 (rat)	D	I	F	G	A	G	F	E	T	V	T	T	A	I	F	W
P4502B1 (rat)	S	L	F	F	A	G	T	E	T	S	S	T	T	L	R	Y
P4504A1 (rat)	T	F	M	F	E	G	H	D	T	T	A	S	G	V	S	W
P4502E1 (human)	D	L	F	F	A	G	T	E	T	T	S	T	T	L	R	Y
P45011A1 (human)	E	M	L	A	G	G	V	D	T	T	S	M	T	L	Q	W
P45021A1 (human)	D	L	L	I	G	G	T	E	T	T	A	N	T	L	S	W

the degree of uncoupling measured, and hence that factor cannot be addressed for these mammalian enzymes.

The other residue involved in forming the kink, Gly 248, is also highly conserved as either alanine or glycine (except for P4504A1, which has an unusual glutamate at this position), and is part of a nonpolar region (244-249) which contacts the heme surface in P450$_{cam}$. Although the overall nonpolarity of this region is conserved among all P450s, positions 244 and 247 are not necessarily conserved. In P450$_{cam}$ these residues contact the substrate, and thus it is proposed that the different substrate specificities of P450 enzymes dictate the nature of these residues (Poulos *et al.*, 1985).

The fact that the only ionic residue in this helix, Asp 251, is highly conserved as an acidic residue suggests that this amino acid serves a structural role in the helix. In P450$_{cam}$, Asp 251 points away from the heme to form an internal ion pair with Arg 186, which is postulated to stabilize the kink in the helix (Poulos *et al.*, 1985). The high conservation of an acidic

residue at this position may thus stabilize this unusual conformation in all P450 enzymes.

Membrane Topology

How the mammalian P450 enzymes are anchored to the membrane has been the subject of a number of studies employing such diverse techniques as antibody binding, chemical modification, trypsinolysis, secondary structure predictions and hydropathy profiles. The fact that P450 substrates are typically very hydrophobic and that treatment of microsomes with proteases releases the catalytic part of NADPH-cytochrome P450 reductase, an enzyme purported to have a short membrane anchor, and either destroys or does not touch P450 suggested early on that P450s were integrally associated with the membrane (DePierre and Ernster, 1977; Ingelman-Sundberg, 1986). Sequence analysis of P4502B4 revealed as many as eight hydrophobic segments which could serve as membrane-spanning helices, confirming this picture (Tarr *et al.*, 1983).

However, later studies have disputed this and suggest that microsomal P450s are only peripherally associated with the membrane. More recent hydropathy profiles by Nelson and Strobel (1988) using 34 P450 sequences have agreed that many transmembrane segments are possible; however, experimental evidence rules out all but two of them, they claim, suggesting an N-terminal membrane anchor for microsomal P450s (Figure 1.12b). Experimental evidence against transmembrane segments occurring in the middle of the protein includes antibody recognition of P4502B1 using antibodies raised from internal segments of the P450 sequence (De Lemos-Chiarandini *et al.*, 1987). Also, more recent proteolysis experiments indicate

40

that everything but the N-terminus of P450s can be cleaved (Brown and Black, 1989; Vergeres *et al.*, 1989), suggesting that the bulk of the enzyme resides on the cytosolic side of the membrane.

Whether or not there is one transmembrane helix or two is currently subject for debate, as there is evidence for both sides. Proteolysis studies suggest that residues 1-21 span the membrane, requiring only one transmembrane helix (Vergeres *et al.*, 1989; Figure 1.12a). Antibody recognition of residues 24-38 in P4502B1 requires these residues are cytosolic, thus supporting a single transmembrane helix (De Lemos-Chiarandini *et al.*, 1987). However, chemical modification of the N-terminus of P4502B4 by membrane-impermeable fluorescein isothiocycnate indicates that it must be cytosolic, requiring two transmembrane helices (Bernhardt *et al.*, 1983; Figure 1.12b).

Studies of the ability of the first 20 amino acids of P4502B1 to serve as a signal peptide conclude that both orientations occur (Monier *et al.*, 1988).

(a)   (b)
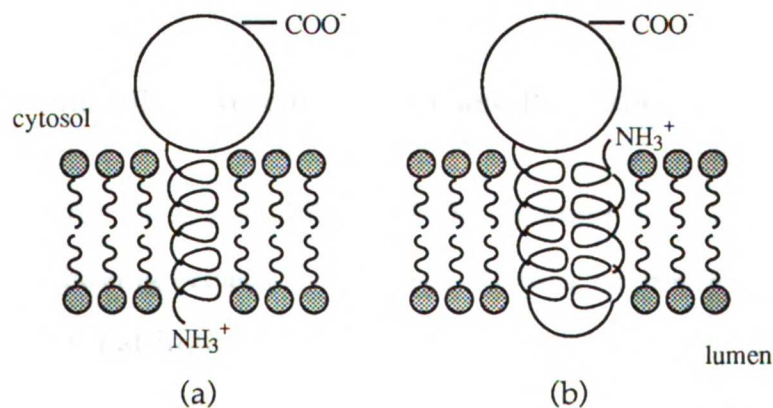
Figure 1.12: *A schematic of the two current proposed models for microsomal P450 integration into the endoplasmic reticulum. In (a), only one N-terminal peptide spans the membrane, locating the N-terminus on the lumen side of the membrane. In (b), two N-terminal peptides span the membrane, placing the N-terminus on the cytoplasmic side of the membrane.*

These authors found that a signal peptide cleavage site, inserted just after the first 20 amino acids of the P450 sequence, was recognized by a lumenally-located signal peptidase. This suggests that the amino terminus initially inserts into the membrane in a loop configuration. It reorients later, they postulate, as a protein attached to the N-terminus of the P450 was found to be on the lumen side of the membrane (Monier *et al.*, 1988).

In either of the two cases, a great deal of support for the bulk of the protein residing on one side of the membrane comes from sequence comparisons with P450$_{cam}$. Secondary structure predictions of membrane-bound P450s and P450$_{cam}$ indicate that almost all of the α-helices and β-structure found in P450$_{cam}$ are predicted to be present in mammalian P450s (Edwards *et al.*, 1989; Tretiakov *et al.*, 1989; Nelson and Strobel, 1988; Gotoh *et al.*, 1983). This high similarity to P450$_{cam}$ suggests that a multi-transmembrane structure is highly unlikely, and that a globular structure more like P450$_{cam}$ is probable. This is true even for the mitochondrial P450s, which lack the hydrophobic N-terminal tail typical of the microsomal P450s.

1.3.2   Factors Controlling Reaction Stereo- and Regiospecificity

Although the drug-metabolizing P450 enzymes have long been characterized as having broad substrate specificities, several pieces of evidence indicate that individual isozymes have surprisingly specific substrate requirements. For example, even though the phenobarbital-inducible isozyme 2B1 and the 3-methylcholanthrene-inducible isozymes 1A1 and 1A2 are all able to oxidize large multi-ring compounds--indicating that their active sites are quite spacious--they still have distinct substrate preferences. This is indicated by the fact that P4501A1 oxidizes 7-

ethoxycoumarin and *p*-nitroanisole over 10 times faster than 2B1 and 30-150 times faster than 1A2 (Conney, 1986). P4502B1 however, turns over benzphetamine and hexobarbital much faster than either 1A1 or 1A2.

Even substrates that are oxidized by more than one P450 enzyme show that the active sites of all the enzymes are not created equal. The regioselectivities of testosterone, progesterone and androstenedione hydroxylation, for example, have been shown to depend on the P450 isozyme involved (Conney, 1986; Swinney *et al.*, 1987; see Figure 1.13).
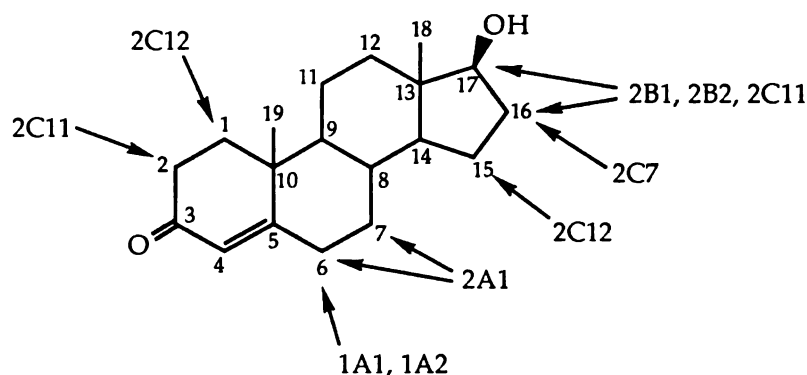
Figure 1.13: *The regioselectivity of testosterone hydroxylation is dependent on which P450 isozymes are involved (data from Conney, 1986).*

What these data suggest is that even though the active site pockets of most of the drug-metabolizing enzymes are ample enough to accommodate large substrates, each of them is distinct. Thus, knowledge of the active site features which make each one unique is important for understanding and predicting the metabolic profiles and substrate specificities of each isozyme.

Mutagenesis Studies

Attempts to define which residues in mammalian P450s are involved in substrate recognition have been frustrated by the lack of a crystal structure of a mammalian P450, and thus efforts to pinpoint active site residues have relied on aligning amino acid sequences with that of $P450_{cam}$ and superimposing the aligned sequences onto the $P450_{cam}$ structure. Since the substrate recognition pocket is going to be different for each isozyme, this method has limited relevance except in regions which are highly conserved, such as in the I helix of $P450_{cam}$. Indeed, mutations of P4501A2 in the region surrounding conserved Thr 319 (aligns with Thr 252 in $P450_{cam}$) indicate that changes in these residues do significantly affect the substrate specificity and regioselectivity of the enzyme, as noted above (Furuya *et al.*, 1989a; 1989b). This was also found to be true for mutants of aromatase, P45019 (Zhou *et al.*, 1992; Graham-Lorence *et al.*, 1991). These results are consistent with those residues forming part of the active site pocket.

Comparison of sequences which vary only in a few amino acids and yet which code for enzymes with vastly different substrate specificities is another way to pinpoint important residues. An allelic variant of P4502D1, which is only four amino acids different and yet has much lower catalytic activity towards bufuralol than the wild-type enzyme, was the impetus for the discovery that a single mutation (L380F) was responsible for the decreased turnover. The mutant enzyme still has normal activity toward debrisoquine, however (Matsunaga *et al.*, 1990), suggesting a subtle active site change.

In another example of the importance of a single residue, mutation of each of the 11 amino acid differences between P4502A5 and P4502A4

pinpointed Phe 209 as one of the key residues which convey 7-hydroxylation of coumarin specificity to P4502A5. Mutation of this phenylalanine to leucine switched the enzyme specificity to that of P4502A4, i.e., 15α-hydroxylation of testosterone (Lindberg and Negishi, 1989). The identity of residue 209 was found to closely affect the spin equilibrium in the P4502A5 mutants, suggesting that it is located near the heme aqua ligand (Iwasaki *et al.*, 1991).

These studies indicate the importance a single amino acid residue can have on the specificity of an enzyme, and demonstrate one way to determine which residues line the active site pocket of the enzyme. The effect of mutations without the benefit of a crystal structure must, however, be interpreted with restraint, as the observed effect could be due to a global change in protein structure and not necessarily to a local one.

Chemical Studies

In contrast to mutagenesis studies which pinpoint important residues in substrate recognition but give no structural data as to where the residues are located, chemical studies using metabolite stereo- and regioselectivity and heme alkylation have painted topological profiles of individual P450 active sites.

One of the earliest studies demonstrating this approach was done by Jerina and coworkers, who determined the stereochemistry of epoxidation of benzo[a]pyrenes by P450 1A1 (Jerina *et al.*, 1982). By overlaying the structures of the various epoxide products, each time aligning the epoxide oxygen, they proposed a picture of the 1A1 active site which is flat and hydrophobic, but restrictive enough to allow only certain orientations of the substrate (see Figure 1.14). Not only was this model predictive for epoxidation of

45

polycyclic aromatic hydrocarbons, but it was also able to rationalize the preferential abstraction of the pro-*S*-hydrogen in the O-deethylation reaction with 7-ethoxycoumarin (Tullman *et al.*, 1984).
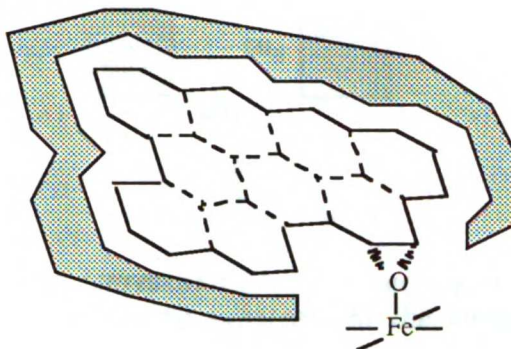
Figure 1.14: Proposed active site topology for P4501A1 based on the stereoselective epoxidation of benzo[a]pyrenes. The size of the planar binding pocket is just large enough to accommodate the 9 aromatic rings shown (adapted from Jerina et al., 1982).

Regioselective oxidation has also been used to argue for a tight active site in P4504A1 (CaJacob *et al.*, 1988). This P450 oxidizes fatty acids solely at the terminal, or ω position, and not at the thermodynamically favored ω-1 and ω-2 positions. In order to overcome the natural preference for ω-1 and ω-2 hydroxylation, it is argued that the protein residues in the active site of P4504A1 must restrict access of the substrate to the ferryl oxygen species such that only the ω carbon is presented (see Figure 1.15).

This hypothesis is supported by the finding that fatty acids with an acetylenic function at the terminal position inactivate P4504A1 by alkylating the protein and not the heme (CaJacob *et al.*, 1988). The rationale centers on the observation that heme alkylation occurs when the oxygen adds to the ω-1 carbon, resulting in N-alkylated porphyrin formation with oxygen at the ω-1 position. Protein alkylation, on the other hand, occurs when the oxygen adds to the ω carbon, giving rise to a ketene intermediate which is either
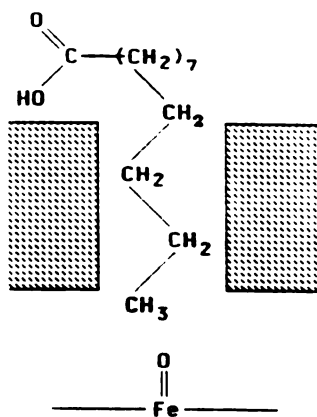
Figure 1.15: *Schematic representation of the active site of P4504A1 in which the protein restricts access of the substrate to the ferryl oxygen species such that only the ω carbon is presented (from CaJacob et al., 1988).*

attacked by a protein nucleophile, leading to protein modification, or by water to yield the corresponding carboxylic acid (Ortiz de Montellano, 1985; see Figure 1.16).
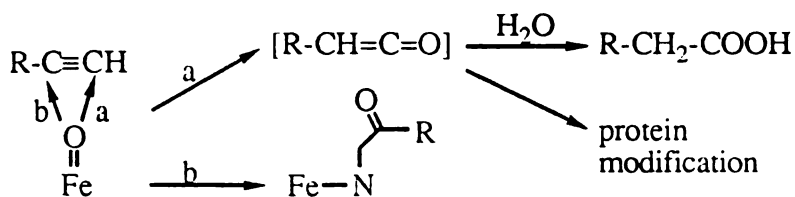
Figure 1.16: *Mechanism for inactivation of P450s by terminal acetylenes via (a) protein modification or (b) heme alkylation (adapted from CaJacob et al., 1988).*

Regioselective heme alkylation has also been used to determine active site topologies for several P450 enzymes. The earliest of such studies looked at the inactivation of P4502B1 by terminal olefins and acetylenes. Small alkyl-substituted olefins and acetylenes such as 1-octene, 1-propene, 1-ethylene, acetylene, 1-octyne and 1-propyne were found to alkylate the heme

nitrogens with surprising regioselectivity: the alkenes were found to only alkylate the D ring nitrogen of the heme, while the acetylenes only alkylated the A ring nitrogen (except for acetylene, which alkylated several nitrogens; Kunze *et al.*, 1983).

This surprising selectivity suggested that not all the heme nitrogens are available for alkylation, and an active site topology was proposed in which the A and D rings of the heme are exposed to solvent and the B ring is covered by protein (see Figure 1.17). Binding of the substrate alkyl chain over the C ring would thus orient the unsaturated bond to attack either the A ring nitrogen in the case of the acetylenes, or the D ring nitrogen in the case of the olefins (Kunze *et al.*, 1983).

The accessibility of the A and D ring nitrogens to solvent in P4502B1 has been confirmed by studies utilizing phenyl-substituted hydrazines as active site probes (Swanson *et al.*, 1991; Tuck and Ortiz de Montellano, 1992). Phenyl hydrazine has been shown spectroscopically and from x-ray crystal
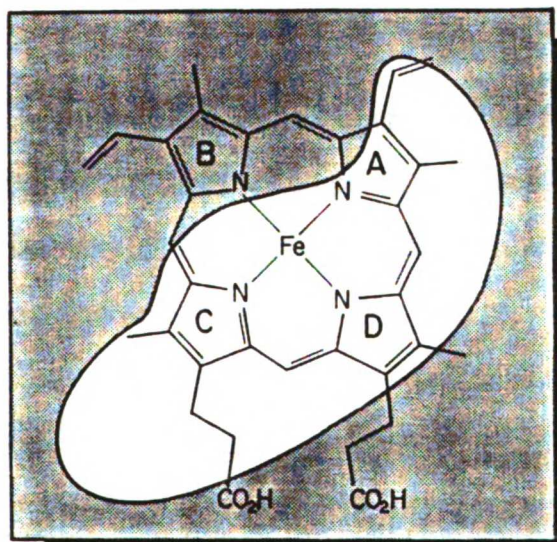
Figure 1.17: Active site topology proposed for P4502B1 based on the regioselective heme alkylation by terminal olefins and acetylenes (from Kunze et al., 1983).

structures to react with P450 enzymes and myoglobin to form a sigma-bonded iron-phenyl complex (Figure 1.18). This complex can be induced to shift under oxidative conditions to form one or more of the N-phenyl protoporphyrin IX isomers. The regioselectivity of the iron to nitrogen shift observed for P450 enzymes is proposed to be due to constraints imposed by protein residues in the active site, since otherwise all four N-phenyl isomers are obtained when the shift takes place outside the enzyme active site (Swanson *et al.*, 1991). Only the A and D ring N-phenyl isomers are obtained when P4502B1 is reacted with phenyl hydrazine, consistent with the proposal that only these two nitrogens are solvent accessible in this protein (Swanson *et al.*, 1991; Tuck and Ortiz de Montellano, 1992).
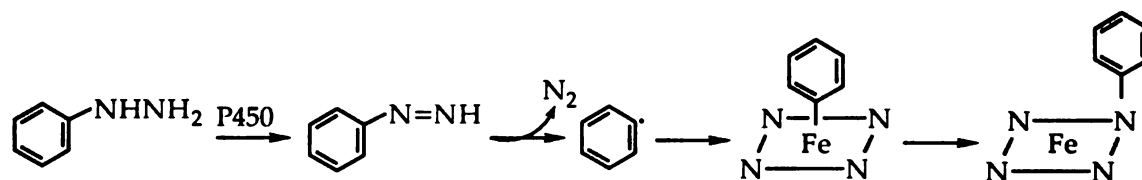
Figure 1.18: Mechanism for formation of N-phenyl adducts from reaction of P450 with phenyl hydrazine.

The active site topologies of a number of other P450 enzymes have been predicted using aryl hydrazines as probes, revealing both subtle and drastic differences between P450 isozymes. The results of these studies are discussed in Chapters 3, 4 and 5.

1.4   Thesis Proposal

Cytochrome $P450_{cam}$ is one of the best characterized P450 monooxygenase systems studied to date. Much of what is known both mechanistically and structurally about P450 enzymes has stemmed from

studies of this enzyme, and in particular from the x-ray crystallograpic structures determined by Poulos and coworkers. The fact that this enzyme and its redox partners are soluble has greatly facilitated these studies, although this property is also what distinguishes this system from the mammalian enzymes, which are membrane-bound. This raises the question of whether or not $P450_{cam}$ would be a good model for the mammalian enzymes.

The high sequence identity between $P450_{cam}$ and all other P450s in the regions which define the heme binding and oxygen binding pockets in $P450_{cam}$ suggests a common structural theme for P450 enzymes. The fact that the overall topology of the mammalian enzymes is predicted to be globular with the number of α-helices comparable to that of $P450_{cam}$ suggests P450 enzymes exhibit a common tertiary structure, regardless of whether they are membrane-bound or soluble. Finally, the fact that $P450_{cam}$ oxidizes hydrophobic substrates and contains a predominantly hydrophobic active site, as is predicted for the mammalian enzymes based on their substrate preferences, suggests this enzyme will serve as a good model for the mammalian enzymes.

Understanding what determines substrate specificity for a given P450 isozyme is crucial for the design of new inhibitors, tailoring the active site for the oxidation of new substrates, and the prediction of drug metabolism. However, since the active site structure is not absolutely known for any of the mammalian P450s, it is not possible to use these enzymes to analyze in detail the relationship between active site topology and substrate specificity. Only the active site structure of $P450_{cam}$ has been determined at a molecular level, and although a great deal has been learned about specific interactions of this protein with its natural substrate, very little is known about what

determines substrate binding preferences with compounds whose structures are distinct from camphor.

The present work examines the protein-substrate interactions which dictate binding preferences for a series of small hydrophobic compounds within the known active site of $P450_{cam}$. These substrates were selected based on their simple structure and small size, and are expected to have access to multiple binding orientations within the active site. The factors which dictate binding preferences are determined from a consideration of the stereoselectivity of the reaction, the mechanism of the reaction, the effect of mutagenesis, and from molecular dynamic simulations of the substrate in the enzyme active site. An assessment is also made of the effects of binding preferences on the extent of uncoupling by the enzyme. The reaction stereoselectivity exhibited by other P450 enzymes with these substrates is discussed in light of the results obtained with $P450_{cam}$.

2.0 MECHANISTIC STUDIES OF OLEFIN OXIDATION: METABOLISM OF *trans*-1-PHENYLVINYLCYCLOPROPANE BY CYTOCHROME P450$_{cam}$

2.1 Introduction

2.1.1 Proposed Mechanisms for Olefin Epoxidation

The primary pathway for olefin metabolism in mammals is epoxidation. Epoxide metabolites are rarely ever observed *in vivo*, however, because of their reactivity with biological macromolecules and because they are efficiently metabolized further by epoxide hydrolases to *vic*-diols and by glutathione transferases to glutathione conjugates.

P450 enzymes constitute the primary epoxidizing enzymes in mammals (Ortiz de Montellano, 1985). Although epoxidation represents a major class of reactions for these enzymes, the mechanism of the reaction remains obscure, with at least four different reaction pathways currently debated (see Figure 2.1).

A concerted mechanism, whereby both carbon-oxygen bonds are formed at the same time (Figure 2.1a), was initially proposed based on the discovery that olefin epoxidation by P450 enzymes occurs with retention of olefin stereochemistry (Watabe *et al.*, 1971; Watabe and Akamatsu, 1974; Ortiz de Montellano *et al.*, 1983). This observation does not necessarily rule out a nonconcerted mechanism, however, as intermediates could be involved in which rotation about the carbon-carbon bond is slow relative to closure of the epoxide ring. The finding that terminal olefins such as *trans*-[1-^{2}H]-1-octene are epoxidized with retention of stereochemistry (Ortiz de Montellano *et al.*, 1983; equation 2.1) indicates that slow carbon-carbon bond rotation cannot be due to steric interactions of substituents with residues in

52
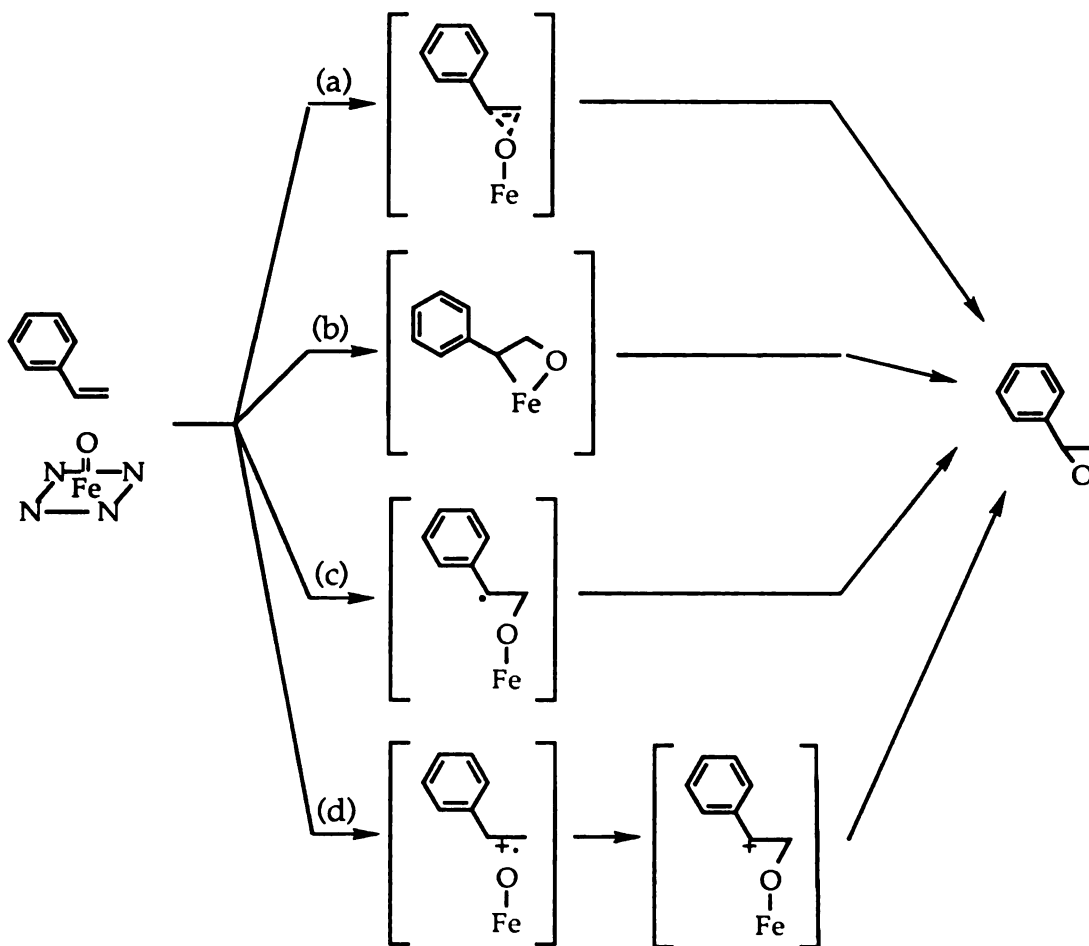
Figure 2.1: *Possible reaction pathways for olefin epoxidation include (a) concerted insertion of the oxygen into the π-bond, (b) intermediacy of a metallaoxetane species, (c) formation of a neutral radical intermediate and (d) initial electron-transfer to form the radical-cation followed by collapse to a cation intermediate. Styrene is shown as an example.*

the enzyme active site, and therefore must be due to the high reactivity of any intermediates involved.

$$(2.1)$$
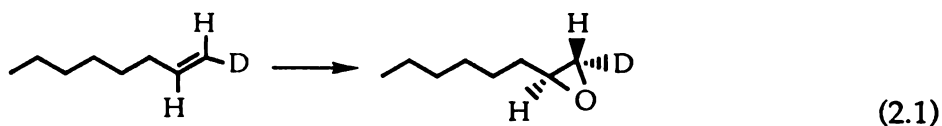
Evidence for a nonconcerted mechanism includes the observation of rearrangement products in the P450-catalyzed oxidation of halogenated and

unhalogenated olefins (Figure 2.1d). The formation of trichloroacetaldehyde from trichloroethylene (Miller and Guengerich, 1982; Henschler et al., 1979) and phenylacetaldehyde from styrene (Mansuy et al., 1984) were found not to be due to rearrangement of the epoxide under the experimental conditions, but rather to derive from the oxidation reaction itself. The finding that olefins substituted with deuterium at the terminal position give aldehydes with migration of deuterium (Liebler and Guengerich, 1983) suggests that these products are formed via a cationic intermediate which undergoes a 1,2-hydride shift analogous to the NIH shift observed for aromatic hydroxylations (Groves and Meyers, 1983; Figure 2.2).
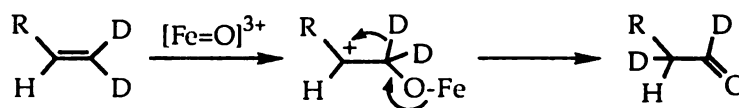
Figure 2.2: *Mechanism which accounts for the migration of deuterium during olefin oxidation. Formation of a cation intermediate leads to a 1,2-hydride shift.*

Heme alkylation by terminal olefins and acetylenes also argues for a nonconcerted mechanism in π-bond oxidation. Incubation of P450 enzymes with alkyl-substituted terminal olefins and acetylenes results in alkylation of the heme at one of the pyrrole nitrogens by what formally looks to be addition of the epoxide metabolite (Figure 2.3). However, incubations with the epoxide as well as stereochemical studies of the heme adducts indicate the epoxide is not the alkylating agent (Ortiz de Montellano et al., 1983). The finding that oxygen addition occurs at the internal carbon in heme alkylation by vinyl fluoride, vinyl bromide, and fluroxene suggests that a cationic intermediate is not involved, as such an intermediate would be expected to show oxygen addition at the terminal carbon due to stabilization
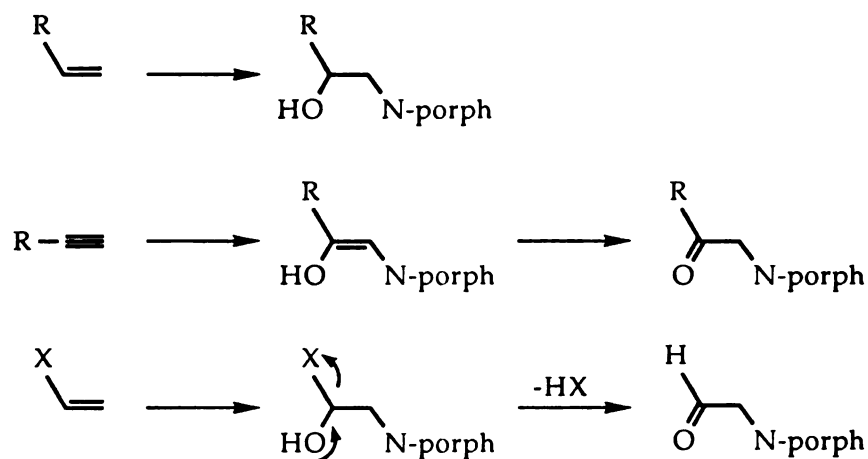
Figure 2.3: Schematic of terminal olefin and acetylene heme alkylation, where R = alkyl and X = F, Br, or OCH₂CF₃. In all cases the ferryl oxygen adds to the internal carbon and the porphyrin nitrogen adds to the terminal carbon (adapted from Ortiz de Montellano, 1985).

of the positive charge by the adjacent π-electron-donating substituent (Ortiz de Montellano *et al.*, 1982). Formation of a radical intermediate, which would show less of a preference for terminal oxygen addition, is therefore the more likely of the two.

The intermediacy of a metallaoxetane species (Figure 2.1b) is postulated to explain spectral intermediates detected during epoxidation reactions with heme model systems (Groves and Watanabe, 1986). Stereospecific hydrogen-deuterium exchange observed during propylene epoxidation by P4502B4 suggests a mechanism which involves formation of a metallaocycle to a carbene (where the H-D exchange occurs) and back to the metallaocycle again (Figure 2.4; Groves *et al.*, 1986). However, the epoxidation of bulky olefins which sterically can not form the metallaoxetane intermediate in heme model systems (Ostovic and Bruice, 1989; Traylor and Miksztal, 1989) suggests that metallaoxetane formation does not constitute a general epoxidation mechanism.
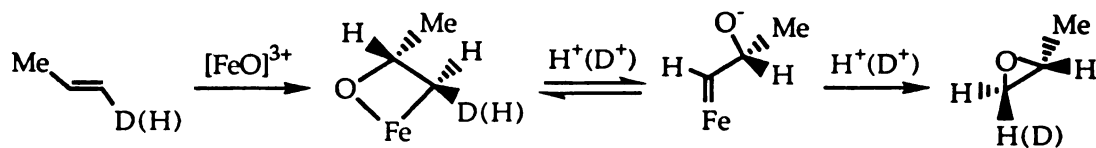
Figure 2.4: *Mechanism proposed to explain stereospecific hydrogen-deuterium exchange which occurs during P4502B4 epoxidation of propylene (from Groves et al., 1986).*

2.1.2 Evidence for Radical Intermediates in P450 Reactions

The intermediacy of radical species in the epoxidation reaction is attractive because it is consistent with the radical nature proposed for the activated iron-oxo species, and with mechanisms postulated for other P450 reactions.

Carbon hydroxylation, for example, has been proposed to proceed via a radical mechanism. Evidence for this includes stereochemical scrambling which occurs during the oxidation of *exo*-tetradeuterated norbornane by rabbit liver microsomes (Groves *et al.*, 1978; equation 2.3). This, together

$$(2.3)$$
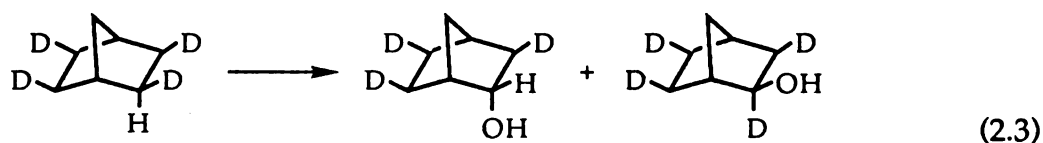
with the finding that P450$_{cam}$ removes either the 5-*endo* or 5-*exo* hydrogen from camphor, yet only forms the 5-*exo*-alcohol (Gelb *et al.*, 1982) suggests that norbornane compounds are hydroxylated via a planar radical intermediate (Figure 2.5).

Further evidence for a radical mechanism includes the allylic rearrangement of double bonds during hydroxylation of 3,4,5,6,-
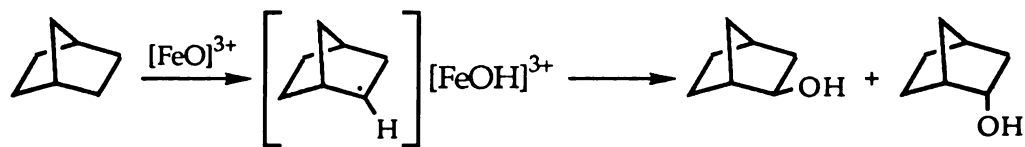
Figure 2.5: A radical mechanism involving a planar radical intermediate is proposed for carbon hydroxylation of norbornane.

tetrachlorocyclohexene (Tanaka *et al.*, 1979) and 3,3,6,6-tetradeuterated cyclohexene (Groves and Subramanian, 1984; equation 2.4). These results are consistent with the formation of an allylically delocalized radical intermediate.

$$\tag{2.4}$$
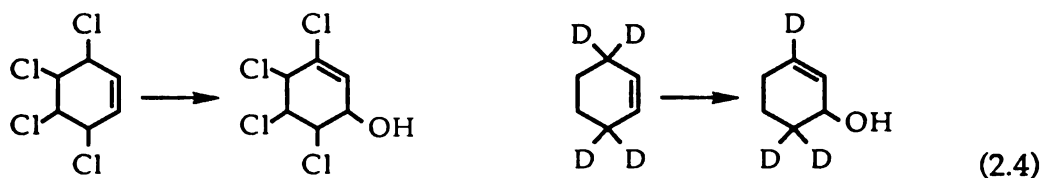
Radical intermediates are also suggested by the large kinetic isotope effects measured for the hydroxylation of compounds containing equivalent hydrogenated and deuterated carbon centers (k_H/k_D = 10-13; Ortiz de Montellano, 1986). The oxidation of quadricyclane to products of radical intermediates (Figure 2.6; Stearns and Ortiz de Montellano, 1985) provides further support for a radical mechanism in carbon oxidation.

Heteroatom oxidation, the third major class of P450 reactions, is also postulated to proceed via a radical mechanism. Alkyl-substituted nitrogen
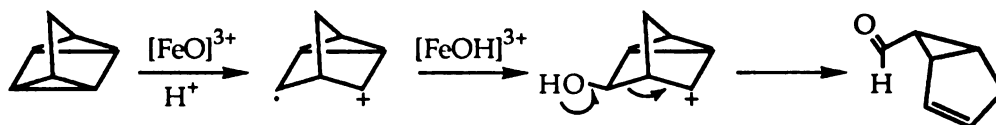
Figure 2.6: Mechanism proposed for P450 oxidation of quadricyclane involves generation of a radical-cation intermediate.

and sulfur atoms are oxidized to the corresponding N- and S-oxides and are dealkylated by P450 enzymes. Oxygen functionalities are also dealkylated; however, the much higher isotope effects measured for O-dealkylation (Miwa *et al.*, 1984) suggest that the mechanism is different for oxygen. The finding that the isotope effects measured for O-dealkylation are comparable to those for carbon hydroxylation suggests that O-dealkylation proceeds via α-carbon hydroxylation, followed by elimination of the alkyl group as the aldehyde (Ortiz de Montellano, 1986; Figure 2.7a).

The isotope effects measured for N- and S-dealkylations, on the other hand, are much lower (Abdel-Monem, 1975; Miwa *et al.*, 1980, 1983). Because these two atoms are more electropositive than oxygen and thus are more likely to undergo electron abstraction, N- and S-dealkylations are proposed to proceed by initial electron abstraction to form the radical-cation, followed by deprotonation to yield the α-hydroxy product. N- and S-oxide formation can also be visualized via a radical-cation intermediate (Figure 2.7b).

Support for one electron oxidation of nitrogen comes from the inactivation of P450s by dihydropyridines. These compounds are oxidized by

$$
\text{(a)} \quad R_2CH\text{-}\ddot{O}R \xrightarrow{[FeO]^{3+}} R_2C\text{-}\ddot{O}R \xrightarrow{[FeOH]^{3+}} R_2\overset{\overset{\displaystyle OH}{|}}{C}\text{-}\ddot{O}R \longrightarrow \text{O-dealkylation}
$$

$$
\text{(b)} \quad R_2CH\text{-}\ddot{N}R_2 \xrightarrow{[FeO]^{3+}} R_2CH\text{-}\overset{\displaystyle .+}{N}R_2 \xrightarrow{[FeO]^{2+}} R_2CH\text{-}\overset{\overset{\displaystyle O^-}{|+}}{N}R_2
$$

$$
\Big\downarrow {}^{\text{-}H^+}
$$

$$
R_2\overset{.}{\underset{..}{C}}\text{-}\ddot{N}R_2 \xrightarrow{[FeOH]^{3+}} R_2\overset{\overset{\displaystyle OH}{|}}{C}\text{-}\ddot{N}R_2 \longrightarrow \text{N-dealkylation}
$$

Figure 2.7: Mechanisms proposed for (a) O-dealkylation and (b) N-oxide formation and dealkylation by P450 enzymes. A similar scheme as in (b) can be drawn for sulfur oxidation and dealkylation (adapted from Ortiz de Montellano, 1986).

P450 enzymes to release the 4-alkyl substituent as a free radical, which then alkylates the heme at one of the pyrrole nitrogens (Augusto *et al.*, 1982). This reaction is best explained by one electron oxidation of the nitrogen, followed by aromatization of the ring and release of the 4-substituent as a radical (Figure 2.8). Direct one electron oxidation of cyclopropylamines to the radical cation is also consistent with the suicide inactivation of P450 enzymes by these compounds (Hanzlik and Tullman, 1982; Macdonald *et al.*, 1982).
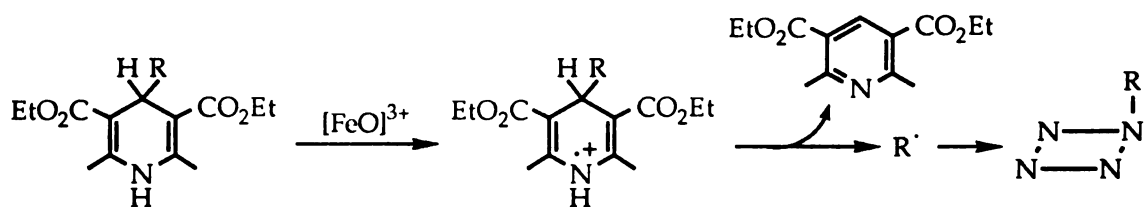
Figure 2.8: *Mechanism proposed for the oxidation of 4-alkyl-dihydropyridines to a radical species which alkylates one of the heme nitrogens.*

In sum, there is substantial evidence for radical pathways in P450 reactions. Although a radical mechanism is fairly well established for carbon and heteroatom oxidations, the evidence for radical intermediates in π-bond oxidation is still not conclusive. A neutral radical mechanism is proposed for heme alkylation, and such an intermediate could explain the formation of rearrangement products as well if the radical intermediate is oxidized to the cation via electron transfer to the iron. This route would most likely constitute a minor pathway in olefin oxidation, and thus is consistent with the observation of only small amounts of rearrangement products in P450 reactions. Hence the development of substrates which can probe for radical intermediates in P450 reactions is of great interest in elucidating the mechanism of olefin oxidation.

2.1.3 Use of Radical Clocks as Mechanistic Probes

The use of compounds containing cyclopropyl rings as probes of radical reactions stems from the very fast rearrangement of the strained ring system to the unstrained linear chain when a radical is generated at the carbon α to the cyclopropyl ring (equation 2.5). The rates of this

$$(2.5)$$
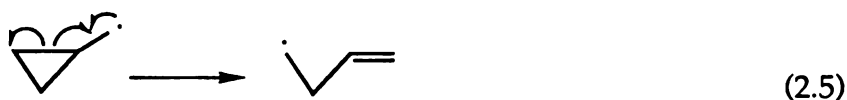
rearrangement for a number of substituted ring systems have been determined from competition experiments with reactions of known rate constants and are summarized in Table 2.1. Knowledge of the rearrangement rates can now be used to determine the rates of other reactions which are in competition with the radical ring-opening, and consequently provide evidence for the intermediacy of such radical species.

To probe the mechanism of P450 reactions, a relatively fast probe must be used. Several groups have determined the rate of the "oxygen rebound" step in P450 enzymes--that is, the rate at which the activated oxygen species recombines with the substrate radical to yield the hydroxylated product (second step in Figure 2.5)--using radical clock probes, and have found it to be on the order of 10^{10} s^{-1} (Ortiz de Montellano and Stearns, 1987; Bowry *et al.*, 1989; Bowry and Ingold, 1991). This suggests that any probe used must accordingly rearrange *at least* as fast as 10^{10} s^{-1}, but may need to be faster in order to trap radical intermediates as the rearranged products.

Castellino and Bruice have developed one of the fastest probes yet for olefinic radical reactions, with a rearrangement rate of $\geq 2 \times 10^{10}$ s^{-1}

60

Table 2.1: *The rates of ring-opening for a number of "radical clocks".*

Radical		Rate constant (s^{-1})
	$1° \rightarrow 1°$	1.6×10^8 [a]
	$2° \rightarrow 1°$	2×10^7 [b]
	$2° \rightarrow 2°$ benzylic	2×10^{10} [c]
	$1° \rightarrow 2°$ benzylic	1.8×10^{11} [d]
	$2° \rightarrow 2°$ benzylic	$\sim 1 \times 10^{10}$

[a] Carlsson and Ingold, 1968   [b] Beckwith and Moad, 1980
[c] Castellino and Bruice, 1988   [d] Newcomb and Manek, 1990

(Castellino and Bruice, 1988). This compound, (Z)-1,2-bis(*trans*-2,*trans*-3-diphenylcyclo-propyl)ethene (2.6), has been used to probe the mechanism of
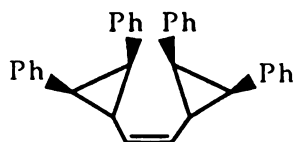
(2.6)

epoxidation by iron and manganese model porphyrin systems. Mass spectral analysis of the non-epoxide reaction products suggest the intermediacy of a radical-cation species, but not a neutral radical species for this reaction. Based on the relative yields of epoxide and non-epoxide products, a rate of

$>1 \times 10^{11}$ to 2×10^{11} s^{-1} was proposed for the collapse of the radical-cation to form the epoxide.

The use of fast radical probes to study the epoxidation reaction by P450 enzymes has so far gone unstudied. The applicability of the Bruice probe is limited, as it is likely to be too big to fit into an enzyme active site. The next fastest substrate, *trans*-1-phenylvinylcyclopropane (Table 2.1), is considerably smaller, but may still be fast enough to capture a radical species in the reaction.

2.2   Results

2.2.1   Identification of P450$_{cam}$ Metabolites

Syntheses of the substrate olefin, *trans*-1-phenyl-2-vinylcyclopropane (1), and standards for the potential metabolites of the P450$_{cam}$ incubation (2-6) were performed by Dr. Vaughn Miller of our laboratory. These standards were used to identify the metabolites of the enzyme incubation by comparison of mass spectrometric data and by GLC co-elution (Miller *et al.*, 1992).
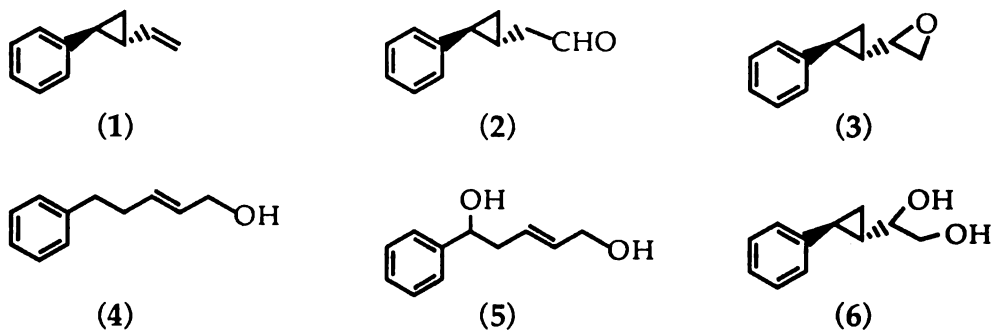
Incubation of the olefin (1) with the purified reconstituted P450$_{cam}$ system for two hours gives five peaks in the GLC chromatogram which are
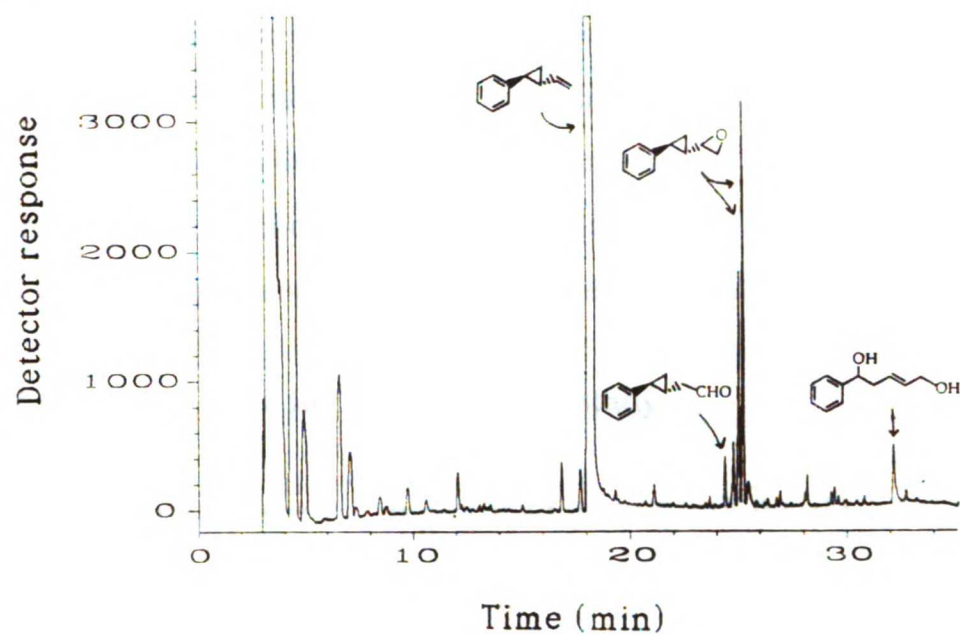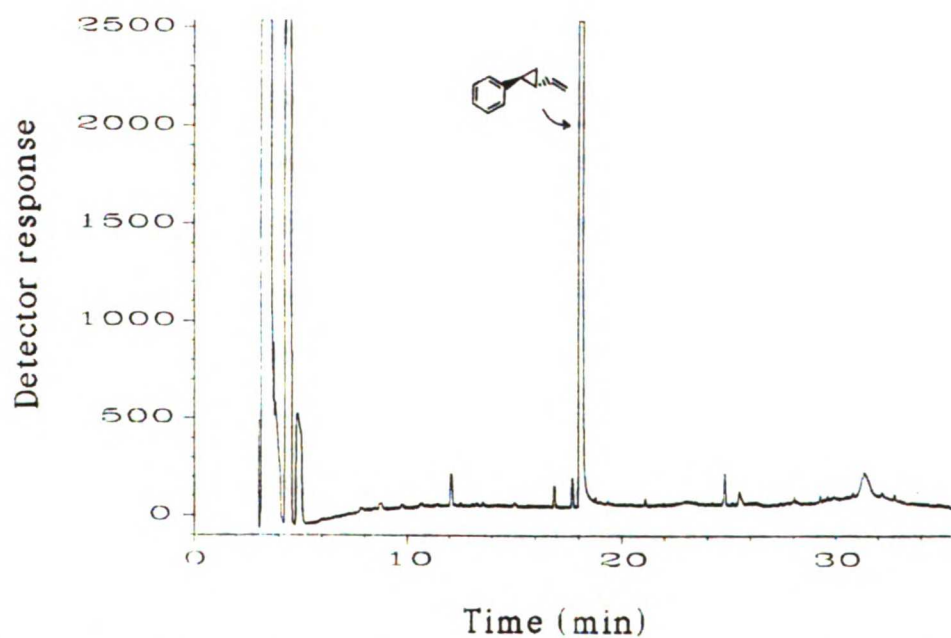
Figure 2.9: GLC chromatograms of the products formed in the incubation of trans-1-phenyl-2-vinylcyclopropane (1) with P450$_{cam}$ (a) in the presence of NADH, and (b) in the absence of NADH (control experiment).

63

not present in a control incubation containing everything except NADH (Figure 2.9). Co-injection with authentic standards, as well as comparison of the GLC/MS data for the standards and metabolites, indicate the peaks correspond to the aldehyde (2), the epoxide (3), and the ring-opened diol (5). The identity of a late-eluting peak at 36.9 minutes is unknown. No trace of the ring-opened alcohol (4) was found (detection limit <1%). Mass spectral data of the metabolites are listed in Table 6.2 of the Experimental Section.

2.2.2   Oxygen Origin in Diol: ^{18}O-Water study

The formation of the ring-opened diol (5) and the aldehyde (2) strongly suggest a nonconcerted mechanism for epoxidation. Important towards proving this is to determine the origin of the oxygens in the products, particularly the diol. The simplest way to do this is to use a different isotope of oxygen such as ^{18}O, as incorporation of this isotope is easily distinguished from the naturally-occurring ^{16}O by mass spectrometry. Because ^{18}O-labeled molecular oxygen was not commercially available at the time, the incubations were run in ^{18}O-labeled water only, and the results compared to those obtained from the normal incubation.

GLC/MS analysis of the metabolites from the H_2^{18}O incubation reveal no change in the molecular ions and fragmentation patterns for the aldehyde and epoxide metabolites, consistent with derivation of the oxygens in these compounds from molecular oxygen.

GLC/MS of the diol product, on the other hand, does show a shift in the mass spectrum. Because GLC/MS of the diol under electron impact (EI) conditions does not give a molecular ion--but does, however, show characteristic fragmentation peaks--this metabolite was analyzed both under

EI conditions and under chemical ionization (CI) conditions after derivatization with BSTFA. The latter method gives a distinct $(M+NH_4)^+$ peak for the diol containing two trimethylsilyl groups (Figure 2.10c).

The EI spectrum of the metabolite from the normal $H_2^{16}O$ incubation shows characteristic fragmentation peaks at 105 and 107 due to cleavage of the C_α-C_β bond adjacent to the phenyl ring (Figure 2.10a). This fragment contains the benzylic hydroxyl oxygen. In the EI spectrum of the metabolite from the $H_2^{18}O$ incubation, these fragment peaks are shifted by two mass units to 107 and 109, indicating the benzylic oxygen is labeled and thus derives from water (Figure 2.10b).

In the CI spectrum of the derivatized metabolite from the $H_2^{18}O$ incubation, the $(M+NH_4)^+$ peak shifts from 340 for the all ^{16}O compound to 342, indicating that the diol contains only one labeled oxygen (Figures 2.10d). Since the benzylic oxygen has previously been shown to be labeled, this indicates that the terminal hydroxyl oxygen is not labeled and thus does not derive from water. The terminal oxygen also does not derive from hydrogen peroxide, as a control experiment containing hydrogen peroxide in place of NADH produced no metabolites. Thus the most likely source of this oxygen atom is molecular oxygen via the heme ferryl oxygen species.

2.2.3   Control Incubations

Two control experiments were performed to determine the role of hydrogen peroxide in the reaction. These experiments are important because it has been shown that P450$_{cam}$ uncouples in the presence of substrates other than camphor. This generates a significant amount of hydrogen peroxide in the incubation mixture which could catalyze oxidation
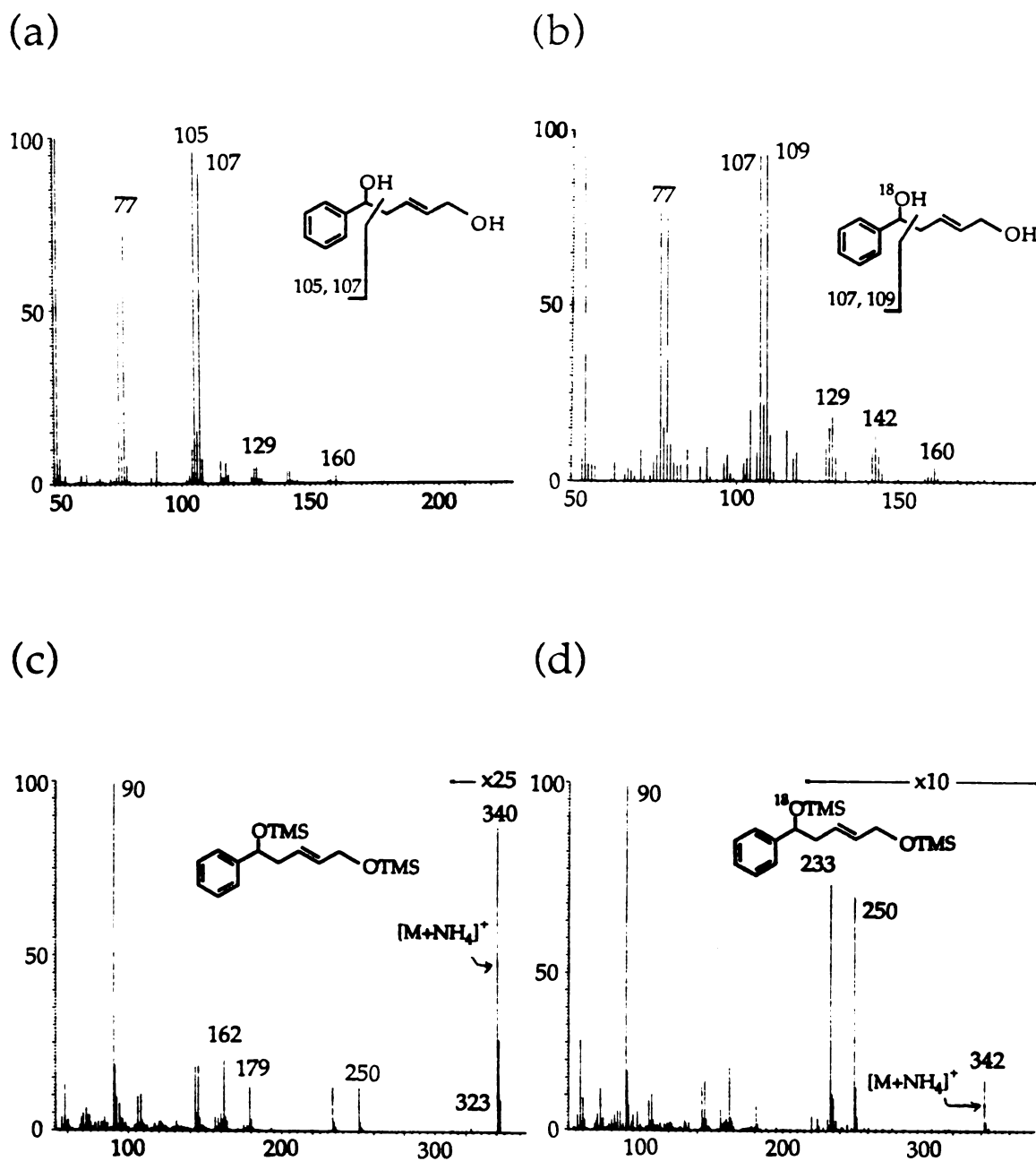
Figure 2.10: Mass spectra of the diol (5) metabolite obtained from incubation of trans-1-phenyl-2-vinylcyclopropane (1) with P450cam in either normal water or ^{18}O-labeled water. (a) EI mass spectrum of the diol from the normal $H_2{}^{16}O$ incubation. (b) EI mass spectrum of the diol from the $H_2{}^{18}O$ incubation. (c) CI mass spectrum of the derivatized diol from the normal $H_2{}^{16}O$ incubation. (d) CI mass spectrum of the derivatized diol from the $H_2{}^{18}O$ incubation.

reactions in addition to those initiated by P450$_{cam}$. Hence it is necessary to determine which, if any, of the metabolites derives from peroxide chemistry.

The first incubation was modified by the addition of catalase, an enzyme which highly efficiently converts hydrogen peroxide to molecular oxygen and water. GLC analysis of the products from this reaction were identical to those generated in the absence of catalase. A second incubation containing 0.5 mM hydrogen peroxide in place of the NADH gave no products, as mentioned previously. Together these results suggest that the observed metabolites of the reaction do not derive from hydrogen peroxide-mediated catalysis.

A second set of control incubations were run in which the olefin was replaced by the synthetic epoxide. These studies were aimed at determining whether any of the metabolites are actually secondary products of the epoxide. Incubation of the epoxide (50 μM) under the same conditions as the olefin did indeed give rise to all three of the other product peaks. Incubation in the presence or absence of NADH gave the same results, indicating that catalytically active enzyme is not necessary for the observed reactions. Incubation of the epoxide in buffer alone produced GLC peaks for the aldehyde (2) and the ring-opened diol (5), but not the late-eluting unidentified peak (rt = 36.9 minutes; see Figure 2.11), suggesting that this compound arises due to an epoxide reaction catalyzed by one of the proteins or with reagents present in their buffers, such as β-mercaptoethanol or glycerol. The epoxide reactions were found neither to be dependent on the buffer used, nor were they inhibited by pretreatment of the buffer with Chelex, thus ruling out metal or buffer catalysis.

To insure that the diol generated in the epoxide reactions was not simply the vic-diol (6) formed by hydrolysis of the epoxide, the product was
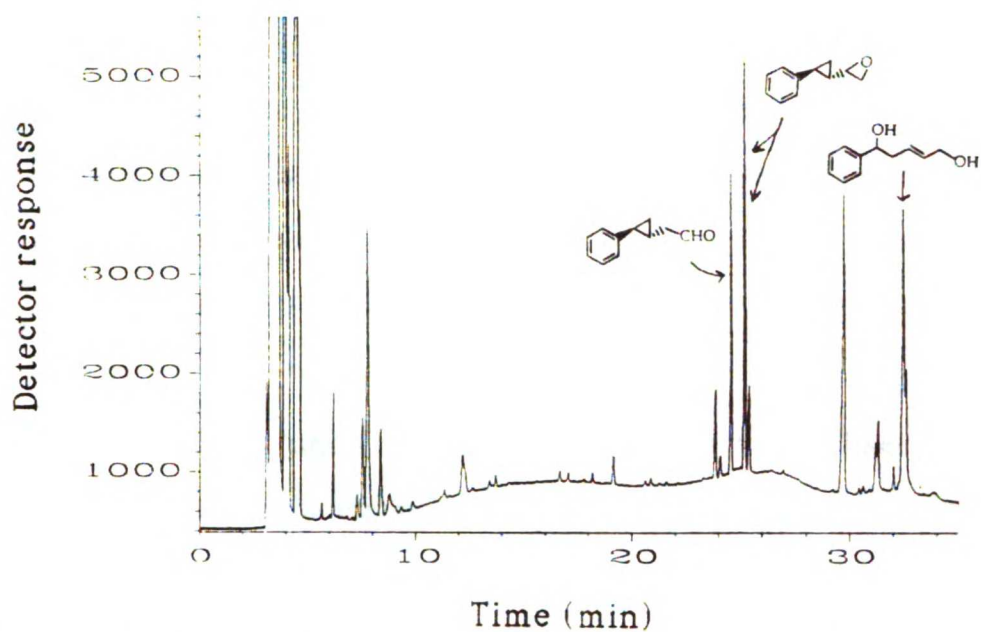
Figure 2.11: GLC chromatogram of the products formed from incubation of the epoxide (3) with buffer.
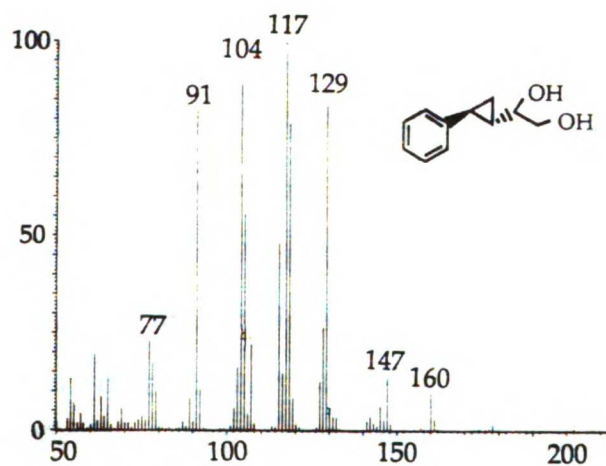
Figure 2.12: EI mass spectrum of the vic-diol (6).

68

analyzed by GLC/MS. This was found to be important as the two diols, the vic-diol and the ring-opened diol (4), virtually co-elute under the GLC conditions employed. GLC/MS analysis indicated, however, that only the ring-opened diol (4) is formed from the epoxide, as its mass spectrum is quite distinct from that of the vic-diol (Figure 2.12).

2.2.4 pH Study

Because the solution reaction of the epoxide is most likely an acid-catalyzed opening of the epoxide ring followed by either a 1,2-hydride shift to form the aldehyde (2), or a cation rearrangement to form the ring-opened diol (5), the effect of pH on the reaction was studied. The fact that this reaction occurs at all at pH 7.0 is surprising. However, raising the pH should diminish the solution reaction but may also diminish the enzyme reaction as well. Although P450$_{cam}$ appears to be stable at pH values as high as 9 (Yu et al., 1974), it is not known how stable putidaredoxin and its reductase are under such basic conditions.

Incubation of the epoxide in buffer at pH 8.0 still yields small amounts of the aldehyde and ring-opened diol, suggesting that even higher pH values are necessary to quench the reactivity of the epoxide. Incubation of the olefin with the P450$_{cam}$ system at this pH indicates some enzyme activity is lost, and thus trying a higher pH would not be productive. Attempts to trap the epoxide before it could react further using cyanide or cytosolic epoxide hydrolase kindly provided by Dr. William Chan, were not successful.

2.3   Discussion

The formation of the epoxide (3), aldehyde (2) and ring-opened diol (5) in the P450$_{cam}$ oxidation of trans-1-phenylvinylcyclopropane appears, at first

sight, to provide support for a nonconcerted epoxidation mechanism. Of the three possible nonconcerted pathways depicted in Figure 2.1, only the radical and radical-cation pathways are reasonable, as the metallaoxetane would not be expected to give ring-opened products.

The intermediacy of a neutral radical species such as that depicted in Figure 2.1c suggests opening of the cyclopropyl ring should occur in competition with closure of the epoxide ring (Figure 2.13). To generate the aldehyde (2) or the ring-opened diol (5) via this route, oxidation of the two radical intermediates to the corresponding cations would have to occur, thus enabling a 1,2-hydride shift to form the aldehyde and water addition to form the ring-opened diol (Figure 2.13). Water addition to the ring-closed cation does not occur, however, as no vic-diol (6) is detected for this reaction. Support for this mechanism comes from the ^{18}O-labeling studies, which indicate the benzylic oxygen derives from water and the terminal oxygen from molecular oxygen.

As discussed previously, oxidation of a neutral radical intermediate to the cation is likely to be only a minor pathway in olefin oxidation. Indeed this is upheld by the fact that the aldehyde (2) and the ring-opened diol (5) are formed in much lower yields than the epoxide (8 and 16%, respectively, based on uncorrected GLC integration).

However, the finding that no ring-opened alcohol (4) is formed within the detection limits of our assay suggests that a neutral radical intermediate is not involved. This product would be expected via hydrogen abstraction by the ring-opened radical (Figure 2.13). For a neutral radical intermediate to be formed but not undergo ring-opening, the collapse to the epoxide would have to occur at a rate of $\sim 10^{12}$ s^{-1} based on the limit of detection of our assay (<1%) and the rate of ring opening ($\sim 10^{10}$ s^{-1}). Given
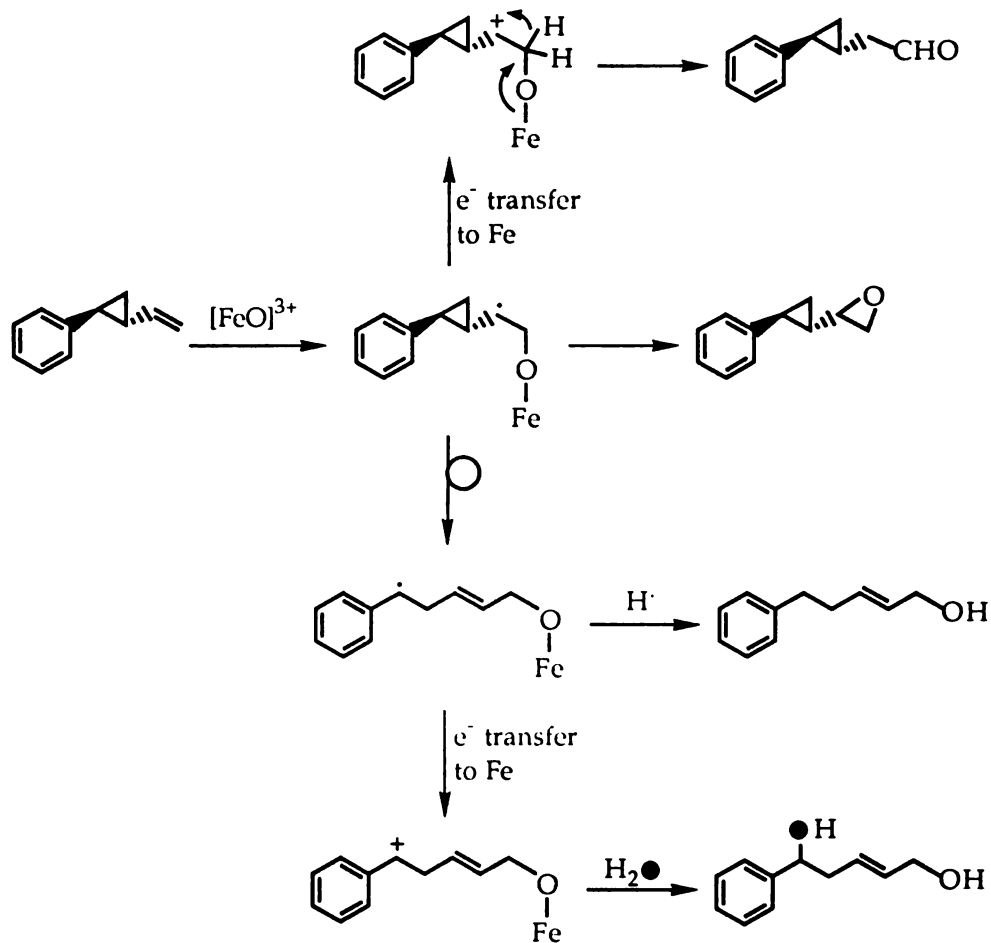
Figure 2.13: A neutral radical mechanism proposed for the oxidation of olefin (1) by $P450_{cam}$. The blackened oxygen denotes an ^{18}O-label.

that molecular vibrations occur on the order of 10^{13} s^{-1}, such an intermediate would only have a lifetime of ~10 molecular vibrations. Such a short lifetime suggests that the species would resemble a transition state rather than a discrete intermediate.

A radical-cation mechanism would also appear to explain the formation of the observed products. The aldehyde could arise from collapse of the ferryl oxygen with the terminal carbon to generate the cation, which then undergoes a 1,2-hydride shift to form the aldehyde (Figure 2.14). The

ring-opened alcohol could arise from radical ring-opening of the cyclopropyl group, which then collapses with the ferryl oxygen and adds water to generate the diol (Figure 2.14).
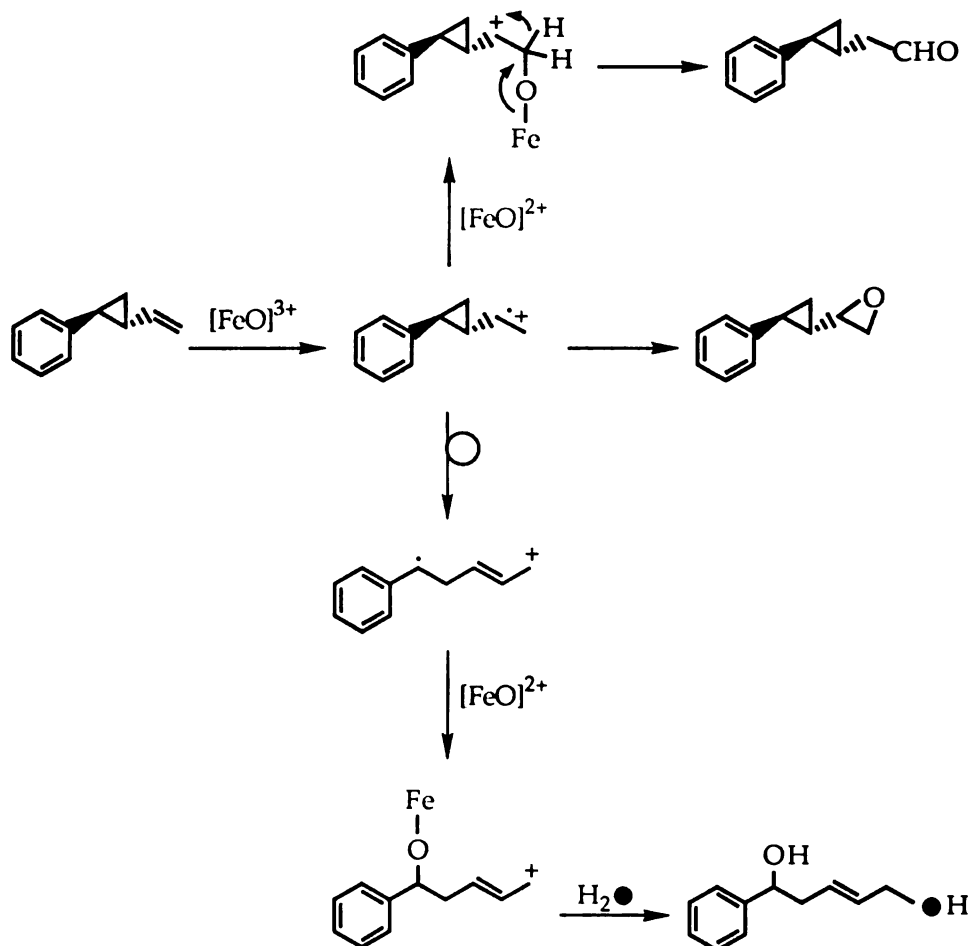
Figure 2.14: A radical-cation mechanism proposed for the oxidation of olefin (1) by P450$_{cam}$. The blackened oxygen denotes an ^{18}O-label.

However, this mechanism, which predicts that the benzylic hydroxyl oxygen comes from molecular oxygen and the terminal oxygen comes from water, is inconsistent with the ^{18}O-labeling studies which found the opposite to be true. A mechanism involving the radical-cation pathway which is in agreement with these studies would require the carbocation, not the radical,

to rearrange. This is highly unlikely, as cyclopropylcarbinyl cations are more stable than the corresponding radicals (Richey, 1972). Also the study by Castellino and Bruice with the radical clock probe (2.6) and model porphyrins found no evidence for cation rearrangement but only radical rearrangement via a postulated radical-cation intermediate (Castellino and Bruice, 1988).

Another possibility is that the radical-cation is so short-lived that no rearrangement occurs, and thus it is the cation that does the rearranging. This certainly explains the products and the lack of any ring-opened alcohol (4). However, it requires the epoxidation reaction to be much slower than previously predicted (Castellino and Bruice, 1988).

The discovery that the epoxide rearranges in solution to form the aldehyde (2) and the ring-opened diol (5) at neutral pH was disappointing and somewhat surprising. This reaction most likely proceeds via acid-catalyzed ring-opening of the epoxide, followed by either 1,2-hydride shift to the aldehyde (2), or ring-opening coupled with water addition at the benzylic carbon to form the ring-opened diol (5) (Figure 2.15). The results from the ^{18}O-labeling studies are consistent with this mechanism.
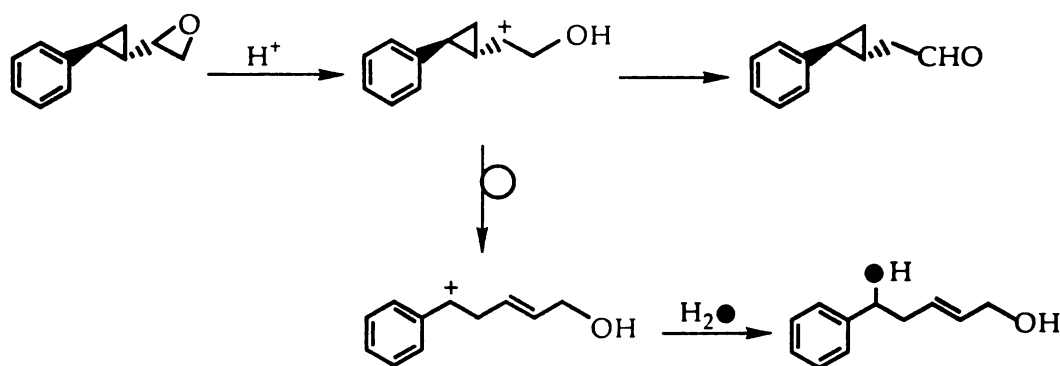
Figure 2.15: Acid-catalyzed ring-opening of the epoxide (3) in solution. The blackened oxygen denotes an ^{18}O-label.

73

The formation of (2) and (5) from the epoxide in solution obscures the detection of these compounds as products of the enzyme reaction. The interference from the solution reaction is difficult to overcome, as the solution reaction occurs to an appreciable extent, thus making it difficult to detect small amounts of enzyme-derived products. The finding that the ratio of (2) to (5) is approximately the same between the enzyme reaction and the epoxide reaction in buffer (~1:2) suggests that almost all of (2) and (5) formed in the enzyme incubation comes from ring-opening of the epoxide.

In conclusion, the finding that the aldehyde (2) and the ring-opened diol (5) derive from the epoxide (3) in the absence of enzyme suggests that observation of these products in the $P450_{cam}$ incubation with olefin (1) is due to the enzyme-independent reaction. However, enzymatic formation of trace amounts of (2) and (5) cannot be entirely ruled out. The complete absence of any ring-opened alcohol (4) argues against the intermediacy of a neutral radical species, as such a mechanism would require the rate of radical closure to the epoxide to be on the order of 10^{12} s^{-1}, close to the theoretical limit between an intermediate and a transition state. A radical-cation mechanism is also argued against based on the $H_2^{18}O$ data.

It should be noted that failure to detect any ring-opened alcohol (4) does not necessarily rule out the possibility of radical intermediates, as work done by Bowry and Ingold on the P450 hydroxylation of radical clock probes found that bulky substrates tend to ring open slower when bound in the enzyme active site than when free in solution (Bowry and Ingold, 1991). Since the rate of ring-opening for small substrates was unaffected by the presence of the enzyme active site, they postulate that steric constraints imposed by the active site effectively slow down the rate of ring opening of bulky substrates.

The likelihood that olefin (1) is sterically constrained in the relatively small $P450_{cam}$ active site is not unreasonable based on Bowry and Ingold's results, and suggests that its ring-opening rate may be comparably slowed when bound. This would lower the rate of epoxide ring closure to $\sim 10^{11}$ s^{-1}, a rate which does not rule out the possibility of a radical intermediate in the P450 epoxidation reaction.

Although *trans*-2-phenyl-1-vinylcyclopropane (1) has been successfully used as a probe of reactions in organic solvents (Fu *et al.*, 1991), the instability of its epoxide (3) in aqueous media indicates that the applicability of this probe for enzymatic reactions is limited. The formation of proton-mediated ring-opened products in solution severely hampers the detection of these compounds as enzyme metabolites, thus making mechanistic evaluations difficult. The fact that the results here provide no concrete evidence for radical intermediates thus must be considered in this light.

3.0 OXIDATION OF STYRENES BY CYTOCHROME P450_cam AND ACTIVE SITE MUTANTS

3.1 Introduction

$P450_{cam}$ has been shown to stereo- and regiospecifically hydroxylate camphor to yield 5-*exo*-hydroxycamphor as the sole product. The protein residues which help determine this high selectivity include Tyr 96, which hydrogen bonds with the camphor carbonyl oxygen, and Leu 244, Val 295 and Val 247, which provide hydrophobic contacts and appropriate steric interactions with the substrate (Poulos *et al.*, 1987). The roles of these residues in specific substrate-protein interactions have been probed using substrate analogs of camphor and by site-directed mutagenesis (Atkins and Sligar, 1988; 1989). These studies have provided a detailed picture of the substrate-protein interactions involved in stereoselective camphor hydroxylation.

Examples of compounds unlike camphor in structure which have been used to probe binding interactions in $P450_{cam}$ are few, however. The x-ray crystallographic studies of the binding of the P450 inhibitor metyrapone, 1-, 2- and 4-phenylimidazoles, and the formation of an iron-phenyl complex from phenyldiazene are some of the only examples (Poulos and Howard, 1987; Raag *et al.*, 1990). The crystal structures of the metyrapone- and the phenylimidazole-bound complexes reveal that these inhibitors bind in the camphor binding pocket while providing a nitrogen ligand to the heme iron. One of the inhibitors that for steric reasons cannot make an iron-nitrogen bond binds higher up in the active site such that one of the nitrogens hydrogen bonds with Tyr 96 (Poulos and Howard, 1987). The iron-phenyl complex generated from the reaction of phenyldiazene with $P450_{cam}$ shows a

phenyl ring sigma-bonded to the heme iron. The phenyl ring is tilted away from the I helix for steric reasons, and the rest of the active site contains two water molecules (Raag *et al.*, 1990).

These studies suggest that although $P450_{cam}$ is tailored to hydroxylate camphor, it may be able to accommodate alternate substrates. The finding that the protein undergoes only small changes upon binding of these inhibitors suggests that the available crystal structures of $P450_{cam}$ can be used to adequately model the binding of new substrates or inhibitors. The ability of theoretical calculations to faithfully depict protein-substrate interactions using these crystal structures is demonstrated by the accuracy of the predictions of norcamphor, 5,5-difluorocamphor and pericyclocamphanone hydroxylation regioselectivity using these methods (Collins and Loew, 1988; Bass *et al.*, 1992).

The finding that mutation of $P450_{cam}$ active site residues significantly affects the hydroxylation regioselectivity of norcamphor but has little effect on camphor hydroxylation (Atkins and Sligar, 1989) suggests that small substrates may be more sensitive probes of changes in the active site architecture than larger, more tightly bound substrates. What determines binding preferences for substrates able to move about the active site has relevance towards understanding reaction regio- and stereoselectivities displayed by the drug-metabolizing P450s, whose active sites are often considered to be loose and floppy because of their ability to oxidize multiple substrates. Hence an understanding of the factors that determine substrate binding in an enzyme whose active site is well defined is highly desirable towards understanding such features in other, as yet unknown P450 binding pockets.

Towards this end, the oxidation stereochemistry of styrene and several of its analogs was studied with $P450_{cam}$. This compound is of general interest due to its widespread use in the manufacture of plastics, and the mutagenic and carcinogenic properties of its biological metabolite, styrene oxide, produced by P450-catalyzed oxidation in the liver (de Meester *et al.*, 1977; Huff, 1984; Ponomarkov *et al.*, 1984; Leibman and Ortiz, 1969). Styrene is of interest for our studies because it is small and structurally distinct from camphor, and thus should interact with the protein much differently than does camphor. The stereochemistry of the epoxidation reaction provides a sensitive probe into substrate binding orientations, and the ability to add substituents onto the hydrophobic core allows for the selective introduction of hydrogen-bonding, polar and steric interactions. The effects of modifying the substrate structure or the protein structure by site-directed mutagenesis can be assessed from the changes in epoxidation stereochemistry, and evaluated based on knowledge of the crystal structure and the results of molecular dynamic simulations.

3.2 Results

3.2.1 Identification of Metabolites

Incubation of styrene with the purified reconstituted $P450_{cam}$ monooxygenase system gives rise to four peaks in the GLC chromatogram which are dependent on the presence of the cofactor NADH. These peaks were identified by co-elution with authentic standards and by GLC/MS as styrene oxide, benzaldehyde, phenylacetaldehyde and a ring-hydroxylated isomer of styrene (see Figure 3.1). The latter metabolite was identified by GLC/MS alone, and thus the position of the hydroxyl group on the ring has

78
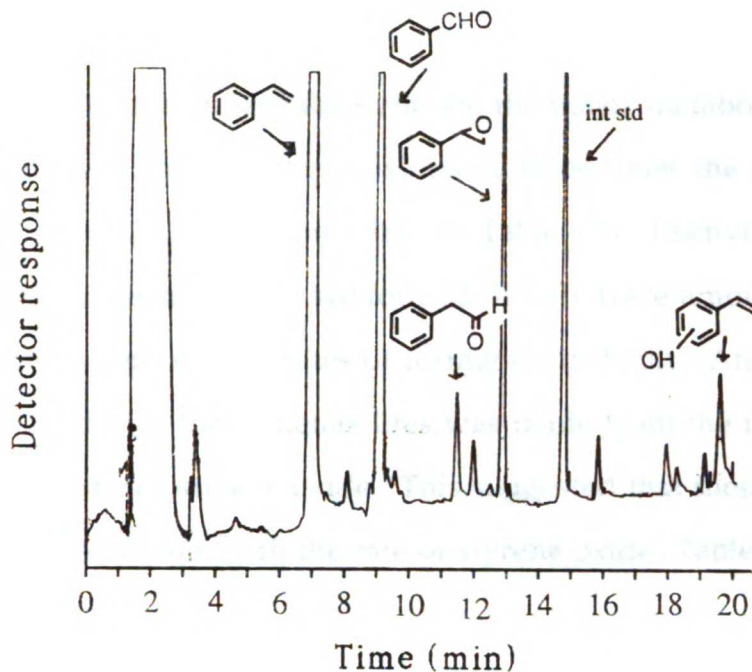
Figure 3.1: GLC chromatogram of the metabolites formed in the reaction of P450$_{cam}$ with styrene.
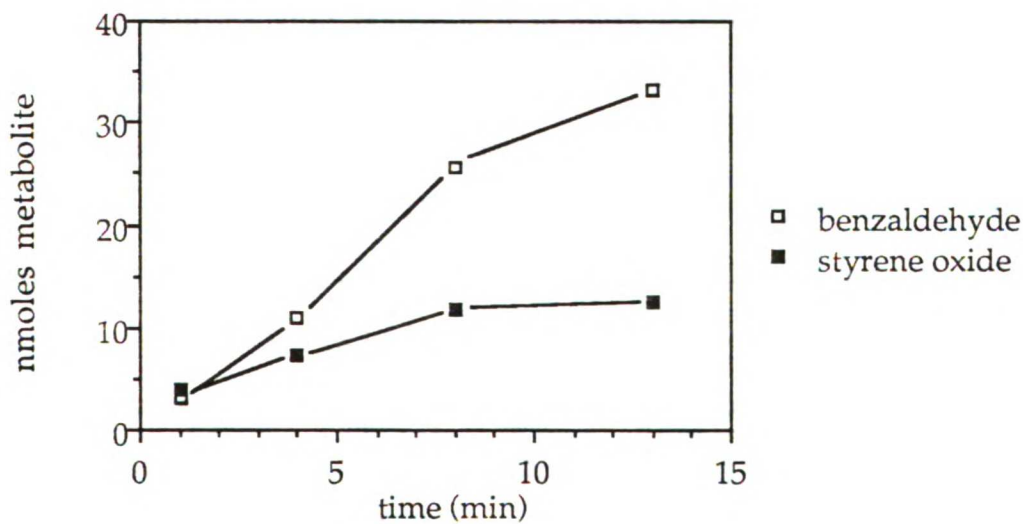
Figure 3.2: Plot of the amount of styrene oxide and benzaldehyde formed versus time in the incubation of P450$_{cam}$ with styrene. The amounts of product formed are normalized to 1 nmole P450$_{cam}$.

not been determined (mass spectrometric data is listed in Table 6.2 of the Experimental Section).

Styrene oxide and benzaldehyde are the major metabolites of styrene, with benzaldehyde formed at approximately three times the rate of styrene oxide (see Figure 3.2; rates summarized in Table 3.1). Phenylacetaldehyde and ring-hydroxylated styrene are formed in only trace amounts, thus making quantitation of their rates of formation difficult. An estimate of the rates of formation for these metabolites was made from the ratio of their GLC peaks to that for styrene oxide. This suggested that these compounds are formed at about one tenth the rate of styrene oxide (Table 3.1).

Incubation of cis-β-methylstyrene with the reconstituted P450$_{cam}$ system results in the NADH-dependent formation of five metabolites (see Figure 3.3). They were identified by GLC co-elution with authentic standards and by GLC/MS as cis-β-methylstyrene oxide, benzaldehyde, cis-3-phenyl-2-propen-1-ol, 1-phenyl-2-propanone and a ring-hydroxylated isomer of cis-β-methylstyrene. The epoxide, benzaldehyde and cis-3-phenyl-2-propen-1-ol constitute the major metabolites, with the epoxide formed just faster than benzaldehyde and about five times as fast as the β-alcohol (see Figure 3.4; rates summarized in Table 3.1). The rearranged aldehyde 1-phenyl-2-propanone and the ring-hydroxylated olefin are formed in only trace amounts at rates estimated to be less than one tenth that for the epoxide.

Incubation of $trans$-β-methylstyrene with the reconstituted P450$_{cam}$ system also results in the NADH-dependent formation of five metabolites, but in much smaller amounts than for either the cis-olefin or for styrene (Figure 3.5). The identities of the metabolites were determined by GLC co-elution with authentic standards and by GLC/MS and found to directly parallel the cis-olefin products. The major metabolites are $trans$-β-
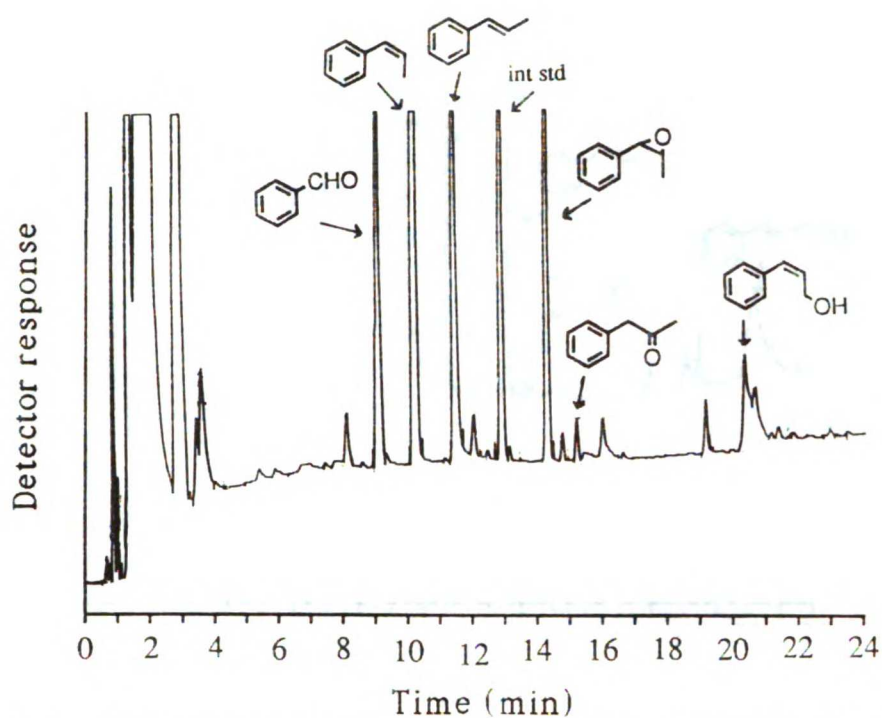
Figure 3.3: GLC chromatogram of the metabolites formed in the reaction of P450$_{cam}$ with cis-β-methylstyrene.
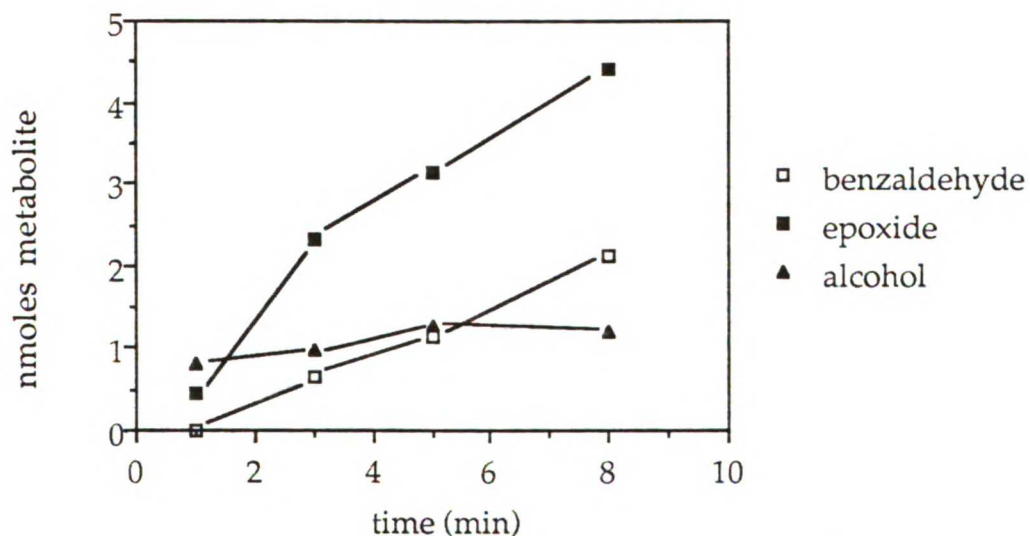
Figure 3.4: Plot of the amount of cis-β-methylstyrene oxide, benzaldehyde and cis-3-phenyl-2-propen-1-ol formed versus time in the incubation of P450$_{cam}$ with cis-β-methylstyrene. The amounts of product formed are normalized to 1 nmole P450$_{cam}$.

Figure 3.5: *GLC chromatogram of the metabolites formed in the reaction of P450_cam with* trans-β-methylstyrene.
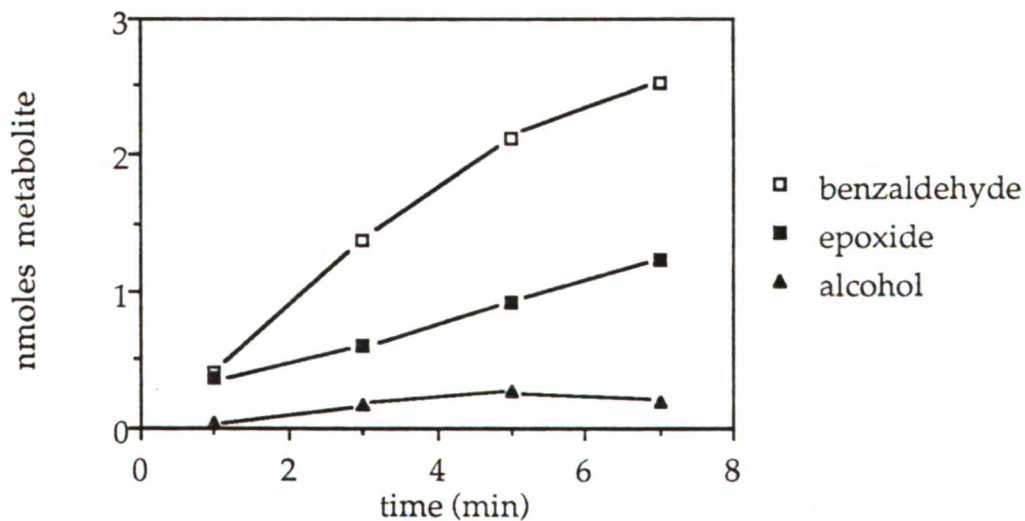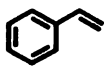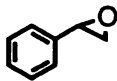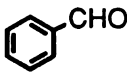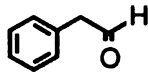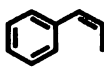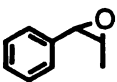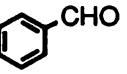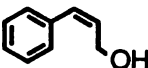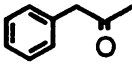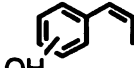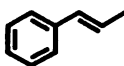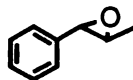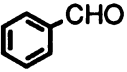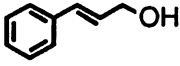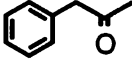
Figure 3.6: *Plot of the amount of* trans-β-methylstyrene *oxide, benzaldehyde and* trans-3-phenyl-2-propen-1-ol *formed versus time in the incubation of P450_cam with* trans-β-methylstyrene. *The amounts of product formed are normalized to 1 nmole P450_cam.*

82

Table 3.1: Summary of the turnover rates for the products formed in the oxidation of styrene, cis-β-methylstyrene and trans-β-methylstyrene by P450$_{cam}$.

Substrate	Products (turnover rate in nmole/nmole P450/min)				
	1.1 ($\pm$ 0.1)	3.2 ($\pm$ 0.3)		~0.09	~0.09
	0.54 ($\pm$ 0.08)	0.31 ($\pm$ 0.03)	0.12 ($\pm$ 0.02)	~0.03	~0.03
	0.15 ($\pm$ 0.03)	0.47 ($\pm$ 0.04)	0.06 ($\pm$ 0.02)	~0.001	~0.01

methylstyrene oxide and benzaldehyde, formed in a ratio of ~1:3, respectively (Figure 3.6). The β-alcohol trans-3-phenyl-2-propen-1-ol is formed at about half the rate of the epoxide, and the rearranged aldehyde 1-phenyl-2-propanone and a ring-hydroxylated product are formed in trace amounts estimated to be 1-10% of the epoxide rate (Table 3.1).

Although all the metabolites detected for styrene and cis- and trans-β-methylstyrene were determined to depend on the presence of catalytically active enzyme, addition of catalase to the incubation mixture was found to inhibit formation of benzaldehyde without detectably altering the formation of the other products. This suggests that some, if not all, of the benzaldehyde formation is supported by hydrogen peroxide generated in situ. This inference is supported by the finding that benzaldehyde, but none of the other products, is obtained if NADH is replaced in the incubation by an

amount of hydrogen peroxide equivalent to that normally produced in the incubation (~1 mM).

Incubation of p-methylstyrene and p-chlorostyrene with the reconstituted P450$_{cam}$ system results in the NADH-dependent formation of the corresponding epoxides and benzaldehydes (Figures 3.7 and 3.8). The epoxides were identified by co-elution with authentic standards on GLC and/or by GLC/MS. The benzaldehydes, formed in a hydrogen peroxide-mediated reaction, were identified by GLC/MS. Analysis of the p-chlorostyrene incubation mixture by normal phase HPLC also revealed small amounts of a ring-hydroxylated product as deduced from the mass spectrum of the collected sample.

Incubations of styrene and p-chlorostyrene with the P450$_{cam}$ active site mutants F87A, F87W and Y96F results in the NADH-dependent formation of the corresponding epoxides and benzaldehydes. The metabolism of p-methylstyrene was studied with the F87A mutant, which gives rise to the epoxide, the benzaldehyde, and a small amount of p-methylphenyl-acetaldehyde.

3.2.2 Epoxidation Stereochemistry

The stereochemistry of epoxidation of styrene, *cis*- and *trans*-β-methylstyrene and p-chlorostyrene by P450$_{cam}$ and the three mutants was determined by chiral GLC. Which enantiomer eluted first for styrene and *trans*-β-methylstyrene oxides was determined by analysis of individual enantiomers purchased from Aldrich Chemical Company. For *cis*-β-methylstyrene the elution pattern was determined from an unequal mixture of the two enantiomers given to us by Dr. Thomas Kodadek. The mixture

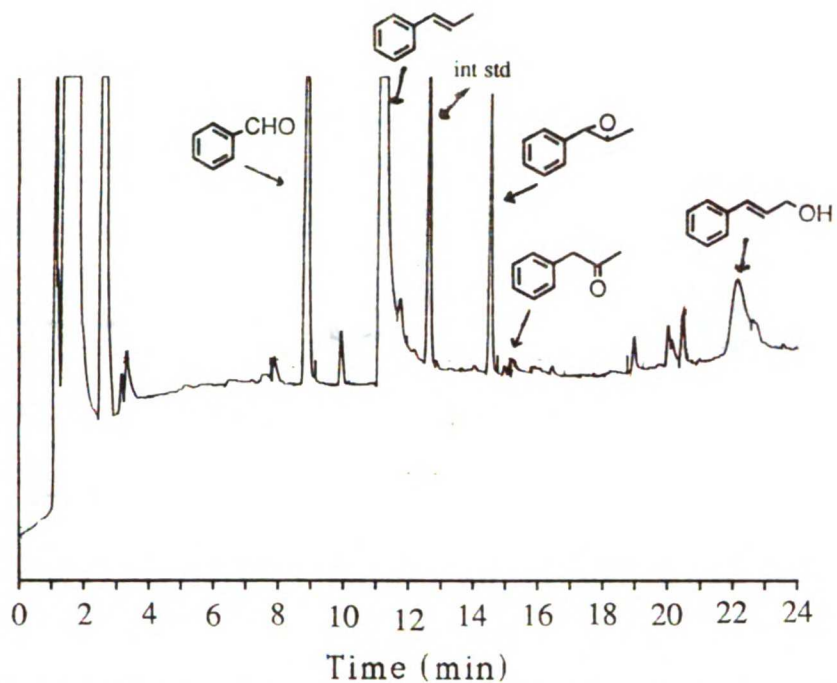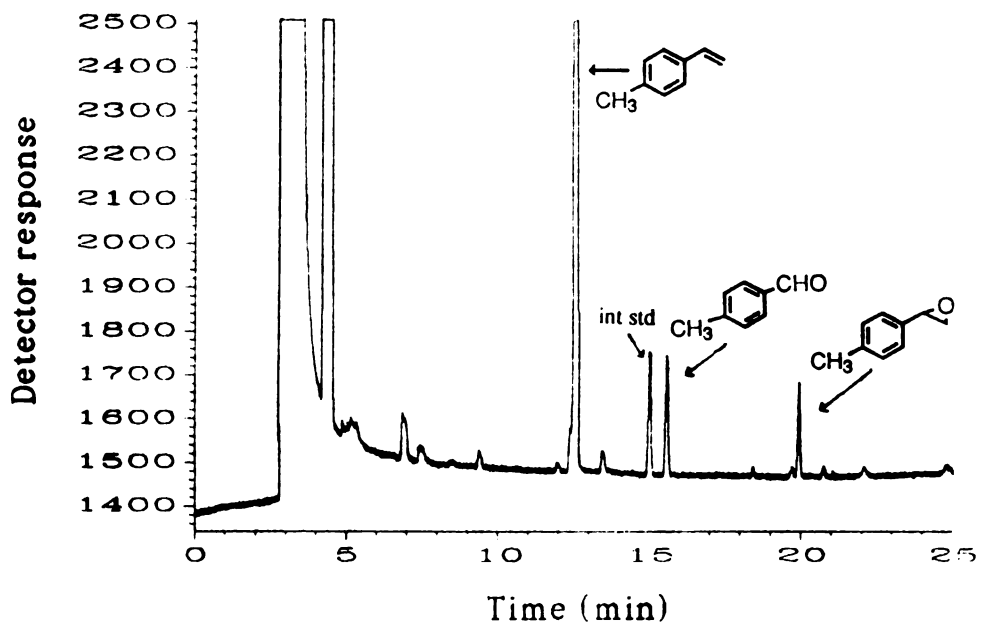**Figure 3.7:** GLC chromatogram of the metabolites formed in the reaction of P450_cam with p-methylstyrene.
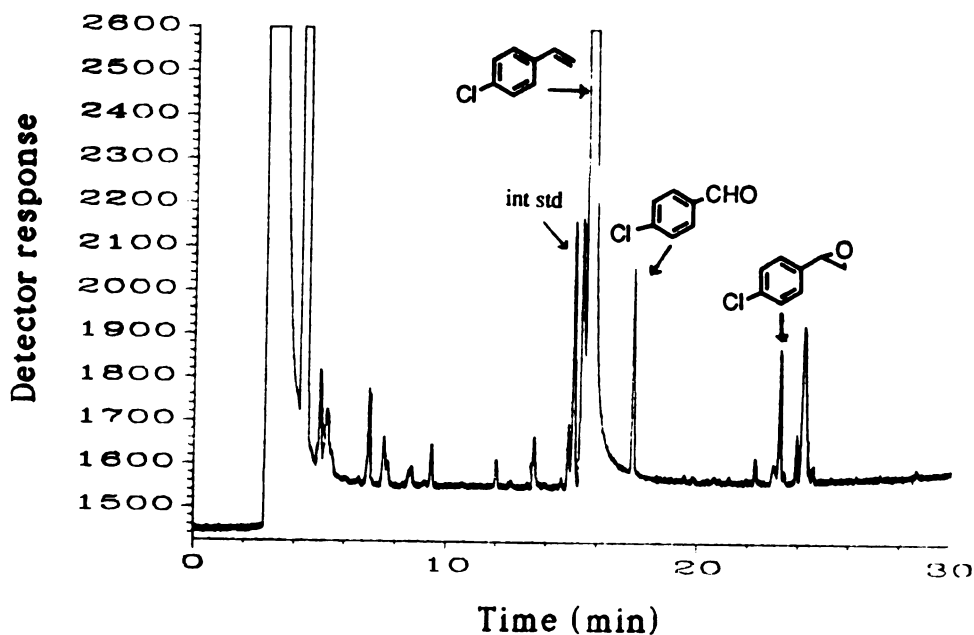
Figure 3.8: GLC chromatogram of the metabolites formed in the reaction of P450_cam with p-chlorostyrene. The peak at 24 minutes is present in the -NADH control.

had been shown by ^{1}H NMR to contain a 70:30 ratio of the 1*S*,2*R*: 1*R*,2*S*

enantiomers, respectively (O'Malley and Kodadek, 1989). In all three cases,

the 1*S* epoxide eluted first. Based on this trend, it was assumed that the 1*S*

epoxide of *p*-chlorostyrene oxide also eluted first.
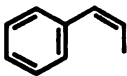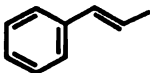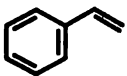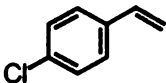
The epoxidation stereochemistry of *p*-methylstyrene could not be

determined due to the instability of this epoxide towards the chiral phase of

the GLC column. The epoxide was found to undergo ring opening while

passing through the column to yield a peak for the corresponding aldehyde.

The broad, tailing aldehyde peak tended to obscure the epoxide peaks, as well

as give unequal peaks for the two epoxide enantiomers even with racemic

epoxide. *p*-Methoxystyrene oxide was found to give only one peak using this

column under a variety of conditions, and it is likely that this peak

corresponds to the ring-opened aldehyde. The chiral phase of the column,

consisting of trifluoroacetyl γ-cyclodextrins, may contain residual

trifluoroacetic acid that is reacting with the epoxides. In any case, our assays

were limited to the epoxides of styrene, *cis-* and *trans*-β-methylstyrene and *p*-

chlorostyrene.

The results, summarized in Table 3.2, indicate that for all four

substrates and for all four proteins, formation of the 1*S*-epoxide enantiomer

is favored over the 1*R*-enantiomer. Some trends are observed in the data,

but overall the changes in stereochemistry are fairly subtle.

3.2.3   Uncoupling Measurements

The observation that benzaldehyde results from the oxidation of the

styrenes by endogenously generated hydrogen peroxide suggests that the

turnover of these substrates is associated with substantial uncoupling of the

Table 3.2: *Summary of the stereochemistry of epoxidation of a number of olefins by P450$_{cam}$ and the mutants F87A, F87W, and Y96F.*

Substrate	P450$_{cam}$	Epoxide stereochemistry (1S : 1R)[a]		
		F87A	F87W	Y96F
(styrene)	89 : 11	ND[b]	ND	82 : 18
(β-methylstyrene)	75 : 25	ND	ND	ND
(α-methylstyrene)	83 : 17	83 : 17	79 : 21	84 : 16
(4-chloro-α-methylstyrene)	74 : 26	66 : 34	71 : 29	70 : 30

[a] 1S and 1R refer to the stereochemistry at the α-carbon. For cis-β-methylstyrene, the ratio is (1S, 2R) : (1R, 2S), and for trans-β-methylstyrene, the ratio is (1S, 2S) : (1R, 2R). All values are ± 1 except for P450$_{cam}$ + cis-β-methylstyrene (± 2) and trans-β-methylstyrene (± 3). [b] Not determined.

epoxidation reaction from the consumption of NADH. In order to evaluate the degree of uncoupling occurring in these reactions, the consumptions of NADH and oxygen were determined and compared against hydrogen peroxide and product formation for the P450$_{cam}$ oxidation of styrene, cis- and trans-β-methylstyrene and camphor. Camphor turnover, which is known to be highly coupled (Atkins and Sligar, 1987a), was included in these studies for comparison.

NADH consumption was measured spectroscopically and found to be linear over the time period monitored (Figure 3.9). Oxygen consumption was measured using an oxygen electrode and found to be linear over only the first 2.5 minutes (Figure 3.10). The leveling off which occurred after that point is most likely due to the low oxygen concentration in the cell at that
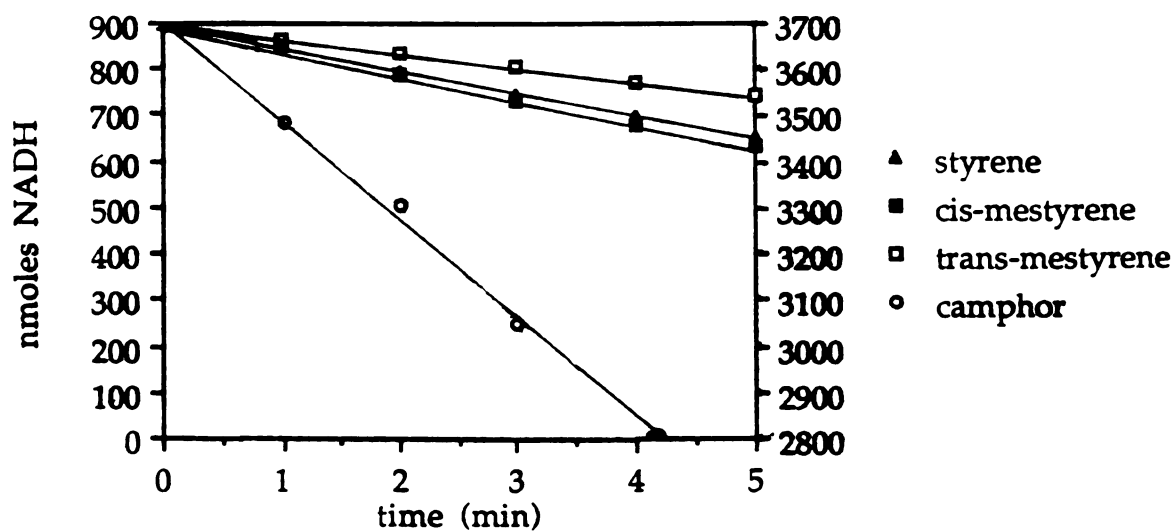
Figure 3.9: Plots of the amount of NADH present versus time during the incubation of P450$_{cam}$ with styrene, cis- and trans-β-methylstyrene (scale on left-hand axis) and camphor (scale on right-hand axis). The amount of NADH consumed is normalized to 1 nmole P450$_{cam}$.
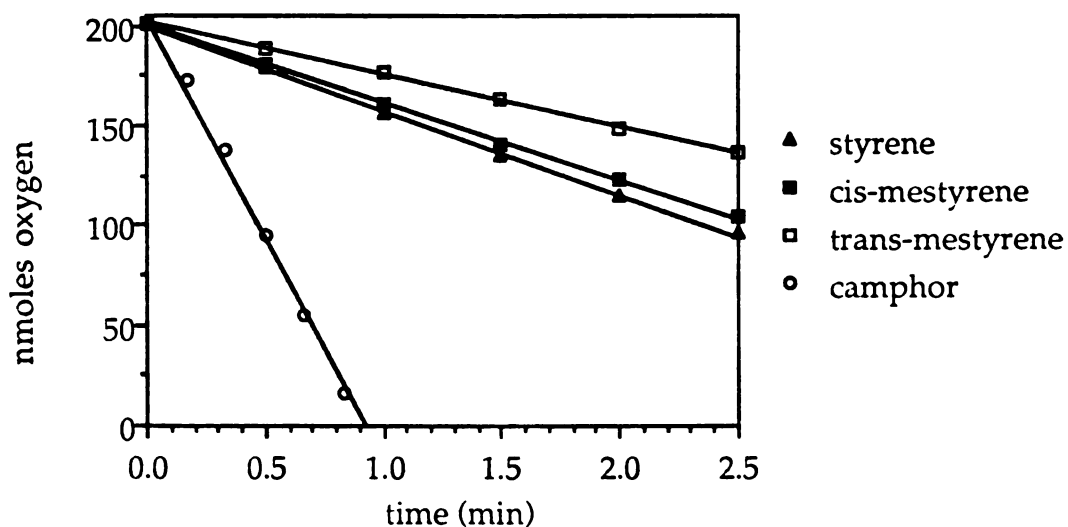
Figure 3.10: Plots of the amount of O$_2$ present versus time during the incubation of P450$_{cam}$ with styrene, cis- and trans-β-methylstyrene and camphor. The amount of O$_2$ consumed is normalized to 1 nmole P450$_{cam}$.

point, which either slowed down the enzymatic reaction and/or favored leakage of oxygen back into the cell. Hydrogen peroxide formation was monitored using a chemical assay and was linear over the time measured (Figure 3.11). Product formation for the olefins was as described previously (Figures 3.2, 3.4 and 3.6). The rate of camphor oxidation to 5-*exo*-hydroxycamphor was determined by GLC (Figure 3.12). In the case of camphor, more so than for the olefins, it was found to be crucial to include protein when making up the standard curve for the metabolites, as the extraction of 5-*exo*-hydroxycamphor is highly sensitive to the presence of proteins in the extraction mixture.

The slightly lower values of oxygen consumption for the olefins as compared to NADH consumption could be due to the reduction of the iron-oxo species to form water, an alternative uncoupling mechanism, but more likely reflects the differences in experimental set-up between the two measurements. Oxygen consumption is measured in an electrode cell with a stir bar, while NADH measurements (as well as hydrogen peroxide and metabolite measurements) are run in a shaking water bath. The fact that varying the spin rate of the stir bar in the oxygen electrode cell affects the oxygen consumption rate makes getting the parameters to be exactly equivalent between the two systems nearly impossible.

The results of these measurements, summarized in Table 3.3, suggest that P450$_{cam}$ oxidation of styrene and *cis*- and *trans*-β-methylstyrenes is accompanied by substantial uncoupling of the enzyme to generate hydrogen peroxide. The fact that the rate of hydrogen peroxide formation is roughly equivalent to the rates of NADH and oxygen consumption suggests that these substrates serve to predominantly uncouple the enzyme to form hydrogen peroxide, forming oxidized product only 0.5-2% of the time.
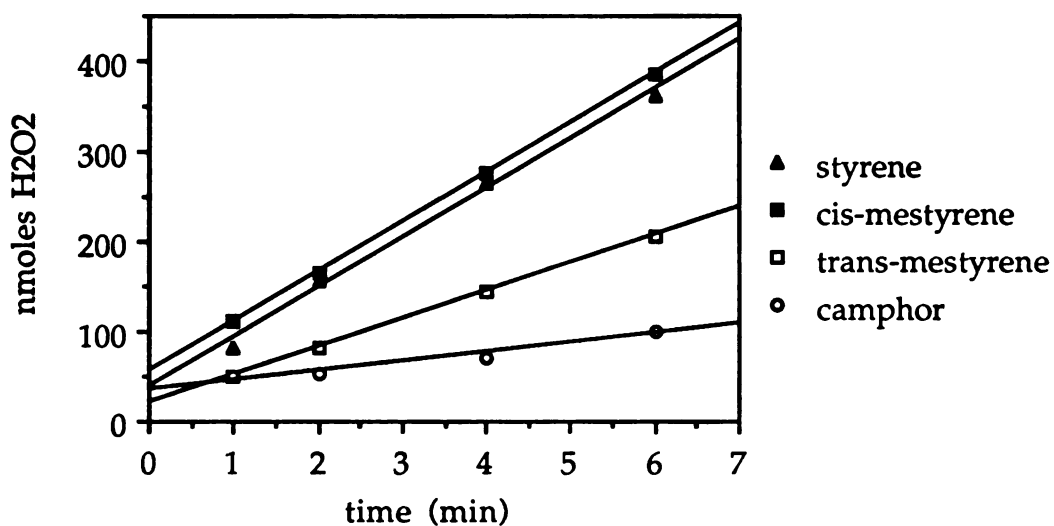
Figure 3.11: *Plots of the amount of* H_2O_2 *formed versus time during the incubation of* $P450_{cam}$ *with styrene, cis- and trans-β-methylstyrene and camphor. The amounts of* H_2O_2 *produced are normalized to 1 nmole* $P450_{cam}$.
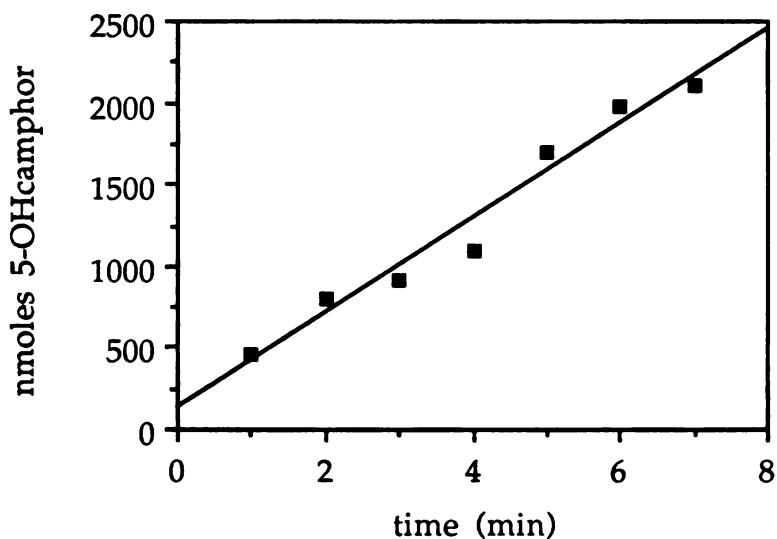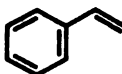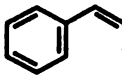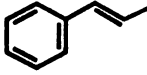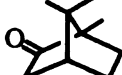
Figure 3.12: *Plot of the amount of* 5-exo-hydroxycamphor *formed versus time in the incubation of* $P450_{cam}$ *with camphor. The amount of product formed is normalized to 1 nmole* $P450_{cam}$.

Table 3.3: *Comparison of the rates of NADH and oxygen consumption with hydrogen peroxide and product formation styrene and* cis- *and* trans-β-*methylstyrene oxidation by* P450$_{cam}$.

Substrate	Rate (nmole/nmole P450/min)			
	NADH	O$_2$	H$_2$O$_2$	Product[a]
	51 ± 3	46 ± 2	53 ± 3	1.1 ± 0.2
	55 ± 2	41 ± 5	56 ± 1	0.54 ± 0.08
	32 ± 1	30 ± 8	29 ± 3	0.15 ± 0.03
	260 ± 20	260 ± 10	9 ± 1	290 ± 10

[a] The product is the epoxide for the styrenes and 5-*exo*-hydroxycamphor for camphor. The rates of product formation from the olefins are slightly higher if the other metabolites are included, although benzaldehyde is not counted as a product for these purposes because it is produced by a peroxide-dependent reaction.

This picture contrasts sharply with the results obtained using camphor as substrate (Table 3.3). The rate of product formation with camphor closely parallels NADH and oxygen consumption and is accompanied by the formation of very little hydrogen peroxide (3%). These results indicate, as has been shown before (Atkins and Sligar, 1987), that the oxidation of camphor by P450$_{cam}$ is tightly coupled to oxygen and NADH utilization.

3.2.4 Molecular Dynamics Simulations

Attempts to predict the epoxidation stereochemistry for styrene and the β-methylstyrenes using a static picture of the P450$_{cam}$ active site pocket were unsuccessful, due primarily to the fact that there are no obvious steric

barriers which favor one enantiomer orientation over the others. In order to understand the energetic factors involved in determining preferred binding orientations within this site, molecular dynamic (MD) simulations of these substrates in the active site were performed by our collaborators Jack Collins, Debbie Camper and Gilda Loew at the Molecular Research Institute in Palo Alto.

The basic protocol they used was to first energy minimize the substrate structures such that the most favorable conformations would be used in the protein interaction studies. For styrene and $trans$-β-methylstyrene, this conformation is planar. For cis-β-methylstyrene, the lowest energy structure is nonplanar, with a dihedral angle of ~40° for τ as defined in Figure 3.14.

These structures were docked into a P450$_{cam}$ active site consisting of the heme prosthetic group, 87 amino acids which define an active site that extends approximately 12 Å from the center of the heme unit, and seven bound water molecules. A ferryl oxygen species is created by placing an oxygen atom axial to the heme iron at a distance of 1.7 Å, the bond length determined for the ferryl-oxo species in peroxidases from EXAFS studies (Chance et $al.$, 1984).

Styrene was docked in two initial orientations: one which, without MD, would give the 1R-enantiomer, and one which would give the 1S-enantiomer. Both cis- and $trans$-β-methylstyrene were docked into the active site in four initial orientations due to the two equivalent low energy conformations for these olefins. The use of two different initial orientations is necessary to show there is no bias towards forming one enantiomer versus the other based on the starting orientation. In all the initial orientations, the phenyl ring is directed away from the iron-oxo species.

The initial substrate-protein complexes were energy-minimized to find the most favorable binding modes for each substrate. These complexes then served as the starting point for MD simulations. Each MD simulation lasted 125 ps, and the positions of the substrate as it moved about the active site were recorded every 0.2 ps. This generated a total of 2500 "snapshots" for styrene and 5000 snapshots each for cis- and trans-β-methylstyrene, which were screened for the likelihood that the complex formed the epoxide.

A given complex was considered to "react" to form the epoxide if the distance between the β-carbon, chosen because it is the most reactive to radical oxygen addition, and the ferryl oxygen was less than 4 Å. Which epoxide enantiomer is formed depends on which face of the π-bond, as defined by the angle between the π-orbitals and the ferryl oxygen (see Figure 3.13), is directed towards the oxygen. An angle of <80° defines a face which would lead to the 1S epoxide of styrene, the 1S,2R epoxide of cis-β-methylstyrene, and the 1R,2R epoxide of trans-β-methylstyrene. An angle of >100°, on the other hand, would lead to the 1R epoxide of styrene, the 1R,2S epoxide of cis-β-methylstyrene, and the 1S,2S epoxide of trans-β-methylstyrene. An angle between 80-100° is considered an edge-on approach, and thus not reactive to epoxide bond formation.

Analysis of the total number of snapshots taken for each substrate reveals that the olefins spend a significant amount of time away from the ferryl-oxo species. Only 49, 12 and 57% of the time were styrene, cis-β-methylstyrene and trans-β-methylstyrene, respectively, close enough to the oxygen to be considered to be in a reactive complex (Fruetel et al., 1992). Of the reactive complexes, the relative amounts of each epoxide enantiomer were determined. Those results are summarized and compared to the experimental results in Table 3.4.
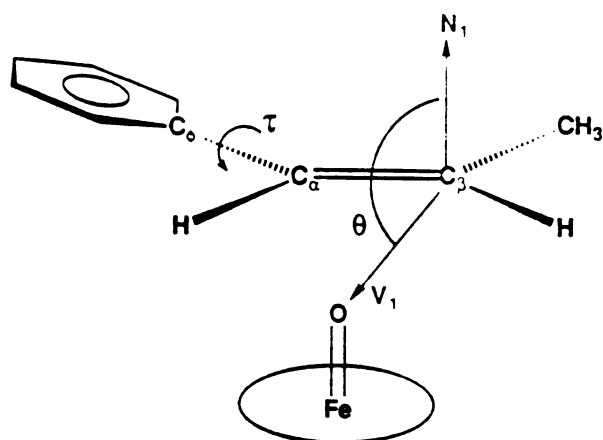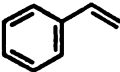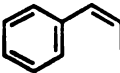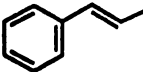
Figure 3.13: *Depiction of a complex between the olefin and the iron-oxo species. Which epoxide enantiomer is formed is defined by the angle theta between the π-orbitals of the olefin and the ferryl oxygen, denoted by the vectors N_1 and V_1.*

Comparison of the theoretical predictions with the experimental results shows good agreement between the two, with the correct enantiomer predicted to be in excess in each case. The results for styrene are the furthest off of the set, and possible reasons for this are discussed.

Table 3.4: *Comparison of the epoxidation stereochemistry results from theoretical predictions and those experimentally determined for $P450_{cam}$ oxidation of styrene, cis-β-methylstyrene and trans-β-methylstyrene.*

	Epoxide stereochemistry ($1S : 1R$)	
Substrate	Theoretical prediction	Experimental results
	65 : 35	83 : 17
	84 : 16	89 : 11
	75 : 25	75 : 25

3.3 Discussion

3.3.1 P450$_{cam}$ and styrene and *cis*- and *trans*-β-methylstyrenes

The P450$_{cam}$-catalyzed turnover of styrene, *cis*-β-methylstyrene and *trans*-β-methylstyrene yields several products for each substrate. The major enzyme-derived metabolite in each case is the epoxide. The only other example of P450$_{cam}$ epoxidation is that of 5,6-dehydrocamphor, an unsaturated analog of camphor, which yields *exo*-5,6-epoxycamphor (Gelb *et al.*, 1982b). Methyl hydroxylation of *cis*- and *trans*-β-methylstyrene constitutes an additional major reaction pathway with these substrates. Minor metabolites include phenyl ring hydroxylation and formation of the rearrangement products phenylacetaldehyde and phenylacetone.

The most unexpected metabolite identified for each of the olefins is benzaldehyde. This compound has not been previously demonstrated for any P450 reaction with styrene, and yet it constitutes one of the major products of the P450$_{cam}$ reactions. The formation of this product is intriguing because it requires cleavage of a carbon-carbon bond. Although carbon-carbon bond cleavage reactions are known for certain P450 enzymes, such as P45019 (aromatase) and P45051 (14α-demethylase), this is the first example of this type of reaction for a non-steroidogenic P450.

The discovery that catalase inhibits, and the addition of hydrogen peroxide promotes, the formation of this product suggests that benzaldehyde is not a product of normal enzymatic turnover, but rather is dependent on the presence of hydrogen peroxide. The detection of benzaldehyde in a model heme system containing *cis*-stilbene, *t*-butylhydroperoxide and a

95

radical chain initiator suggests peroxy radicals are involved in its formation (He and Bruice, 1991).

The influence of catalase on the reaction profiles for these olefins suggests a significant amount of hydrogen peroxide is being produced by the $P450_{cam}$ system. Indeed, measurements of the NADH and oxygen consumption rates, when compared to the product and hydrogen peroxide formation rates, indicate that almost all of the NADH and oxygen consumed are going towards hydrogen peroxide production, and very little is directed towards product formation (Table 3.3). This picture contrasts sharply with camphor oxidation by this enzyme, which is highly coupled and thus yields very little hydrogen peroxide.

The fact that the NADH consumption rate approximately equals the hydrogen peroxide formation rate indicates that only hydrogen peroxide is being formed when the enzyme uncouples. The slight differences in NADH and oxygen consumption rates are most likely due to experimental error, and thus do not indicate excess water is being produced. Whether the hydrogen peroxide is formed directly from the enzyme or via superoxide is not known, as the formation of superoxide was not directly examined. $P450_{cam}$ has been shown to produce superoxide in the absence of substrate (Sligar *et al.*, 1974), and therefore formation of this product is a possibility.

The observation of significant uncoupling with the three olefins suggests these substrates occupy binding modes in the $P450_{cam}$ active site which permit access of water to the iron-dioxygen species. The MD simulations suggest that these substrates have considerable mobility in the active site, including binding in modes which are "unreactive" towards oxygen addition to the π-bond. Whether or not the unreactive binding modes observed in the MD simulations will lead to the discharge of the iron-

dioxygen species to form hydrogen peroxide is not known. However, the relative small size of these substrates suggests water molecules are likely to remain in the active site when the substrate is bound, hence providing a proton source for the formation of hydrogen peroxide. The binding of camphor, in contrast to the styrenes, desolvates the binding pocket of $P450_{cam}$, resulting in very little uncoupling of the enzymatic reaction. MD simulations of camphor in the $P450_{cam}$ binding pocket indicate that reactive complexes are formed nearly 100% of the time (Paulsen and Ornstein, 1990).

The abilities of styrene and *cis*- and *trans*-β-methylstyrenes to move about the active site is reflected not only in the large amounts of uncoupling measured, but also in the fact that both epoxide enantiomers are observed for each substrate. This indicates that the substrates are not so rigidly held that only one enantiomer is obtained, such as is the case in polycyclic aromatic hydrocarbon epoxidations by P4501A1 (Jerina *et al.*, 1982). However, a significant preference for the 1S epoxide enantiomer is observed for each olefin, indicating that the active site does impose a bias in how the substrate is oriented. Analysis of the crystal structure of $P450_{cam}$ with one of the olefins docked inside, however, suggests orientations leading to both epoxide enantiomers are possible, with no obvious steric barriers prohibiting the 1R orientation. Thus a static picture of the active site where the substrates are oriented based on available space in the binding pocket provides little clue as to why one enantiomer is preferentially formed over the other.

Analysis of the energetics of styrene and *cis*- and *trans*-β-methylstyrenes in energy-minimized complexes with the protein also provides little information as to which orientations are the most favorable. Comparison of orientations which lead to the 1R enantiomer with those leading to the 1S enantiomer indicates all the complexes are approximately

the same energy or else predicts the wrong enantiomer to be favored (Fruetel *et al.*, 1992).

The ability of molecular dynamic simulations to correctly predict the enantiomer in excess for the three olefins indicates that a dynamic approach is needed to understand the binding of these substrates. Although the starting orientation of the olefin was not found to bias the final result, several initial orientations as well as initial velocities were determined to be necessary in order to correctly predict the final ratio.

The preferred binding orientations of the three olefins all place the phenyl ring approximately over the D ring of the heme (see Figure 3.14). In this orientation, the phenyl ring contacts the lower edge of Phe 87 and Tyr 96, fitting between these residues and the heme surface. Because of the time-scale of the dynamics, orientations which turn the substrate around such that the phenyl ring is closer to the iron-oxo species are not observed. Such orientations must be possible, however, as small amounts of aryl hydroxy products are detected experimentally.

The results of the MD simulations underline the importance of hydrophobic interactions in determining preferred binding orientations in the absence of any strongly directional parameters such as steric, hydrogen bonding and polar interactions. The fact that *cis*-β-methylstyrene shows slightly stronger preference for the 1*S* enantiomer than does styrene may simply be due to the fact that it has a greater hydrophobic surface and thus prefers to bind in the hydrophobic pocket leading to the 1*S* epoxide. *trans*-β-Methylstyrene, although equally hydrophobic as the *cis*-isomer, may occupy slightly different orientations than either of the other two olefins due to steric interactions of the *trans*-methyl group with the heme surface, and consequently does not show higher selectivity than styrene. The fact that
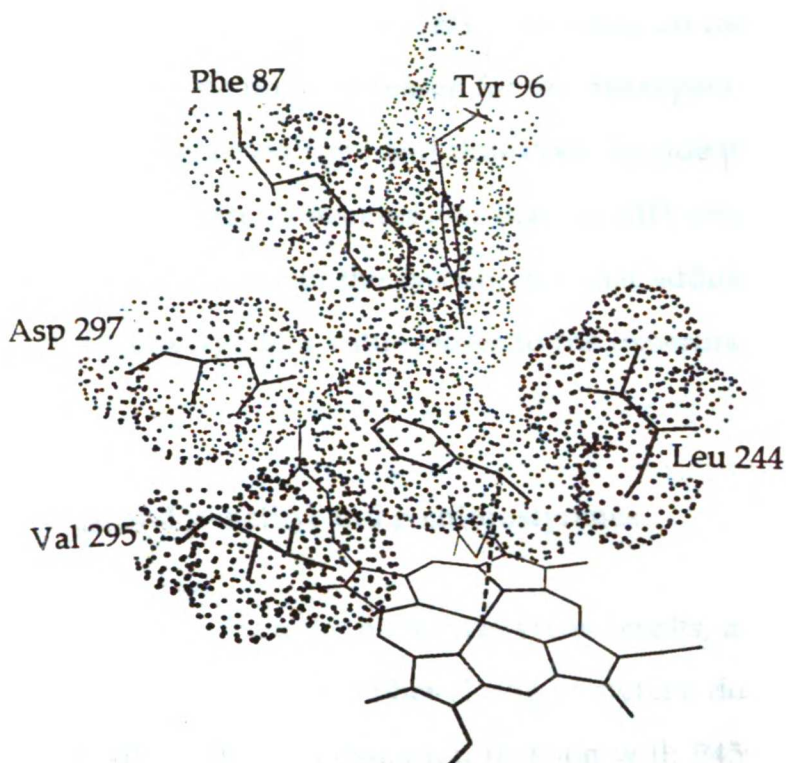
Figure 3.14: *Depiction of the preferred binding orientation of styrene and the β-methylstyrenes as determined from molecular dynamic simulations. Shown is styrene bound in the orientation which would give the 1S-epoxide enantiomer. Note that the phenyl ring binds over the D ring of the heme and under Phe 87 and Tyr 96.*

this substrate is turned over more slowly than the *cis* olefin suggests that it binds with less than optimal alignment of the π-orbitals with the ferryl-oxygen *p*-orbitals, consistent with previous observations that *cis*-olefins are turned over better than *trans*-olefins (Groves and Nemo, 1983).

The reasons for the discrepancy between the MD results and those measured experimentally for styrene are not clear. The smaller size of styrene would suggest this substrate binds more loosely in the active site and thus should give lower selectivity than either *cis*- or *trans*-β-methylstyrenes, in agreement with the MD results. However, styrene is found to give approximately the same *S:R* ratio as *cis*-β-methylstyrene, indicating that the

addition of a *cis*-methyl group has very little effect on the binding of the styrene structure. One possible reason for the discrepancy in the results is the active site model is too rigid and thus does not adequately simulate the dynamics of the protein. It also may be that the MD simulations did not fully sample the dynamics of the system, and that additional runs will reveal that the ratios converge to a value closer to the experimentally determined one.

3.3.2 P450$_{cam}$ and *p*-methyl and *p*-chlorostyrenes

As can be seen from the β-methylstyrene results, addition of a methyl group either *cis*- or *trans*- to the phenyl ring of styrene does not greatly affect the stereoselectivity of the epoxidation reaction with P450$_{cam}$. Whether or not that same amount of bulk added somewhere else to the styrene structure will have the same effect cannot be predicted from these results.

The general availability of *para*-substituted styrenes made this family of compounds an attractive one with which to study this question. However, the inability of our chiral GLC assay to reliably resolve *para*-substituted styrene oxides other than *p*-chlorostyrene oxide greatly limited our efforts. We were able, however, to address some of the same questions using *para*-substituted thioanisoles (see Chapter 4).

The stereochemistry results for *p*-chlorostyrene suggest that addition of a chloro group to the phenyl ring makes very little difference in the reaction stereochemistry (Table 3.2). This suggests that the active site can readily accommodate a *p*-chloro substituent with little effect on substrate binding as reflected in the reaction stereochemistry. The lower stereoselectivity observed for *p*-chloro as compared to *p*-hydrogen is also

seen with the thioanisoles (Chapter 4). The reasons why this might be are discussed more fully in Chapter 4.

The finding that for both styrene and p-chlorostyrene the S-epoxide enantiomer is preferentially formed suggests that hydrophobic contacts between the core styrene structure and protein residues in the P450$_{cam}$ active site continue to direct the reaction stereochemistry in spite of the introduction of a more polar substituent. The finding that styrenes in general show higher oxidation stereoselectivities than the less hydrophobic thioanisoles (Chapter 4) is also consistent with hydrophobic interactions acting as a strong determinant for S-epoxide preference. It would have been interesting to test the limits of this hypothesis with the other styrene substrates; however, our studies were limited by the assay system.

It is interesting that para-substituted benzaldehydes are formed in the reaction of P450$_{cam}$ with p-chloro and p-methylstyrenes, suggesting that oxidation of these substrates, like that of styrene and the β-methylstyrenes, is accompanied by significant uncoupling. The rate of hydrogen peroxide formation was not determined for the para-substituted olefins. However, measurements of oxygen consumption indicate that both p-chloro and p-methylstyrene consume oxygen at rates slower than styrene by about one third (data not shown). The rate of epoxide formation was also not quantitatively measured for the para-substituted olefins. However, it is estimated to be less than that determined for styrene based on relative peak height to an internal standard for a 30 minute incubation.

These trends are similar to that observed for trans-β-methylstyrene which, although it consumes less oxygen than styrene, is not necessarily less uncoupled due to a slower epoxide formation rate (Table 3.3). These results suggest that the addition of a para-substituent to the styrene structure does

not necessarily force the substrate into productive complexes with the ferryl oxygen more often than styrene. This might otherwise be expected based on the "tighter" fit of a *para*-substituted styrene in the binding pocket.

It should be noted that the elution order of the two *p*-chlorostyrene oxide enantiomers on the chiral GLC column was not absolutely determined but is assumed to be the same as for styrene and *cis*- and *trans*-β-methyl-styrene oxides. Thus it is possible that the stereochemical preference observed with this substrate is actually the opposite of the rest of the olefins. However, the strong trend in the enzymatic stereoselectivity seen with this enzyme and the three mutants (Table 3.2) suggests that the assignment is correct.

3.3.3 F87A, F87W, Y96F and styrene, *p*-chloro- and *p*-methylstyrenes

Protein residues Phe 87 and Tyr 96 are two of three aromatic residues which help define the active site pocket in P450$_{cam}$. Both residues contact camphor in the camphor-bound crystal structure (Poulos *et al.*, 1985; 1987), and thus serve important roles in orienting that substrate for 5-*exo* hydroxylation. Tyr 96 was determined to be particularly important in camphor hydroxylation, as the crystal structure shows that it hydrogen bonds with the camphor carbonyl oxygen (Figure 1.5).

MD simulations of styrene and the β-methylstyrenes in the P450$_{cam}$ active site reveal that the phenyl rings of these olefins contact the lower edges of Phe 87 and Tyr 96 in the orientation which leads to the 1S-epoxide (Figure 3.15). These results suggest that mutation of these residues would affect the binding of these substrates in this orientation, causing the

S-epoxide to be more or less favored depending on the mutation and the consequence of residues moving in response to the mutation.

To test this, mutants of Phe 87 and Tyr 96 were constructed by Dr. Sandra Graham-Lorence in this lab, expressed in *E. coli*, and purified to homogeneity by either Dr. Graham-Lorence or myself. Two mutants of Phe 87, F87A and F87W, and one mutant of Tyr 96, Y96F, were studied.

Analysis of the epoxidation stereochemistry of styrene and *p*-chlorostyrene with these three mutants reveals very little change in epoxidation stereochemistry from the native enzyme (Table 3.2). This was somewhat surprising given the significant changes in size, particularly for Phe 87, that were made.

One possible explanation for the lack of stereochemical change is that radical changes in the active site structure are compensated for by movement of other active site residues. This compensation may in effect negate the change made by the mutation such that the overall structure of the active site remains relatively unchanged. Evidence to support movement of other protein residues in the active site of the mutants comes from phenyl and biphenyl hydrazine studies, which found that the extent of heme nitrogen arylation did not correlate with the postulated "space" opened up by the F87A or Y96F mutations or closed down by the F87W mutation, assuming that the rest of the protein structure remained the same as that in the crystal structure of the native enzyme (Tuck *et al.*, in press). Details of the substrate binding pockets in these mutants are explored further with *para*-substituted thioanisoles in Chapter 4.

4.0 OXIDATION OF THIOANISOLES BY CYTOCHROME P450$_{cam}$ AND ACTIVE SITE MUTANTS

4.1 Introduction

The results of the styrene epoxidation studies reveal that P450$_{cam}$ can catalyze stereoselective reactions with substrates structurally very different from camphor. These substrates are small enough to occupy multiple orientations within the active site, often binding in unproductive modes that lead to enzyme uncoupling rather than substrate oxidation. The stereochemistry of the epoxidation reaction provided a sensitive probe into preferred substrate orientations in the productive complexes. These studies indicate the importance of hydrophobic interactions in determining binding orientations within the active site when other strongly directional parameters such as polar, hydrogen-bonding or steric interactions are not in effect.

One could envision developing sensitive probes of P450 active site structure by the selective introduction of polar, hydrogen-bonding or steric groups into the otherwise hydrophobic substrate structure. To do this, a series of compounds is needed in order to understand changes in substrate binding as reflected in the reaction stereochemistry. Initial studies with *p*-methyl- and *p*-chlorostyrene indicate that a *para*-substituent can be accommodated within the P450$_{cam}$ active site, and that this substituent alters the stereochemistry of the reaction. Hence a series of *para*-substituted compounds may provide new information on how substrates bind in the P450$_{cam}$ active site. Because of the problems encountered with the styrene epoxidation assay, however, a new series of compounds was needed for such a study. The new substrate chosen was thioanisole.

104

Thioanisole is an attractive compound because it is structurally similar to styrene yet its oxidation involves a new reaction. This is important towards testing the hypothesis that substrate binding determines the reaction stereochemistry, regardless of the particular reaction involved.

The product of P450 oxidation of thioanisole is the sulfoxide, which is chiral due to a lone pair of electrons on the sulfur (equation 4.1). The

$$S\text{-sulfoxide} \qquad R\text{-sulfoxide} \tag{4.1}$$
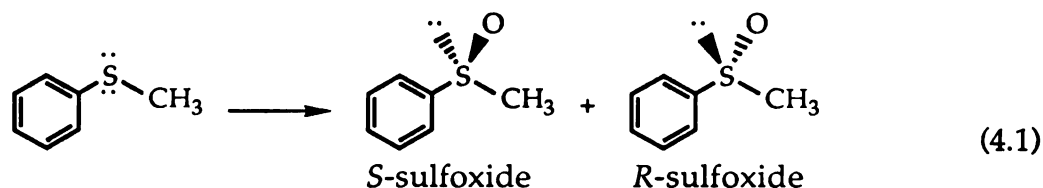
oxidation stereochemistry of this and similar compounds has been studied with a variety of enzymes, including chloroperoxidase (Colonna *et al.*, 1990), rat liver P450s (Waxman *et al.*, 1982), flavin monooxygenases (Light *et al.*, 1982; Rettie *et al.*, 1990) and bacterial enzymes from *A. niger* and *M. isabellina* (Holland, 1988). The strong sulfoxidation stereoselectivities demonstrated in these studies suggest that each enzyme shows its own characteristic selectivity towards these substrates, and that this may be one way to identify such enzymes in impure mixtures such as microsomes (Light *et al.*, 1982). The results of these studies and those from the previous chapter suggest that thioanisole and its analogs may serve as sensitive probes of binding orientation within the $P450_{cam}$ active site structure.

4.2 Results

4.2.1 Identification of Metabolites

Incubation of $P450_{cam}$ with thioanisole or one of five *p*-substituted thioanisoles (methyl, methoxy, chloro, cyano and nitro) results in the

NADH-dependent formation of the corresponding sulfoxides as determined by co-elution with synthetic sulfoxide standards on a Chiracel OB HPLC column. The identities of the sulfoxide peaks were also confirmed by comparison of the UV/visible spectra of the HPLC peaks with those of synthetic standards. Representative HPLC chromatograms of each substrate after incubation with $P450_{cam}$ are shown in Figures 4.1 - 4.6.

Addition of catalase to the incubation mixture alters the yield and ratio of the two sulfoxide peaks, suggesting that the sulfides are to some extent oxidized to the sulfoxide by exogenous hydrogen peroxide in solution. The hydrogen peroxide is most likely produced by uncoupling of the enzyme (see Section 4.2.3), and the change in sulfoxide stereochemistry is due to the fact that the solution reaction forms racemic sulfoxide while the enzymatic reaction does not. Because the solution reaction interferes with the enzyme results, catalase was included in all the thioanisole and p-substituted thioanisole incubations to minimize this problem.

Metabolites other than the sulfoxides were identified only in the case of p-methylthioanisole. Chiral HPLC analysis of the $P450_{cam}$ incubation revealed the presence of an NADH-dependent peak which ran very closely but just before the S-sulfoxide peak (see Figure 4.2). Some days, depending on the temperature, it co-eluted with the S-sulfoxide peak; however, this could be detected by examining the UV/visible spectrum of the peak, as the two compounds are spectrally distinct. Based on integration of the HPLC peaks and GLC peaks of the compound derivatized with BSTFA, this product constitutes 12-14% of the sulfoxide.

GLC/MS analysis of the new metabolite derivatized with BSTFA indicated that it has a molecular ion at 226, consistent with p-hydroxy-methylthioanisole with one trimethylsilyl group attached. A fragment ion
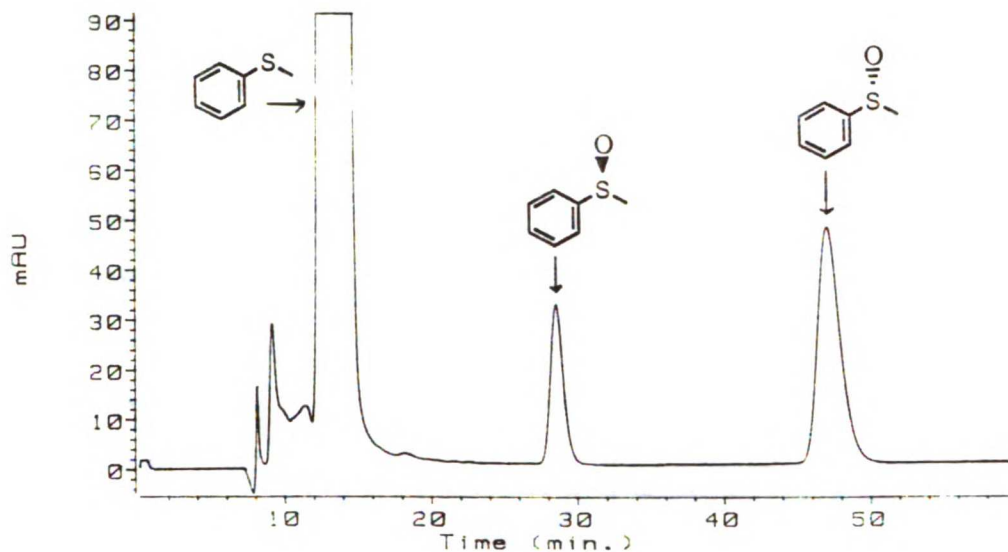
Figure 4.1: Chiral HPLC chromatogram of the sulfoxide enantiomers formed in the reaction of $P450_{cam}$ with thioanisole.
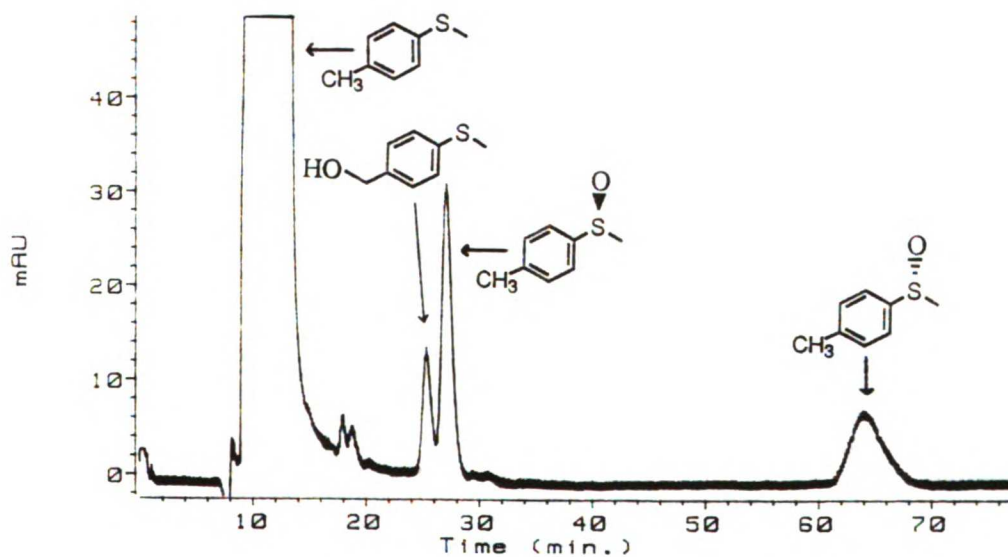
Figure 4.2: Chiral HPLC chromatogram of the sulfoxide enantiomers formed in the reaction of $P450_{cam}$ with p-methylthioanisole.
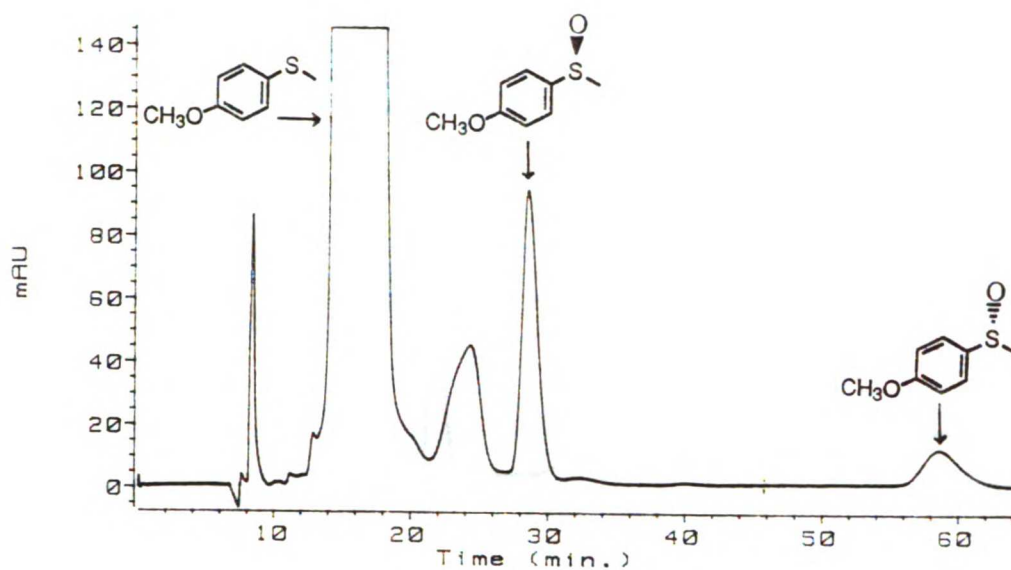
Figure 4.3: *Chiral HPLC chromatogram of the sulfoxide enantiomers formed in the reaction of P450$_{cam}$ with p-methoxythioanisole.*
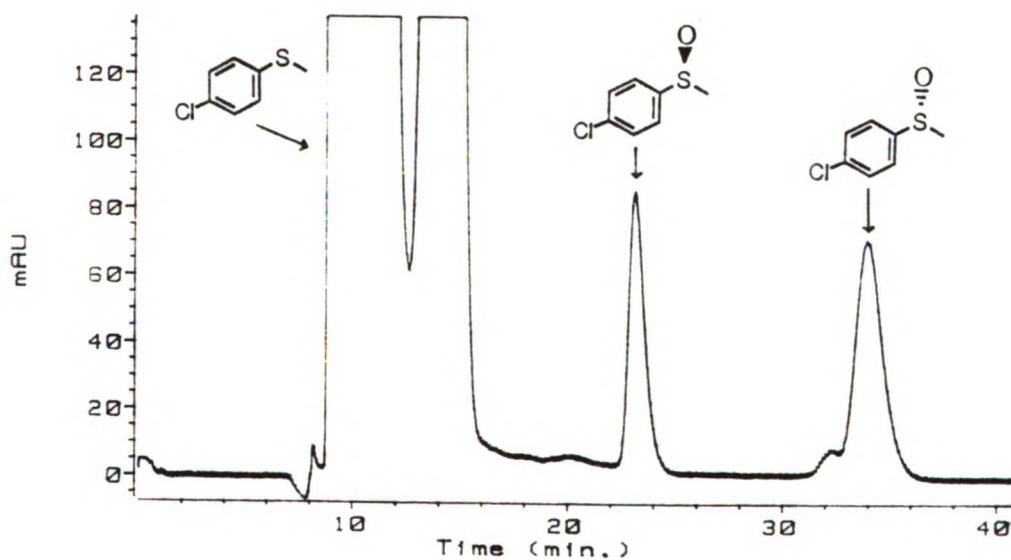
Figure 4.4: *Chiral HPLC chromatogram of the sulfoxide enantiomers formed in the reaction of P450$_{cam}$ with p-chlorothioanisole.*
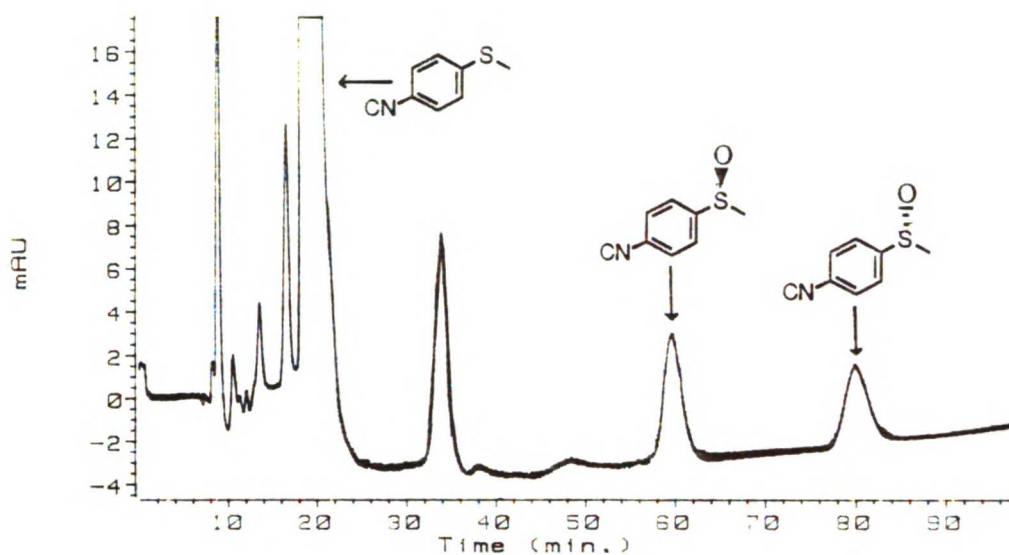
Figure 4.5: Chiral HPLC chromatogram of the sulfoxide enantiomers formed in the reaction of P450$_{cam}$ with p-cyanothioanisole.
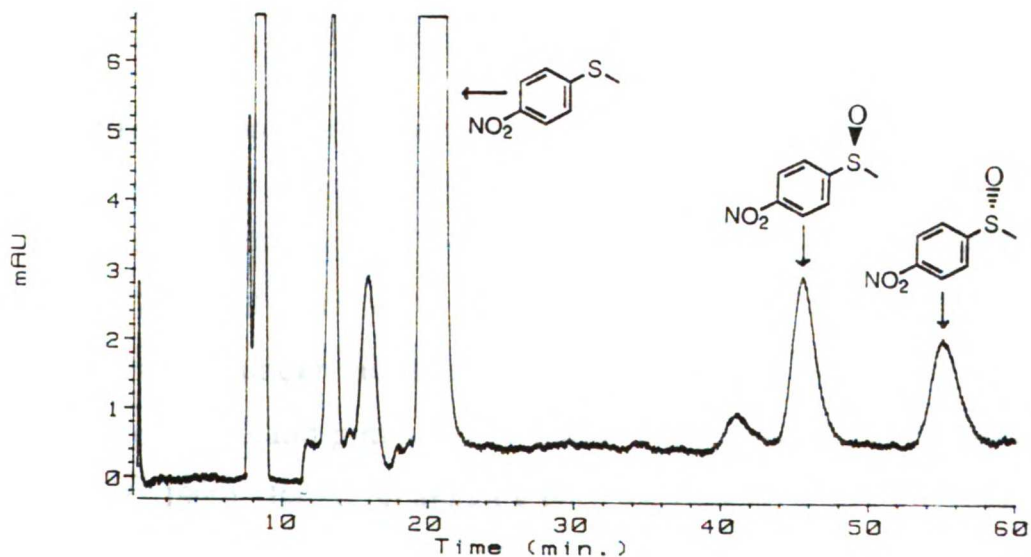
Figure 4.6: Chiral HPLC chromatogram of the sulfoxide enantiomers formed in the reaction of P450$_{cam}$ with p-nitrothioanisole.

109

at 179 (loss of SCH₃) confirmed that the hydroxyl is not attached to the sulfur methyl, and the base peak fragment ion at 137 (loss of OTMS) is consistent with formation of a stable benzyl cation in the mass spectrometer (mass spectrometric data is listed in Table 6.2 of the Experimental Section).
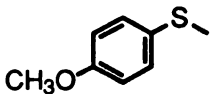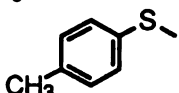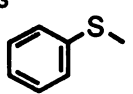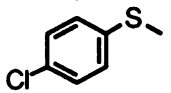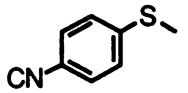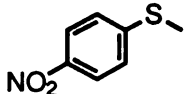
Incubation of five of the thioanisoles (p-nitrothioanisole was not run) with the $P450_{cam}$ active site mutants F87A, F87W and Y96F also results in the NADH-dependent formation of the corresponding sulfoxides. Again catalase was added to these incubations to minimize the hydrogen peroxide side reaction. In the F87W incubations, the hydroxymethyl metabolite of p-methylthioanisole was observed by chiral HPLC in approximately the same ratio to sulfoxide as seen with the native enzyme (~12% of the epoxide). For F87A, only a small amount of this product was seen (estimated at ~5% of the epoxide), while for the Y96F mutant, no hydroxymethyl product was observed. No O-demethylation product was seen with p-methoxythioanisole; however, a specific search for this particular metabolite was not conducted.

4.2.2 Sulfoxidation Stereochemistry

The stereochemistry of the sulfoxidation reaction was determined using a Chiracel OB HPLC column. This system cleanly separates the two enantiomers, and under the conditions employed, the S-enantiomer elutes first for thioanisole and p-methyl, methoxy, chloro and nitrothioanisoles (Rettie et al., 1990). Based on analogy with the other five thioanisoles, the S-enantiomer of p-cyanothioanisole is also assumed to elute first.

The results of the sulfoxidation stereochemistry for the six thioanisoles are summarized in Table 4.1. Analysis of this data suggests that
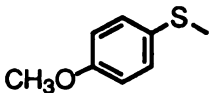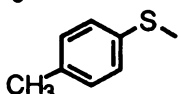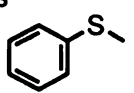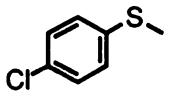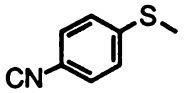
Table 4.1: *Summary of the stereochemistry of oxidation of a number of p-substituted thioanisoles by P450$_{cam}$.*

Substrate	Sulfoxide stereochemistry (R:S)
	25 : 75 (± 3)
	48 : 52 (± 1)
	72 : 28 (± 1)
	61 : 39 (± 2)
	49 : 51 (± 2)
	46 : 54 (± 6)

the presence of a *para*-substituent greatly influences the stereochemistry of the reaction, and that the extent of change depends on the nature of the substituent.

The stereochemistry results for thioanisole oxidation by the three active site mutants F87A, F87W and Y96F are summarized in Table 4.2. Mutation of Phe 87 to alanine in general increases the formation of the S-sulfoxide, while mutation to tryptophan generally disfavors this enantiomer, but only by a small extent as compared to the native enzyme. Mutation of Tyr 96 to phenylalanine, like the F87A mutation, increases favoritism for the S-sulfoxide, but to a greater extent. The exception to all of these trends is the sulfoxidation stereochemistry observed for p-methoxythioanisole.

111

Table 4.2: *Summary of the stereochemistry of oxidation of* p-substituted *thioanisoles by the P450$_{cam}$ active site mutants F87A, F87W and Y96F.*

Substrate	Sulfoxidation stereochemistry ($R : S$ ($\pm$ 1))		
	F87A	F87W	Y96F
CH_3O—⬡—S (structure)	29 : 71	55 : 45	35 : 65
CH_3—⬡—S (structure)	36 : 64	54 : 46	28 : 72
⬡—S (structure)	62 : 38	78 : 22	59 : 41
Cl—⬡—S (structure)	45 : 55	63 : 37	24 : 76
CN—⬡—S (structure)	35 : 65	52 : 48	24 : 76

4.2.3 Uncoupling Measurements

The oxidation of thioanisole by hydrogen peroxide generated *in situ* suggests that enzymatic oxidation of these substrates is accompanied by substantial uncoupling of the enzyme. To determine the extent of the uncoupling by P450$_{cam}$ with thioanisole and *p*-methylthioanisole, the rates of NADH and oxygen consumption were measured and compared against the rates of hydrogen peroxide and metabolite formation for these two substrates.

NADH consumption was measured spectrophotometrically, and found to be linear over the time period monitored (see Figure 4.7). Some scatter in the data is observed that is attributable to alternating between two different cuvettes over the time course of each experiment. As a

consequence of the scatter, the NADH measurements were carried out longer than the other assays in order to get enough time points to accurately determine the rate.

Oxygen consumption was monitored by an oxygen electrode and was found to be linear over the first 2.5 minutes (see Figure 4.8). The leveling off which occurs after 2.5 minutes is most likely due to the low oxygen concentration in the cell at that point, which may both slow down the enzymatic reaction and favor leakage of oxygen back into the cell. Hydrogen peroxide and sulfoxide formation were measured by a chemical assay and by GLC, respectively. Their plots are shown in Figures 4.9 and 4.10.

The small discrepancy between the rates for NADH and oxygen consumption could be due to reduction of the iron-oxo species to water in the case of thioanisole, but more likely reflects the differences in experimental set-up between the two measurements. Oxygen consumption was measured in an electrode cell with a stir bar, while NADH measurements (as well as the hydrogen peroxide and metabolite measurements) were run in a shaking water bath. Also, the finding that the hydrogen peroxide formation rates closely agree with the NADH consumption rates suggest that hydrogen peroxide is the primary product of enzymatic uncoupling, and no or little excess water is being formed. Whether the hydrogen peroxide is formed directly from the enzyme or via superoxide is not known, as the formation of superoxide was not directly tested.

The results of these measurements, summarized in Table 4.3, suggest that $P450_{cam}$ oxidation of thioanisole and p-methylthioanisole, like its oxidation of styrene and the β-methylstyrenes, is accompanied by a significant amount of uncoupling. The rates for NADH, oxygen and

113
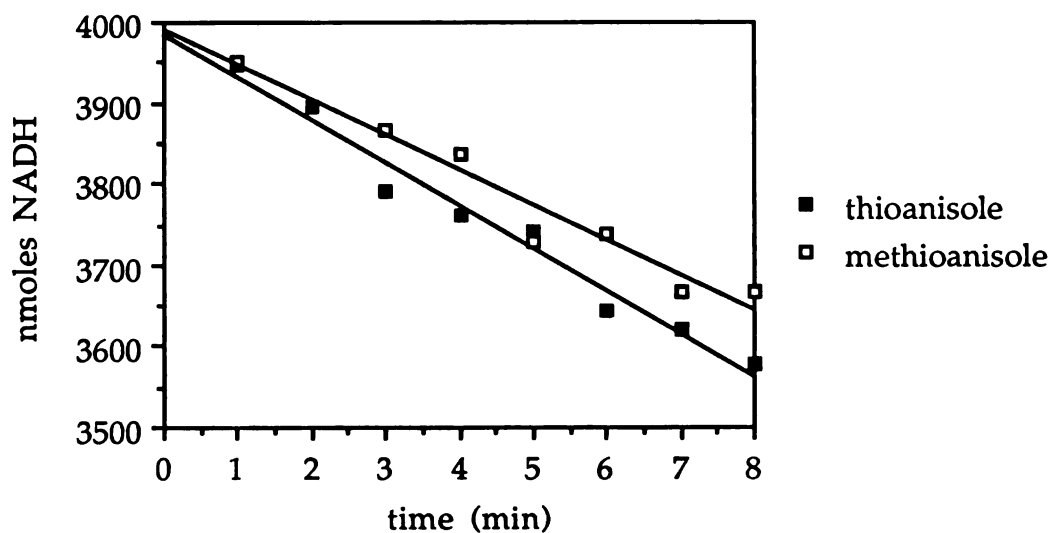
Figure 4.7: Plots of the amount of NADH present versus time during the incubation of P450$_{cam}$ with thioanisole and p-methylthioanisole. The amount of NADH consumed is normalized to 1 nmole P450$_{cam}$.
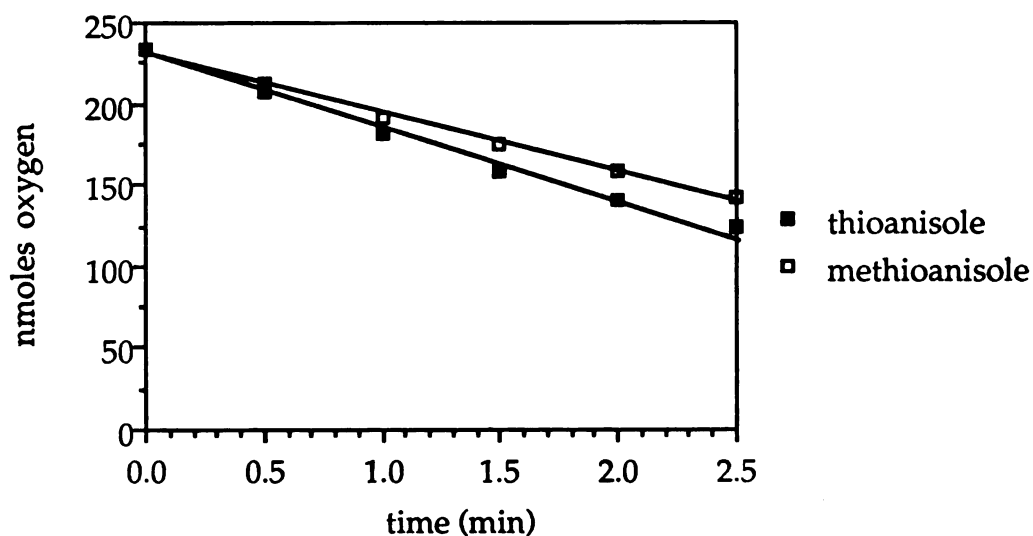
Figure 4.8: Plots of the amount of O$_2$ present versus time during the incubation of P450$_{cam}$ with thioanisole and p-methylthioanisole. The amount of O$_2$ consumed is normalized to 1 nmole P450$_{cam}$.

114
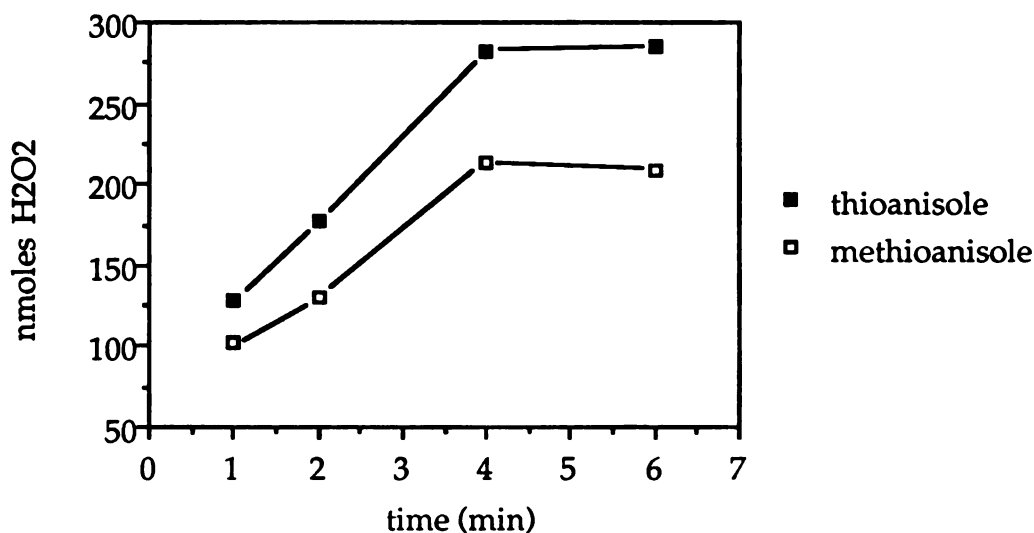
Figure 4.9: *Plots of the amount of H_2O_2 formed versus time during the incubation of $P450_{cam}$ with thioanisole and p-methylthioanisole. The amount of H_2O_2 formed is normalized to 1 nmole $P450_{cam}$.*
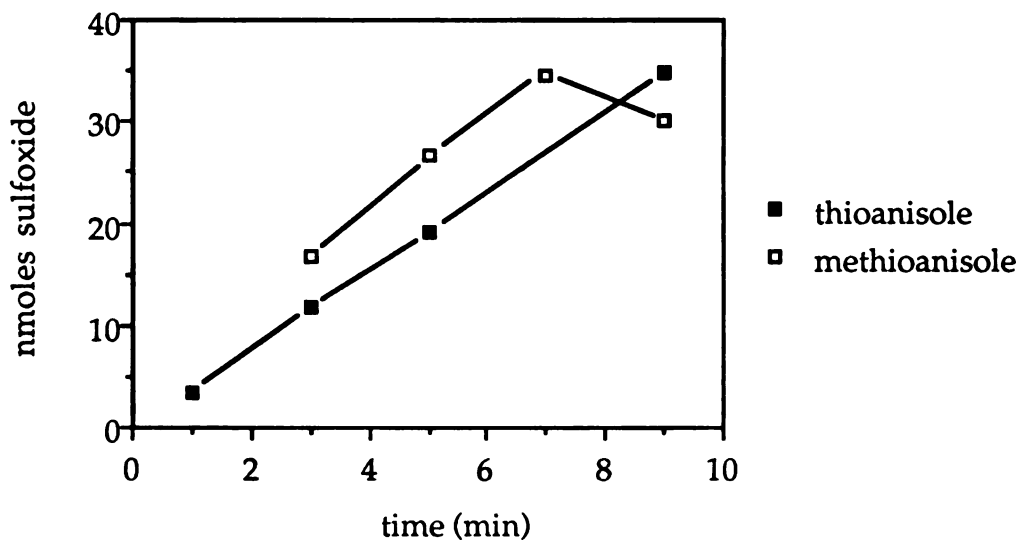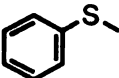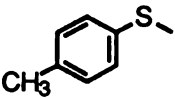
Figure 4.10: *Plots of the amount of sulfoxide formed versus time during the incubation of $P450_{cam}$ with thioanisole and p-methylthioanisole. The amounts of product formed are normalized to 1 nmole $P450_{cam}$.*

115

Table 4.3: Comparison of the rates of NADH and oxygen consumption with hydrogen peroxide and product formation for the oxidation of thioanisole and p-methylthioanisole by P450_cam.

| Substrate | Turnover (nmole/nmole P450/min) | | | |
	NADH	O_2	H_2O_2	sulfoxide
	49 (± 8)	41 (± 5)	48 (± 5)	3.5 (± 0.5)
	42 (± 8)	48 (± 5)	37 (± 2)	4.0 (± 0.5)

hydrogen peroxide are similar to those measured for styrene and *cis*-β-methylstyrene, but the product formation rates are 3-8 times higher for the sulfur compounds. Nonetheless, sulfoxide formation only accounts for 7-10% of the NADH consumed in the reaction, indicating that the oxidation of these compounds is much less tightly coupled than is the oxidation of camphor by this enzyme (Chapter 3).

4.2.4 Molecular Dynamics Simulations

In order to get a better understanding of the protein-substrate interactions which determine the observed stereochemical preferences in thioanisole and *p*-methylthioanisole oxidation by P450_cam, molecular dynamic (MD) simulations were run of these substrates in the active site pocket by Jack Collins, Yan-Tyng Chang and Gilda Loew at Molecular Research Institute. The procedure followed was very similar to that used with styrene and the β-methylstyrenes (see Chapter 3), and differences are noted below.

Energy minimization of the two substrates resulted in planar conformations for both. These structures were docked into the enzyme active site in six distinct orientations, three of which would lead, without MD, to formation of the R-sulfoxide enantiomer, and the other three to the S-enantiomer. In each case, the initial sulfur-oxygen distance was between 3.0 and 3.5 Å.

MD simulations of 125 ps were run on each of the six substrate-protein complexes with the coordinates of the complex saved every 0.2 ps. Two different initial velocity distributions were used for each initial complex, generating a total of 7500 "snapshots" which were screened for the likelihood of the complex to form the sulfoxide. The criteria used to determine which complexes will form sulfoxide were (1) the sulfur-oxygen distance is less than 4 Å, and (2) the face angle theta (defined in Figure 4.11) is either < 80° (will form the S-sulfoxide) or >100° (will form the R-sulfoxide). Snapshots where theta is between 80° and 100° were disregarded, since they correspond to a much less stable transition state. The enantiomeric ratios predicted were
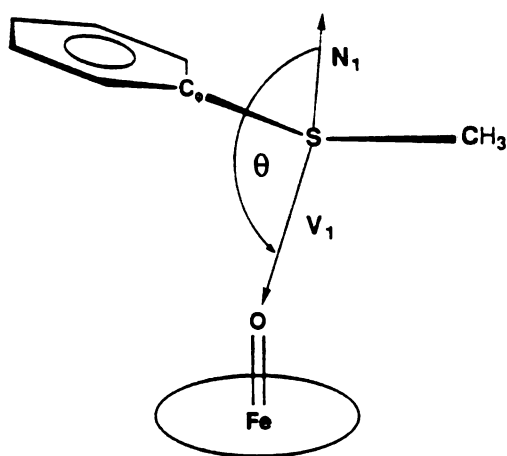
Figure 4.11: Depiction of a complex between thioanisole and the iron-oxo species. Which sulfoxide enantiomer is formed is defined by the angle theta between the normal to the C-S-C plane (N_1) and the S to O vector (V_1).

then calculated as the relative number of snapshots leading to one enantiomer versus the other.

Analysis of the initial energy-minimized protein-substrate complexes was done to see if an energy criterion alone would be sufficient to predict the enantiomeric ratios of the sulfoxide products. Comparison of the interaction energies of each of the complexes, however, revealed them all to be approximately the same, giving no hint as to which enantiomer should be preferentially formed (Fruetel *et al.*, submitted).

Totalling up the number of orientations leading to the *S*-enantiomer versus the number of orientations leading to the *R*-enantiomer for all 12 simulations (six initial orientations times two initial velocities each) gives a predicted ratio of *R* : *S* sulfoxides of 65 : 35 for thioanisole, and 22 : 78 for *p*-methylthioanisole. Changing the sulfur-oxygen cut-off distance for a "reactive" complex from 4.0 Å to 3.5 or 4.5 Å made very little difference in the final product ratios. Also, changing the protein backbone harmonic force from 100 kcal/Å^2 to 1 kcal/Å^2, thus making the protein residues less rigid, made very little difference in the product ratio for *p*-methylthioanisole.

The MD results suggest that thioanisole prefers to bind in an orientation which is similar to that preferred by styrene. This orientation places the phenyl ring of the substrate approximately over the D ring of the heme, with the sulfur atom closest to the C ring (Figure 4.12). The addition of a *p*-methyl substituent changes this preference, however, such that preferential formation of the *S*-sulfoxide is now predicted. This orientation places the phenyl ring still over the D ring but now the sulfur atom is closer to the A ring of the heme (Figure 4.13).
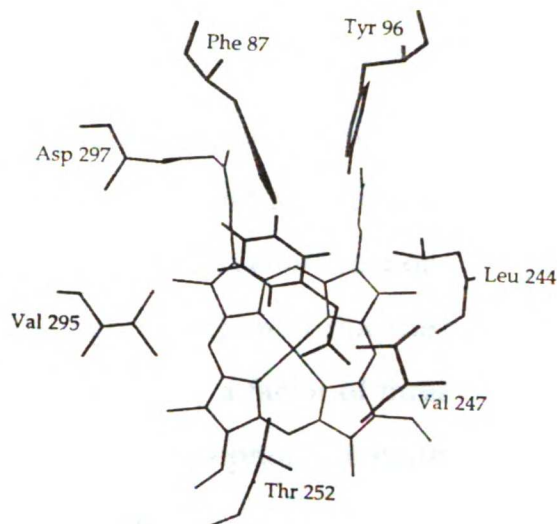
Figure 4.12: *Overhead view of thioanisole bound in the active site of P450$_{cam}$ in the preferred orientation as determined by molecular dynamic simulations. The orientation shown would lead to the R-sulfoxide.*
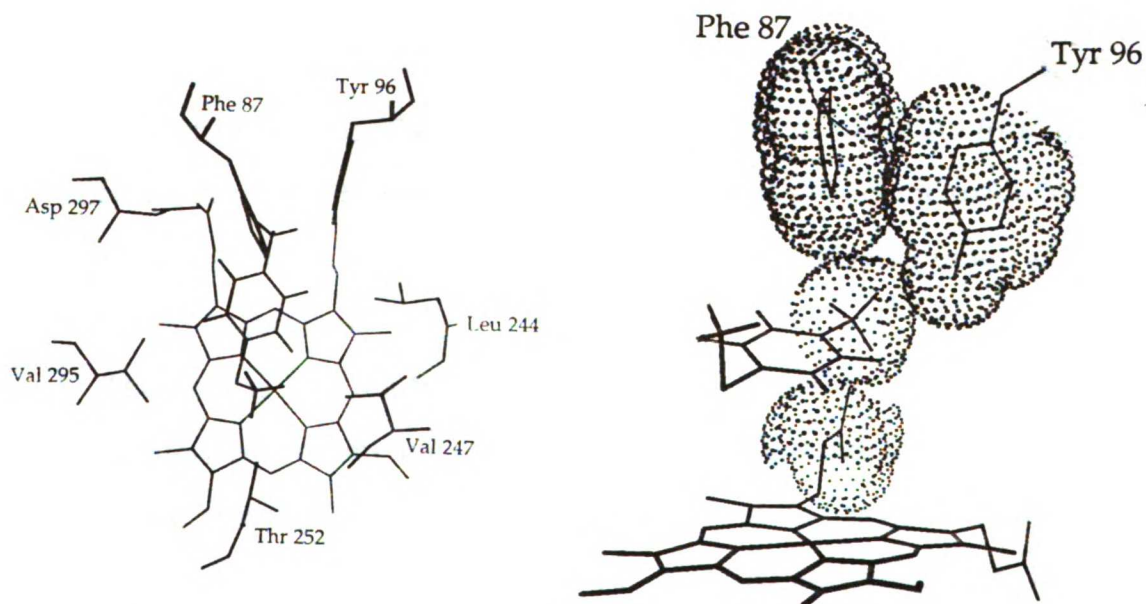
Figure 4.13: *View of p-methylthioanisole bound in the active site of P450$_{cam}$ in the preferred orientation as determined by molecular dynamic simulations. Left is an overhead view. Right shows the p-methyl substituent in the cleft defined by Phe 87, Tyr 96 and a heme propionic side chain. The orientation shown would lead to the S-sulfoxide.*

119

4.3 Discussion

4.3.1 P450$_{cam}$

The P450$_{cam}$-catalyzed oxidation of thioanisole and its p-methyl, p-methoxy, p-chloro, p-cyano, and p-nitro analogs to the corresponding sulfoxides represents a new class of reactions not previously demonstrated for P450$_{cam}$. Although oxidation of thioanisole to the sulfoxide is faster than the epoxidation of styrene by a factor of three or so, it is significantly slower than the hydroxylation of camphor, the natural substrate for P450$_{cam}$, by a factor of about 80 (Chapter 3).

The discovery that catalase affects the sulfoxide enantiomeric ratio suggests that the sulfides are partially oxidized by hydrogen peroxide generated *in situ*. Specific detection of time-dependent formation of hydrogen peroxide revealed that it is formed at rates approximately equivalent to the rates of NADH and oxygen consumption with thioanisole and p-methylthioanisole (Table 4.3). Since the rates of sulfoxide formation are only about one-tenth this fast, this indicates that enzymatic oxidation of these two compounds, like that of styrene and the β-methylstyrenes, is significantly uncoupled.

The finding that the NADH and hydrogen peroxide rates are approximately equivalent suggests that hydrogen peroxide is the sole product of enzymatic uncoupling. The slight discrepancy in the oxygen and NADH rates for thioanisole most likely represents experimental differences in the measurements, and thus does not indicate that excess water is being produced. Whether the hydrogen peroxide is actually enzymatically-generated superoxide that is detected as hydrogen peroxide is not known, as the formation of superoxide was not directly tested.

The measurement of significant uncoupling with thioanisole and p-methylthioanisole suggests these compounds, like styrene and the β-methylstyrenes, occupy binding modes in the P450$_{cam}$ active site which permit access of water to the iron-peroxo species. The MD simulations suggest that thioanisole, and to a lesser extent p-methylthioanisole, have a fair amount of mobility in the active site, thus consistent with these substrates binding in unproductive complexes with the iron-dioxygen species. The finding that p-methylthioanisole tends to "lock" into one binding orientation while thioanisole is free to move about during the MD simulations, however, is inconsistent with the comparable amounts of uncoupling measured for the substrates.

Comparison of the HPLC peak heights for the sulfoxides of the different thioanisoles reveals that p-cyano- and p-nitrothioanisoles give much smaller sulfoxide peaks than the p-methoxy and p-methyl analogs, suggesting that the electron-poor thioanisoles are turned over much more slowly than the electron-rich ones. This is in agreement with a radical mechanism proposed for sulfur oxidation in which the first step is electron abstraction from the sulfur atom (Ortiz de Montellano, 1986).

The stereochemistry results for sulfur oxidation by P450$_{cam}$ indicate that thioanisole is preferentially oxidized to the R-enantiomer in a ratio of 72 : 28 $R:S$ sulfoxides. Comparison of this result with the fact that styrene is oxidized in a ratio of 83 : 17 $S:R$ epoxides (Chapter 3), and ethyl benzene is preferentially oxidized to the R-alcohol in a ratio of 80 : 20 $R:S$ alcohols (DeVoss, J. and Ortiz de Montellano, P.R., unpublished results) indicates these substrates are all preferentially oxidized to the same relative enantiomer in approximately the same ratios (note that although they are denoted oppositely, the S-epoxide has the same relative positioning of the

oxygen, phenyl ring, and adjacent carbon as does the *R*-sulfoxide and *R*-alcohol; see equation 4.2). These results suggest that all three substrates bind similarly in the P450$_{cam}$ active site, and that the factors which determine favorable binding for one substrate also determine it for the others.

MD simulations of the two substrates in the active site pocket reveal that the preferred binding orientations for thioanisole and styrene are very

R-sulfoxide *S*-epoxide *R*-alcohol

(4.2)
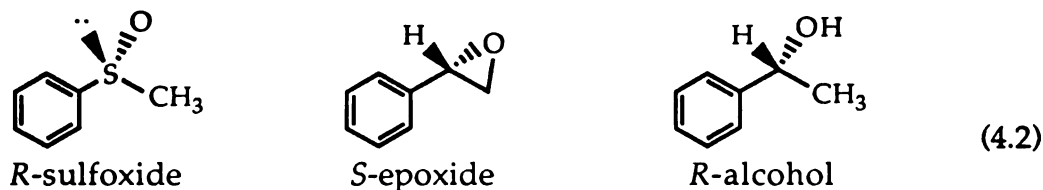
similar. As shown in Figure 4.12, the orientation which leads to the *R*-sulfoxide places the phenyl ring of thioanisole over the D ring of the heme, with the SCH$_3$ group closer to the C ring of the heme near the ferryl oxygen. This orientation is likely preferred due to favorable hydrophobic contacts between the phenyl and methyl groups of the substrate and hydrophobic residues Phe 87, Tyr 96, Val 247 and Val 244. Orientations which place the phenyl ring over the A or C rings of the heme are not likely due to steric clashes with the protein. The slightly different stereochemical ratio obtained with styrene as compared to thioanisole is most likely due to differences in the reaction geometries, the greater polarity of the sulfur atom, and/or the relative reactivities of the substrates.

Comparison of the epoxidation stereochemistry of styrene and *p*-chlorostyrene reveals that addition of a *p*-chloro group causes a small decrease by ~10% in the stereochemical preference for the *S*-epoxide (Chapter 3). These results suggest that introduction of the appropriate *para*-substituent may destabilize otherwise preferred binding orientations such that the stereochemical preference of the reaction is reversed. This

possibility was explored more fully with the thioanisoles presented here. The results from these studies indicate that indeed the stereochemical preference can be reversed; however, the degree of change depends highly on the substituent involved.

The presence of a p-methyl substituent, for example, decreases the preference for R-sulfoxide formation such that both enantiomers are equally favored. A p-methoxy substituent continues this trend even further by decreasing the R-sulfoxide favoritism such that the S-sulfoxide is favored, effectively inverting the thioanisole oxidation stereochemistry. The trend observed with these three substrates at first suggested that there might be an electronic factor in determining the reaction stereochemistry. Indeed a plot of the Hammett sigma$^+$ constant versus the % of S-enantiomer gives a linear correlation for these three sulfides. However, the stereochemistry results with p-chloro, p-cyano and p-nitrothioanisole do not continue this trend (Table 4.1), indicating that electronic effects alone do not explain the observed stereochemistries.

The presence of a $para$-substituent does, in general, decrease the favoritism for the R-sulfoxide. This is most likely due to increased steric interactions between the $para$-substituent and Phe 87, Asp 297, Ile 395 and Val 295 when the substrate is bound in the R-sulfoxide orientation (Figure 4.12). MD simulations of p-methylthioanisole in the P450$_{cam}$ active site pocket reveal that this substrate tends to bind such that the p-methyl substituent fits into a cleft defined by the lower edges of Phe 87 and Tyr 96 and the heme propionic group of the D ring (Figure 4.13). With the methyl substituent bound in this cleft, the predominant enantiomer formed is the S-sulfoxide, suggesting that the tendency of the p-methyl substituent to fit into

this pocket is the reason why more S-sulfoxide is observed with this substrate as compared to the unsubstituted thioanisole.

The finding that the MD simulations overpredict the S-sulfoxide favoritism, postulating a ratio of 22 : 78 R:S in contrast to the 48 : 52 ratio found experimentally may reflect the tendency of the substrate to "lock" into this position during the dynamics, even though lowering the backbone harmonic force constant of the residues had little effect on the MD values. The discrepancy in the results suggests that the protein is more fluid than the dynamics indicate, and highlights one of the problems of using a noncontinuous segment of the protein to model the dynamics of an entire protein.

The results of the MD simulations do, nonetheless, indicate the correct trend in going from unsubstituted to p-methylthioanisole, and suggest a plausible explanation for the general observance of more S-sulfoxide with $para$-substitution. Manually docking the other four $para$-substituted thioanisoles--methoxy, chloro, cyano and nitro--into the P450$_{cam}$ active site suggests that all but the nitro substituent will fit into the cleft, although the methoxy is a tight fit and allows only certain orientations of the methoxy group.

Another possible explanation for the observed increase in S-sulfoxide formation with $para$-substituted thioanisoles is that these substrates bind such that the $para$-substituent fits into a space at the top of the active site pocket defined by Thr 185, Phe 193, Met 184, Phe 98 and Phe 87 (Figure 4.14). This orientation places the substrate in a much more vertical position than those favored by the MD simulations, with the axis of the substrate roughly perpendicular to the heme plane rather than almost parallel to it. Since the roof of the active site is asymmetrical, interaction of the $para$-substituent

with residues here could also affect the stereochemistry of the reaction. The greater height over the C ring of the heme (see Figure 4.14) suggests that the *para*-substituent would fit into this space. Manually docking the substrates into the active site in that orientation suggests that formation of the *S*-sulfoxide would be favored, in agreement with the experimental results.
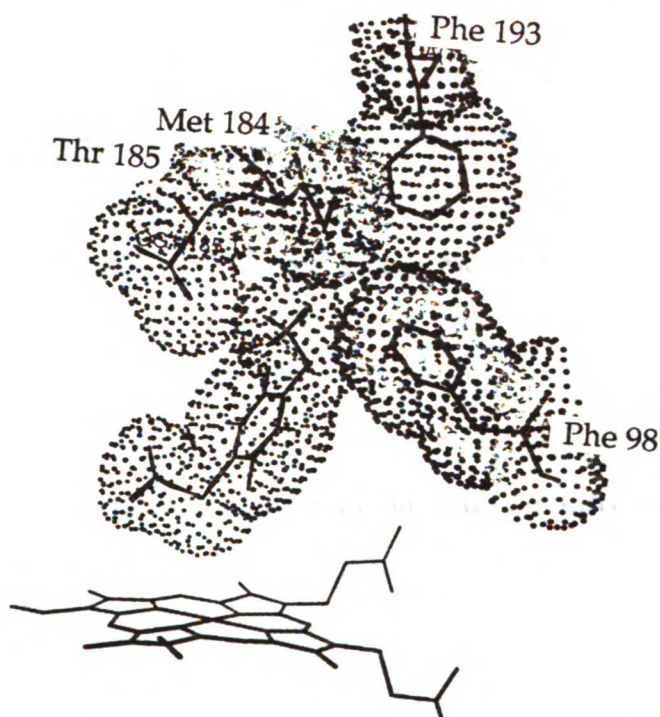
Figure 4.14: View of p-methoxythioanisole bound in a "vertical orientation" whereby the methoxy group binds in a pocket over the C ring of the heme defined by Thr 185, Phe 193, Met 184, Phe 98 and Phe 87.

MD simulations of thioanisole and *p*-methylthioanisole docked into vertical positions, however, found that very few "reactive" complexes were formed during these runs (Fruetel *et al.*, submitted). These results suggest that the vertical orientations generally do not contribute significantly to the stereochemistry results. Possible experiments designed to determine the significance of such binding orientations include mutating residues which

define this pocket but do not contact the cleft between the heme propionics, such as Thr 185, Phe 193, Met 184 and Phe 98.

An interesting feature of both the vertical and parallel substrate orientations is that in either orientation the *para*-substituent contacts Tyr 96. One possible explanation of why *p*-methoxythioanisole shows higher stereoselectivity than any of the other substituents may be its ability to weakly hydrogen bond with the hydroxyl group of Tyr 96. This possibility could be tested by comparing sulfoxide stereochemistries of *p*-methoxythioanisole with the *p*-ethyl or *p*-formyl substituted sulfides, for example, or by comparing the native enzyme with the Y96F mutant enzyme.

4.3.2 F87A, F87W and Y96F

The MD simulations of thioanisole and *p*-methylthioanisole suggest that Phe 87 and Tyr 96 are important residues in determining the selectivity of the reaction because they directly contact the substrates as well as define the binding cleft for the *para*-substituent. There is also the possibility that Tyr 96 hydrogen bonds with *p*-methoxythioanisole. Hence, mutation of these two residues could have a significant effect on the stereo- and regioselectivity of the reaction.

Towards this end, the metabolism and sulfoxidation stereochemistry was analyzed for three P450$_{cam}$ mutants: one where Phe 87 is replaced by alanine (F87A), one where it is replaced by tryptophan (F87W) and one where Tyr 96 is replaced by phenylalanine (Y96F). In a simplistic model where the overall protein structure remains the same as that in the crystal structure, the F87A and Y96F mutations would be expected to open up space in the active site over the D and C rings of the heme, respectively, while the

F87W would be expected to decrease space in the active site over the D ring of the heme. These mutations should thus significantly affect the binding, and consequently the oxidation stereochemistry, of the thioanisoles.

Analysis of the sulfoxidation stereochemistry observed with these mutant enzymes reveals that both large and small changes in stereochemistry occur, and trends in the data are apparent for all but the *p*-methoxy analog (Table 4.2). F87A oxidation, for example, shows a 10-15% decrease in *S*-sulfoxide formation as compared to the native enzyme for all the substrates except for the *p*-methoxy analog, which is oxidized similarly to the native enzyme. The F87W mutation causes very little change in the sulfoxidation stereochemistry from the native enzyme (slight decrease in *S*-sulfoxide formation) except for the *p*-methoxy analog, which shows a large decrease (30%) in *S*-sulfoxide formation. The Y96F mutation causes a 15-35% increase in *S*-sulfoxide formation as compared to the native enzyme for all the substrates except, once again, the *p*-methoxy analog, which shows a 10% decrease in preference for the *S*-sulfoxide.

The trends observed in the data if the *p*-methoxy substituent is excluded suggest that, in general, mutations which decrease the size of the residue (F87A and Y96F) favor increased *S*-sulfoxide formation while mutations which increase the size (F87W) disfavor the *S*-sulfoxide. Attempts to translate these results into a picture of the substrate binding pocket in the mutant enzymes are complicated by the aberrant *p*-methoxy results as well as by heme arylation studies, which find that the changes predicted based on a static model of the protein do not explain the observed heme arylation patterns (Tuck *et al.*, in press; Tuck, S.F., Graham-Lorence, S. and Ortiz de Montellano, P.R., unpublished results).

Analysis of the N-aryl porphyrin isomers obtained with phenyl and biphenyl hydrazine and the F87A mutant enzyme suggest that this mutation, instead of increasing space over the D ring by shrinking the size of this residue, actually decreases the amount of D ring arylation relative to the C and A rings (Tuck *et al.*, in press). The heme arylation pattern obtained with the F87W mutant and phenyl hydrazine is not significantly different from the native enzyme; however, the reaction with the larger biphenyl hydrazine shows increased amounts of D ring arylation--not decreased amounts, as might be expected from the increased bulk of a tryptophan over the D ring of the heme (Tuck *et al.*, in press). The Y96F mutation also gives results contrary to those predicted. Thus, instead of increasing space over the C ring by shrinking the size of the amino acid side chain, this mutation decreases the amount of C ring arylation relative to the D ring (Tuck, S.F., Graham-Lorence, S. and Ortiz de Montellano, P.R., unpublished results).

The results of these experiments indicate that active site residues have moved relative to their positions in the native enzyme in response to the mutations. Although this is not surprising, it does make interpretation of the thioanisole results more difficult.

The mutation which appears to have caused the fewest changes in the active site topology is F87W. The small differences in sulfoxidation stereochemistry with this mutant as compared to the native enzyme for most of the thioanisoles are in agreement with the small changes observed in the phenyl (but not biphenyl) hydrazine shift studies, and in hydroxylation patterns determined for camphor, norcamphor and thiocamphor with the F87W mutant enzyme (Graham-Lorence, S. and Ortiz de Montellano, P.R., unpublished results). The finding that similar amounts of the *p*-hydroxymethyl metabolite are formed from *p*-methylthioanisole by

the F87W mutant as with the native enzyme (estimated at 10-15% of the sulfoxide) also suggests that the *p*-methyl analog binds similarly in the mutant and the native enzymes.

The one substrate that gives different results for the two enzymes is *p*-methoxythioanisole. Two features which distinguish the methoxy substituent from the others are that it is slightly larger and it is able to weakly hydrogen-bond. The size of the substituent could be a factor if the mutation causes a decrease in the size of the binding cleft between the two heme propionic side chains. This decrease in size cannot be so large that binding of *p*-methylthioanisole is affected, however. Another possibility is that the mutation affects residues at the top of the active site pocket, and binding of *p*-methoxythioanisole in a vertical position causes the substituent to interact with these residues, thus affecting the reaction stereochemistry. Evidence which suggests that the two active sites are different high up in the active site comes from heme arylation studies which find that shifts of the biphenyl-iron complex are sensitive to changes in the two enzymes while shifts of the phenyl-iron complex are not (Tuck *et al.*, in press).

Size alone cannot be the determining factor, however, as this would suggest that *p*-cyanothioanisole should show similar shifts in stereochemistry as *p*-methoxy with the mutant, and it does not. Hence, it seems probable that a combination of factors is involved, including hydrogen-bonding of the methoxy substituent with the Tyr 96 hydroxyl group. In either the "parallel" orientation, where the methoxy group binds in the cleft between the heme propionics, or the "vertical" orientation, where the substituent binds high in the active site, analysis of the substrate manually docked in the active site suggests that the methoxy group can interact with Tyr 96.

p-Methoxythioanisole sulfoxidation by the F87A mutant, on the other hand, shows very little change in stereoselectivity from the native enzyme. The other substituted and unsubstituted thioanisoles show slightly larger differences (10-15% increase in *S*-sulfoxide); however, the overall effect of the mutation on the sulfoxidation stereochemistry is surprisingly minor given the nonconservative nature of the mutation. It is interesting, for example, that the conservative mutation Y96F yields much larger stereochemical differences than the F87A mutation.

It would seem reasonable that the loss of a hydrophobic phenyl ring in a predominantly water-filled pocket should cause larger changes in local protein structure than the loss of a polar hydroxyl group. Mutation of Phe 87 to alanine would disrupt π-stacking interactions between Phe 87 and Tyr 96, and thus movement of Tyr 96 and other hydrophobic residues in this region of the active site is highly likely. However, the relatively small effect this mutation has on the reaction stereochemistry suggests that the net effect of this protein movement is to retain an active site topology much like that in the native enzyme. This assessment is upheld by phenyl and biphenyl hydrazine studies, which show that relatively small changes in arylation patterns occur with this mutant (Tuck *et al.*, in press).

The results of the Y96F mutation generally show a substantial increase in formation of the *S*-sulfoxide (15-35%) over the native enzyme. This could occur by either favoring *S*-sulfoxide formation or by disfavoring *R*-sulfoxide formation. *S*-Sulfoxide formation may be favored due to the changes in active site structure caused by this mutation. Heme arylation studies reveal more room is available over the D ring of the heme in this mutant (Tuck, S.F., Graham-Lorence, S. and Ortiz de Montellano, P.R., unpublished results), and this increase in space may favor binding to yield the *S*-sulfoxide.

Another possibility is that binding to give the *R*-sulfoxide is disfavored in the mutant. MD simulations of thioanisole bound in the P450$_{cam}$ active site suggest that binding to give *R*-sulfoxide formation is preferred because of favorable hydrophobic contacts between the substrate and Phe 87, Tyr 96, Val 247 and Val 244. Thus, one way to disfavor *R*-sulfoxide formation would be to break up these hydrophobic contacts. Although replacement of Tyr 96 with phenylalanine would be expected to increase the hydrophobicity in this region, it may be that the reduction in size of the residue permits a water molecule to bind where the hydroxyl group was, and that the presence of this water disfavors binding of the hydrophobic substrate in the *R*-sulfoxide orientation.

The trend for increasing *S*-sulfoxide formation with the Y96F mutant holds for all the thioanisoles except *p*-methoxy, which actually shows decreased formation of the *S*-enantiomer. The reversal of the trend seen with the other substrates, together with the fact that this mutation removes the hydrogen-bonding properties of Tyr 96, strongly suggests that hydrogen bonding between the methoxy substituent and Tyr 96 plays a role in determining the sulfoxidation stereochemistry of this substrate. The interpretation that hydrogen-bonding interactions with Tyr 96 promote formation of the *S*-sulfoxide is consistent with the greater preference for *S*-sulfoxide formation observed for the *p*-methoxy substrate as compared to the other thioanisoles in the native enzyme.

In sum, the stereochemistry studies of thioanisole sulfoxidation with the P450$_{cam}$ mutants F87A, F87W and Y96F indicate that the binding of these substrates is sensitive to mutation of these residues. Interpretation of the results, however, is complicated by apparent movement of active site residues in response to the mutations. The results suggest that the F87W

mutant is the most like the native enzyme. The F87A and Y96F mutations both caused increased formation of the *S*-sulfoxide, with the conservative mutation Y96F giving rise to greater changes in stereochemistry than the nonconservative mutation F87A. For all three mutant enzymes, the changes in oxidation stereochemistry of *p*-methoxythioanisole did not follow the trend for the other substrates, suggesting that hydrogen-bonding interactions, among others, may play a role in the binding of this substrate.

5.0 OXIDATION OF STYRENES AND THIOANISOLES BY MICROSOMAL AND BACTERIAL CYTOCHROMES P450

5.1 Introduction

Efforts to define the active site topologies of P450 enzymes whose crystal structures are not known has been an active area of interest in the P450 field. Sequence alignment studies which fit the mammalian sequences onto the P450$_{cam}$ template suggest that the structures of the mammalian enzymes are grossly similar to that of P450$_{cam}$, except for the presence of a membrane-binding domain at the amino-terminus of the mammalian proteins (Nelson and Strobel, 1989; Tretiakov *et al.*, 1989). Such alignments, however, do not give much detail concerning the differences between the P450 substrate binding pockets. Mutagenesis studies which indicate certain amino acid residues are important in determining substrate binding and specificity are also insufficient for definition of an active site without a protein framework from which to work.

Attempts to define an active site topology without foreknowledge of the protein tertiary structure or the relevant amino acid residues have utilized metabolite analyses and chemical modification of the heme. These techniques have painted pictures of individual P450 active sites based on accessibility of the given probe to the iron-oxo species, in the case of metabolite studies, or to one or more of the heme nitrogens, in the case of the heme modification studies. Although these elegant studies have suggested a distinct shape for individual active sites, they still leave unanswered the question of how does the shape of the active site determine substrate specificity.

133

The studies of substrate binding in P450$_{cam}$ described in the previous two chapters suggest that many factors play a role. The binding orientations of hydrophobic substrates small enough to occupy multiple orientations are controlled by complementary hydrophobic interactions. Making the substrate large enough such that it can no longer "bounce" around reveals clefts in the active site which can bind one end of the molecule, thus keeping it relatively fixed. The influence of hydrogen bonding and polar interactions was also suggested by these studies. Finally, the ability of the substrate to bind away from the iron-peroxo species and thus permit access of water to the ferryl oxygens is reflected in the amount of enzymatic uncoupling observed during catalysis.

The ability to extrapolate these results to P450 enzymes whose active sites are relatively unknown presents a new challenge. The P450 enzymes chosen for this study are the bacterial enzymes P450$_{terp}$ (P450108) and P450$_{BM-3}$ (P450103), and the microsomal enzyme P4502B1. These enzymes have vastly different substrate requirements--from terpenes to fatty acids to polycyclic drugs and steroids--and thus more or less represent the broad spectrum of P450 enzymes encountered in nature.

P450$_{terp}$ is a soluble enzyme purified from a *Pseudomonas* isolated by culture enrichment techniques for its ability to grow on α-terpineol as its sole carbon source (Peterson *et al.*, 1992). This enzyme shows significant sequence identity with P450$_{cam}$ (25%) and, similar to P450$_{cam}$, requires for its redox partners an iron-sulfur protein, terpredoxin, and an FAD-containing reductase, terpredoxin reductase (Peterson *et al.*, 1992). The ability of this enzyme to accept substrates other than α-terpineol is not known; however, the originating *Pseudomonad* will not grow on other monoterpenes such as

camphor, cymene, or linalool (Peterson *et al.*, 1992), raising the possibility that this enzyme may not be able to oxidize such substrates.

The product of the reaction of $P450_{terp}$ with α-terpineol is not known, nor are the ensuing steps in the catabolic breakdown of terpineol as a carbon source. Heme arylation studies of this enzyme using phenyl hydrazine find that only the D ring nitrogen can be arylated, suggesting that only the D ring of the heme is solvent accessible (Tuck *et al.*, 1992). The finding that the iron-phenyl complex is unstable in this enzyme is also consistent with the presence of protein residues in close proximity to the heme iron.

These results indicate that the active site of $P450_{terp}$ is one of the most restrictive examined so far by this technique, as it is the only one which gives only one N-phenyl isomer. Determination of the metabolite(s) of α-terpineol and the products obtained from oxidation of *para*-substituted styrenes and thioanisoles should provide additional information into how such an active site topology translates into reaction regio- and stereoselectivity.

$P450_{BM-3}$ is also a bacterial enzyme, isolated from *B. megaterium*, but it is significantly different from $P450_{terp}$ and $P450_{cam}$ both structurally and functionally. Sequence comparison studies indicate that this enzyme more closely resembles the hepatic fatty acid hydroxylases such as P4504A1 than any of the bacterial P450 enzymes (Ruettinger *et al.*, 1989). Substrate turnover studies confirm that this enzyme readily hydroxylates fatty acids of variable chain lengths at the ω-1, ω-2 and ω-3 positions (Narhi and Fulco, 1986; Boddupalli *et al.*, 1992). The fact that the redox partner of this enzyme is a flavoprotein, not an iron-sulfur protein, and requires NADPH as a cofactor further suggests this enzyme more closely aligns with the microsomal enzymes (Ruettinger *et al.*, 1989). However, $P450_{BM-3}$ is

135

distinguished by the fact that it is soluble rather than membrane-bound, and that the P450 and reductase enzymes are expressed as a single 115 kDa protein--the first time this has ever been observed for a P450 enzyme (Ruettinger *et al.*, 1989). These features make it a unique P450 enzyme which may serve as a convenient model for the mammalian enzymes.

The finding that $P450_{BM-3}$ can hydroxylate fatty acids containing up to 21 carbons suggests that the active site is quite accommodating (Narhi and Fulco, 1986; Boddupalli *et al.*, 1992). Studies of the formation of N-phenyl porphyrins from reaction of $P450_{BM-3}$ with phenyl diazene reveal that all the heme nitrogens can be arylated, although the A ring isomer is favored over the rest by a factor of 5 or so (Tuck *et al.*, 1992). These results suggest an active site which is relatively spacious but asymmetrical about the heme iron (see Figure 5.1).

P4502B1 is a microsomal P450 which is the primary P450 isozyme induced by phenobarbital in rat liver. The natural substrate for this enzyme
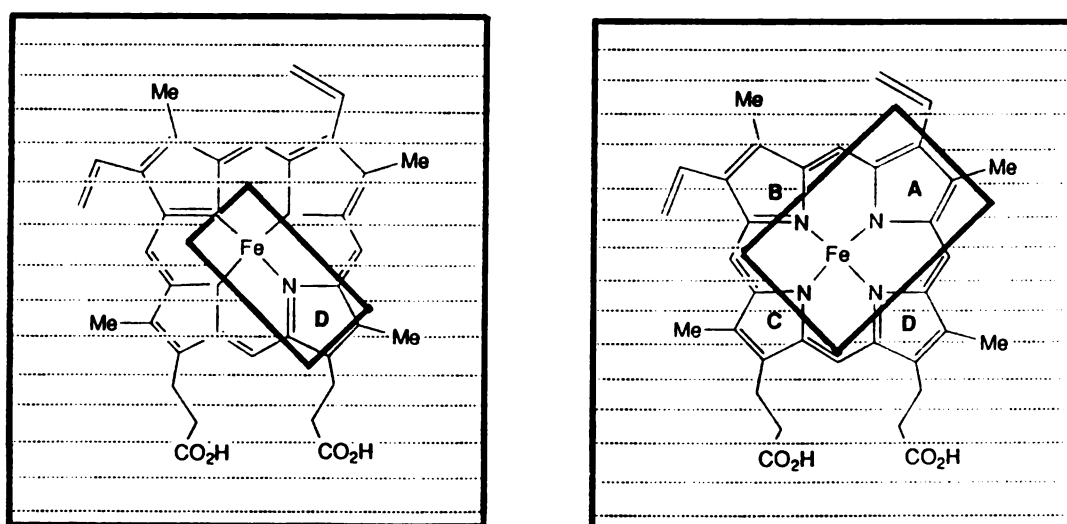
Figure 5.1: Models of the active site topologies of $P450_{terp}$ (left) and $P450_{BM-3}$ (right) based on the N-arylated porphyrins isolated from reaction of the enzymes with phenyl diazene (Tuck et al., 1992).

136

is unknown, but it has been found to show the greatest specificity for benzphetamine N-demethylation and hexobarbital 3-hydroxylation of any of the drug-metabolizing enzymes studied (Conney, 1986).

Attempts to define an active site for P4502B1 using phenyl, naphthyl and biphenyl hydrazines indicate the regions over the A and D rings are accessible to the probes (Swanson *et al.*, 1991; Tuck and Ortiz de Montellano, 1992). The finding that biphenyl but not naphthyl hydrazine can arylate the A ring nitrogen suggests that little lateral space is available over the A ring (Figure 5.2). This suggests that large substrates such as benzphetamine, aminopyrine, and testosterone cannot bind over this ring, and instead must bind over the D ring of the heme. This proposal is confirmed by substrate protection studies which found that binding of these substrates diminishes the amount of D ring arylation (Tuck and Ortiz de Montellano, 1992).
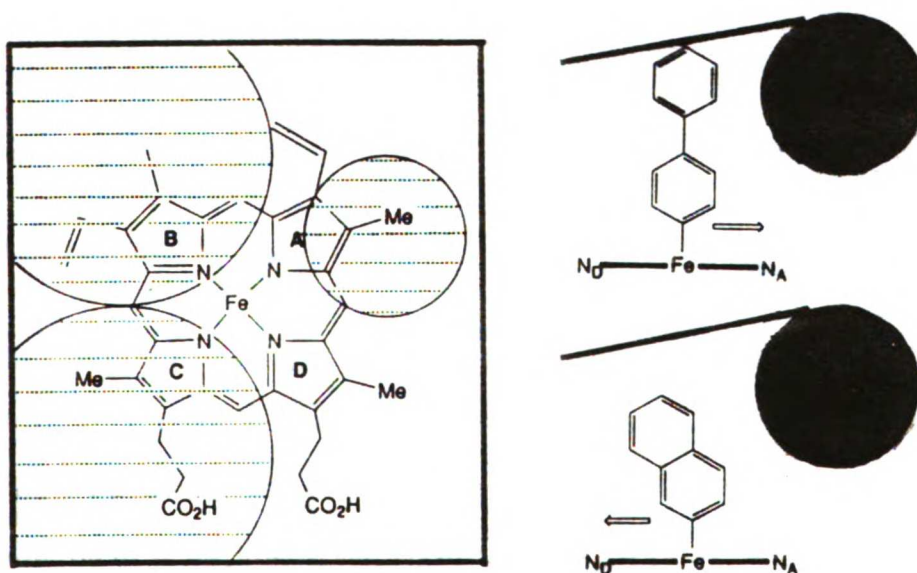
Figure 5.2: Model of the active site topology of P4502B1 based on the N-arylated porphyrins obtained from reaction of the enzyme with phenyl, naphthyl and biphenyl hydrazine (Tuck and Ortiz de Montellano, 1992).

These more recent studies are in agreement with earlier studies of heme alkylation in P4502B1 by terminal olefins and acetylenes which found that only the A and D rings of the heme are alkylated (Kunze *et al.*, 1983). These studies suggested that the alkyl chains bound over the C ring of the heme in order to properly orient acetylenes to alkylate the A ring and olefins to alkylate the D ring. Such a binding pocket cannot be ruled out if it is located over the protein residues which block alkyl- and arylation of the C ring nitrogen.

Taken together, the proposed active site topologies for $P450_{terp}$, $P450_{BM-3}$ and P4502B1 suggest very different binding pockets for the three enzymes. How a restrictive or spacious or asymmetric active site translates into reaction regio- and stereoselectivity is not immediately obvious from such studies. It is hoped that by analyzing the metabolites and reaction stereochemistries of a series of related compounds that a better understanding of the parameters involved in determining substrate specificity and reactivity is attained.

5.2   Results

5.2.1   Cytochrome $P450_{terp}$

Incubation of $P450_{terp}$ with its natural substrate α-terpineol (**1**) results in the formation of only one product which is dependent on the presence of the cofactor NADH (other peaks in the chromatogram are present as contaminants of α-terpineol; see Figure 5.3). That product (10-20 mgs) was purified from an incubation run by Julian Peterson and coworkers at the University of Texas Health Sciences Center in Dallas, and analyzed by NMR, mass spectrometry and GLC co-elution with authentic standards. The mass
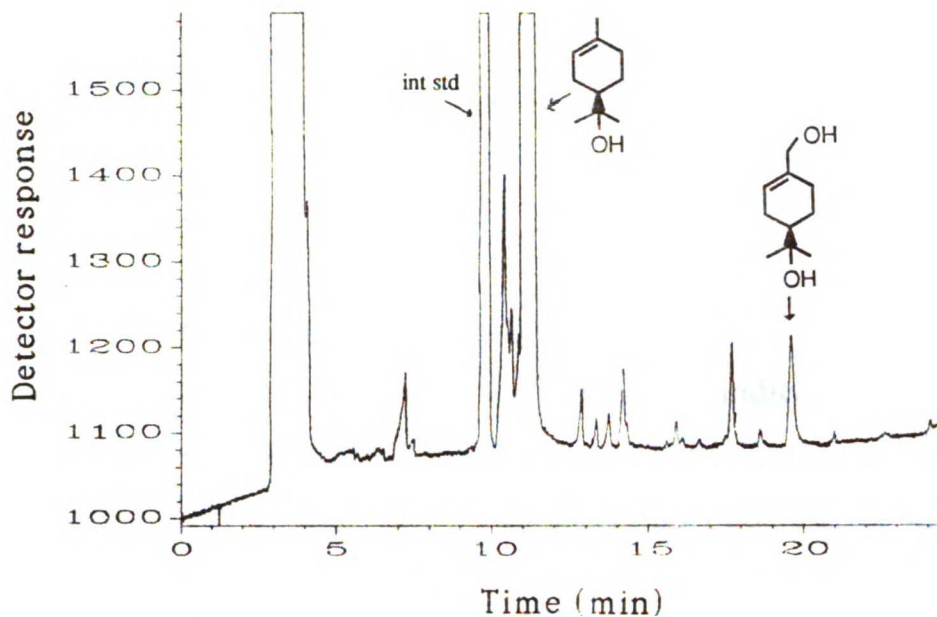
Figure 5.3: *GLC chromatogram of the metabolite formed in the reaction of* *P450${}_{terp}$ with α-terpineol. Unidentified peaks are contaminants in the α-terpineol sample.*

spectrum of the metabolite under EI conditions gives a molecular ion at m/z 170, equivalent to the molecular weight of terpineol plus an oxygen (see Table 6.2 in the Experimental Section for mass spectrometric data). This suggests the metabolite is either an alcohol or an epoxide.

The ^{1}H and ^{13}C NMR spectra are not consistent with the epoxide, however, nor do they match those published for uroterpenol (**2**) (Carman *et al.*, 1986). GLC analysis indicates that the metabolite does not co-elute with *trans*-6-hydroxyterpineol (**3**), another possibility. The GLC and NMR spectral data are consistent, however, with 7-hydroxyterpineol (**4**).

To confirm the identity of the metabolite as the 7-alcohol (**4**), 7-hydroxyterpineol was prepared from the reaction of β-pinene oxide and mercuric nitrate by the method of Bluthe and coworkers (Bluthe *et al.*, 1980). Comparison of the ^{1}H and ^{13}C NMR and mass spectral data with the P450${}_{terp}$

(1) (2) (3) (4)
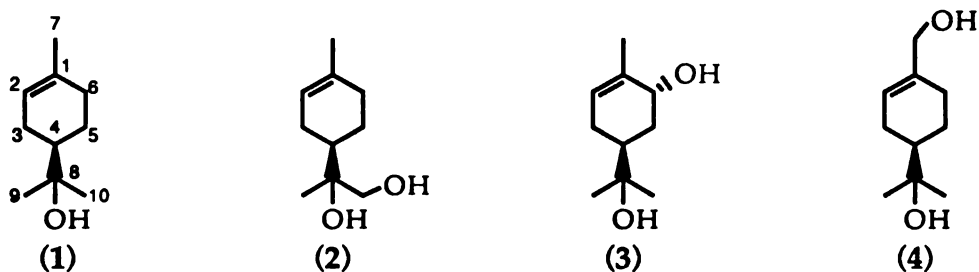
metabolite indicates the spectra are superimposible. GLC and TLC analysis of the metabolite and the synthetic 7-hydroxyterpineol indicates the two co-elute in both systems, further confirming the identity of the metabolite.

Incubation of P450$_{terp}$ with *para*-substituted thioanisoles, where the *para*-substituent is either a hydrogen, methoxy, chloro or cyano group, gives the corresponding sulfoxides as the primary products as evidenced by chiral HPLC analysis of the metabolites. The *p*-methoxythioanisole incubation gave several peaks in the HPLC chromatogram, but only the sulfoxide was positively identified by GLC/MS of the collected peaks. No evidence was found for the O-demethylated product.

P450$_{terp}$ incubations with *p*-methylthioanisole contrasts with those of the other thioanisoles in that the primary product of the reaction is not the sulfoxide but the *p*-hydroxymethyl sulfide. The hydroxylated product constitutes ~98% of the total product formed as determined by integration of the HPLC peaks for the sulfoxide and hydroxymethyl products (see Figure 5.4). This contrasts with the results for P450$_{cam}$, where the *p*-hydroxy metabolite constituted only 10-15% of the total product (Chapter 4). The large amount of the hydroxy product in the P450$_{terp}$ incubations presented some problems assaying the stereochemistry of the sulfoxides, as the hydroxymethyl product elutes very closely to the *S*-sulfoxide on the chiral HPLC column, and thus the large hydroxymethyl peak obscures the much
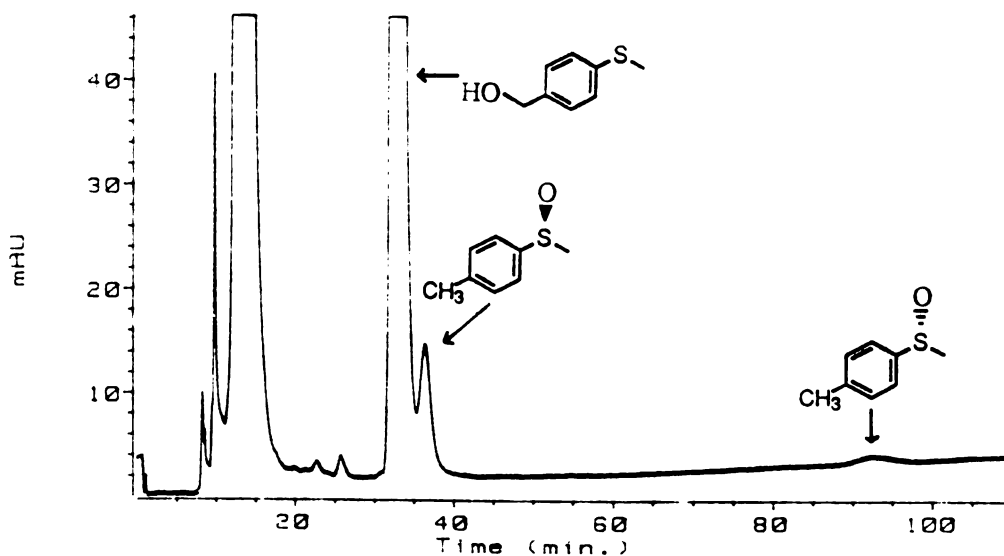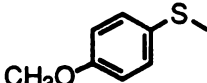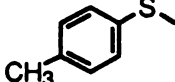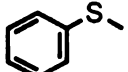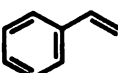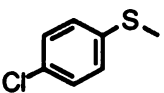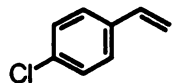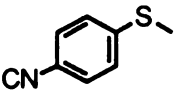
Figure 5.4: *Chiral HPLC chromatogram of the metabolites formed in the reaction of P450_terp with p-methylthioanisole.*

smaller sulfoxide peak. A slightly less polar solvent system was found necessary to separate the two peaks for adequate integration.

The results of the sulfoxidation stereochemistry assays, presented in Table 5.1, indicate that $P450_{terp}$ shows very high sulfoxidation stereoselectivity towards these substrates. In each case formation of the S-sulfoxide is favored, with the highest selectivities observed for the more electron-poor substrates.

Styrene and *p*-chlorostyrene are also stereoselectively oxidized by $P450_{terp}$ to predominantly the *R*-epoxide (Table 5.1). The slight increase in selectivity for the more electron-poor substrate suggests a similar trend to that observed with the thioanisoles; however, the greater uncertainty in these measurements due to the small size of the GLC peaks obscures such a trend.

141

Table 5.1: *Summary of the stereochemistry of oxidation of* p-substituted *thioanisoles and styrenes by* P450$_{terp}$.

Substrate	Sulfoxide stereochemistry ($R : S \pm 2$)	Substrate	Epoxide stereochemistry ($S : R \pm 3$)
CH$_3$O-C$_6$H$_4$-S (4-methoxythioanisole)	20 : 80		
CH$_3$-C$_6$H$_4$-S (4-methylthioanisole)	10 : 90		
C$_6$H$_5$-S (thioanisole)	5 : 95	styrene	12 : 88
Cl-C$_6$H$_4$-S (4-chlorothioanisole)	3 : 97	4-chlorostyrene	9 : 91
CN-C$_6$H$_4$-S (4-cyanothioanisole)	<1 : 99		
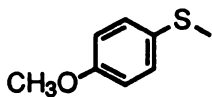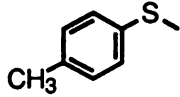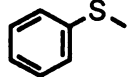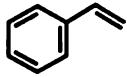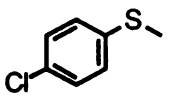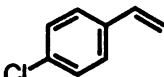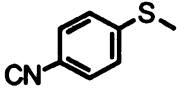
p-Methylstyrene is also epoxidized by P450$_{terp}$, and although the stereochemistry of the reaction could not be determined due to problems with the chiral GLC assay, normal-phase GLC analysis suggested that approximately equimolar amounts of the epoxide and a new metabolite, *p*-hydroxymethylstyrene, are formed. The *p*-hydroxymethyl product was identified by GLC/MS as both the BSTFA-derivatized and underivatized product. The derivatized product gave a molecular ion at m/z 206, consistent with *p*-hydroxymethylstyrene with one trimethylsilyl group attached, and a fragment ion at 117, suggesting loss of the OTMS group (mass spectrometric data is listed in Table 6.2 of the Experimental Section). *p*-Methylbenzaldehyde, as identified by GLC/MS, is also detected in these incubations, but in amounts much smaller than that observed with P450$_{cam}$ (~2-3% of the total product formation).

5.2.2 Cytochrome P450$_{BM-3}$

Incubation of P450$_{BM-3}$ with *para*-substituted thioanisoles and styrenes reveals that these substrates are turned over very rapidly by this enzyme—styrene is epoxidized, for example, ~100-fold faster by P450$_{BM-3}$ than by P450$_{cam}$. This is the fastest P450 that has been found with these substrates.

The product of P450$_{BM-3}$ turnover of *para*-substituted thioanisoles is exclusively the sulfoxide, and styrene is turned over solely to the epoxide. No *p*-hydroxymethyl products are observed for either *p*-methylthioanisole or *p*-methylstyrene, nor is any benzaldehyde observed with the styrene substrates. This latter result suggests very little uncoupling occurs during the oxidation reaction.

Table 5.2: Summary of the stereochemistry of oxidation of p-substituted thioanisoles and styrenes by P450$_{BM-3}$.

Substrate	Sulfoxide stereochemistry $(R : S \pm 1)$	Substrate	Epoxide stereochemistry $(S : R \pm 1)$
CH₃O	59 : 41		
CH₃	55 : 45		
	49 : 51		40 : 60
Cl	55 : 45	Cl	27 : 73
CN	50 : 50		

143

The results of the stereochemistry assays are summarized in Table 5.2. These results suggest that although these substrates are turned over well, little or no stereoselectivity is observed for the thioanisoles. The styrenes show slightly higher selectivities; however this is still less in general than $P450_{cam}$ and much less than $P450_{terp}$, the other two bacterial enzymes studied.

5.2.3   Cytochrome P4502B1

Incubation of *para*-substituted thioanisoles and styrenes with P4502B1 reveals that these substrates are oxidized to the corresponding sulfoxides and epoxides, respectively. Very little hydroxymethyl metabolite is formed from *p*-methylthioanisole (<1% of sulfoxide as determined from the chiral HPLC traces). Neither the formation of *p*-hydroxymethylstyrene from *p*-methylstyrene nor the formation of benzaldehyde from any of the styrenes was determined.
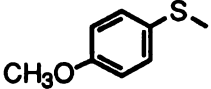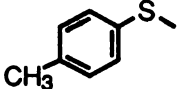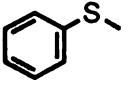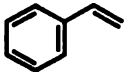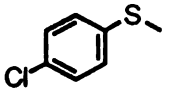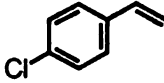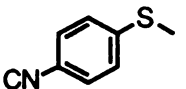
The results of the stereochemistry assays are summarized in Table 5.3. The selectivity of the reaction was found to depend on the identity of the *para*-substituent, with the lowest selectivities observed for the unsubstituted substrates.

5.3   Discussion

5.3.1   Cytochrome $P450_{terp}$

$P450_{terp}$ oxidation of α-terpineol yields 7-hydroxyterpineol as the sole metabolic product. Hydroxylation at this position is not unexpected, as hydrogen abstraction to form a radical at this carbon would be favorable due

Table 5.3: *Summary of the stereochemistry of oxidation of* p-*substituted thioanisoles and styrenes by P4502B1.*

Substrate	Sulfoxide stereochemistry $(R:S \pm 1)$	Substrate	Epoxide stereochemistry $(S:R \pm 1)$
	28 : 72		
	20 : 80		
	38 : 62		64 : 36
	6 : 94		17 : 83
	7 : 93		

to allylic delocalization and stabilization of the radical intermediate. However, delocalization of the radical center would suggest that other hydroxylated products, namely 2- and 6-hydroxyterpineol, would also be formed. Such products are observed, for example, in the hydroxylation of cyclohexene (Groves and Subramanian, 1984). The finding that only one product is formed suggests that protein residues in the active site restrict access of the 2- and 6-positions to the ferryl oxygen. The fact that terpineol is hydroxylated at a sterically unencumbered end of the molecule also suggests that the substrate channel to the ferryl oxygen is highly restrictive and does not allow presentation of highly substituted carbon centers to the ferryl oxygen.

Heme arylation studies of P450$_{terp}$ using phenyl hydrazine indicate that only ring D of the heme is exposed to the probe (Tuck *et al.*, 1992). These

results suggest that the P450$_{terp}$ active site is smaller than in other P450s, which, in general, show nitrogen arylation of at least two heme nitrogens (Swanson *et al.*, 1991; Tuck *et al.* 1992; Tuck and Ortiz de Montellano, 1992). The finding that only the D ring of the heme is accessible suggests that the substrate binding pocket is located over the D ring.

The results of the thioanisole and styrene stereochemistry studies reveal that the restrictive binding pocket in P450$_{terp}$ not only exerts control over the regiochemistry of the reaction, but the stereochemistry of the reaction as well. The extremely high stereoselectivities observed particularly for *p*-chloro- and *p*-cyanothioanisoles suggest very limited binding orientations are available to these substrates.

The trend that higher selectivities are observed for substrates which are electron-poor suggests that the electronic properties of the substrate play a role in the reaction. Indeed a plot of % *S*-sulfoxide versus sigma$^+$, a parameter which indicates the relative degree of charge stabilization by the *para*-substituent for a positively-charged transition state (Ritchie and Sager, 1964), suggests a linear relationship between the two (Figure 5.5).

Such an effect may be envisioned where the degree of electron-richness or poorness of the sulfur is reflected in the length of the sulfur-oxygen bond in the transition state of the reaction. This difference is then translated into a stereochemical difference by an active site which is asymmetric about the ferryl oxygen. Steric interactions, for example, could disfavor the binding of a long-bond transition state in a particular orientation while having little effect on the same orientation for a short-bond transition state.

Such a scenario would suggest highly restrictive binding pockets for either the phenyl ring or the sulfur methyl group, or both. The fact that
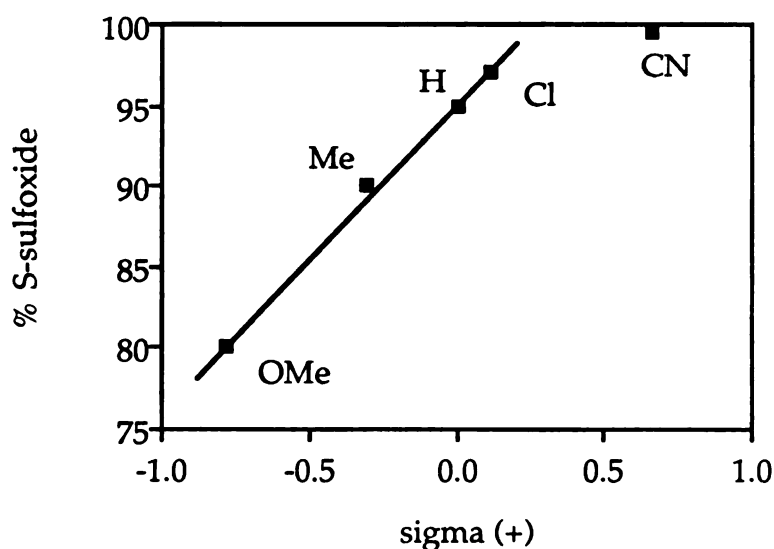
Figure 5.5: *Hammett plot of the % S-sulfoxide formed by P450$_{terp}$ versus σ^+.*

P450$_{terp}$ overwhelmingly favors hydroxylation of p-methylthioanisole at the p-methyl group over the much easier sulfur oxidation suggests that access of the bulkier SCH$_3$ group to the ferryl oxygen is hindered. This suggests that the binding pocket for the SCH$_3$ group is tighter than that for the phenyl ring, and it may be protein-substrate interactions with this group that dictates the reaction stereochemistry.

The finding that p-chlorostyrene, but not styrene, is preferentially oxidized to the R-epoxide (which has the same relative configuration as does the S-sulfoxide of thioanisole) suggests that the interactions governing the binding of p-chlorostyrene are similar to those determining the thioanisoles. Styrene, on the other hand, shows the opposite preference to all the other substrates studied. Why styrene is different is not clear. It may be that its small size and lack of polar groups permits it to bind differently than all the other substrates.

The small amounts of benzaldehyde formed with the styrene substrates indicates that some uncoupling occurs during the oxidation of these substrates; however, this uncoupling is much less than that observed with P450$_{cam}$. This suggests that the substrate channel to the iron-oxo species is long as well as narrow, allowing the styrenes to bind far enough away from the heme to permit water to reach the ferryl-dioxygen species and thus promote uncoupling. A picture of the active site of P450$_{terp}$ based on the results presented here is shown in Figure 5.6.
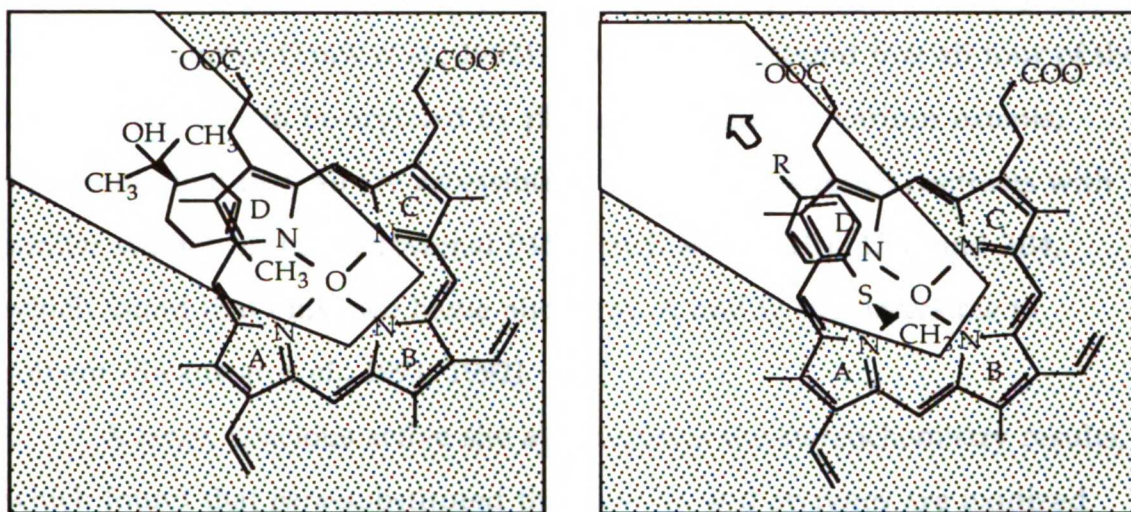
Figure 5.6: *Depiction of the active site of P450$_{terp}$ with (a) α-terpineol or (b) a para-substituted thioanisole bound. The orientations of the substrates shown are those which give the identified metabolites. The open arrow in (b) indicates possible mobility of styrene or thioanisole in the binding pocket such that uncoupling can occur.*

5.3.2 Cytochrome P450$_{BM-3}$

The results obtained with another bacterial P450, P450$_{BM-3}$, contrast sharply with those from the P450$_{terp}$ studies. This enzyme readily oxidizes *para*-substituted thioanisoles and styrenes to the corresponding sulfoxides and epoxides, respectively, but with little or no stereoselectivity. The failure

to detect benzaldehyde or *p*-chlorobenzaldehyde in styrene and *p*-chloro-styrene incubations, respectively, indicates that turnover of these substrates is also highly efficient, with little or no uncoupling of the oxidative reaction. The rapid and efficient turnover of these substrates is somewhat surprising considering this enzyme is proposed to be a fatty acid hydroxylase based both on sequence identity with P4504A1 and its high turnover of fatty acids (Ruettinger *et al.*, 1989; Narhi and Fulco, 1986; Boddupalli *et al.*, 1990).

The ability of this enzyme to accommodate a wide variety of substrates is most likely due to its relatively spacious active site as revealed by phenyl hydrazine studies (Tuck *et al.*, 1992). These studies found that all four of the heme nitrogens can be arylated by phenyl hydrazine to various extents, suggesting that they all are accessible to solvent. This result contrasts with similar studies of the microsomal P450s such as P4502B1, 1A1, and 2B4, which found that only two heme nitrogens, A and D, are accessible to solvent (Swanson *et al.*, 1991; 1992).

A large, spacious active site also explains the stereochemistry results, which found that *para*-substituted thioanisoles and styrenes are oxidized with little or no stereoselectivity. The finding from the phenyl hydrazine studies that the A ring nitrogen was preferentially alkylated over the other three suggests there is some chirality to the active site (Tuck *et al.*, 1992); however, little of that is reflected in the thioanisole sulfoxidations. The styrene epoxidations show slightly higher stereoselectivities, similar to what was seen with P450$_{cam}$, and that may reflect stronger hydrophobic interactions of these substrates with residues in the enzyme active site.

A large, spacious active site does not appear to be consistent with highly efficient enzymatic turnover of small substrates such as styrene and thioanisole based on the observations with P450$_{cam}$. Molecular dynamic

simulations of styrene and thioanisole in the $P450_{cam}$ active site suggested that these substrates have significant mobility in the active site, and this, together with their small size, may permit water to access the iron-peroxo species and thus promote uncoupling of the oxidative reaction (Chapter 3). Since very little uncoupling is observed with $P450_{BM-3}$, the protein active site, although large enough to accommodate much bigger substrates, must somehow bind small substrates in a way which prevents access of water to the iron-dioxygen species, or in some other manner prevent uncoupling. The question of how it accomplishes such a feat may be revealed when the crystal structure of this enzyme is published sometime in the near future.

5.3.3   Cytochrome P4502B1

Analysis of a microsomal P450, P4502B1, reveals that it oxidizes *para*-substituted thioanisoles and styrenes very rapidly to the corresponding sulfoxides and epoxides, respectively, in a manner intermediate in selectivity between the two bacterial enzymes--i.e., it is not as selective as $P450_{terp}$, but is more so than $P450_{BM-3}$. The stereoselectivity observed depends to a large extent on the identity of the substituent, but in all cases the same enantiomer, either the *S*-sulfoxide or *R*-epoxide, is favored.

The finding that the unsubstituted substrates show the lowest stereoselectivity of the group indicates that a *para*-substituent helps to increase the reaction stereoselectivity. This could be accomplished by either increasing favorable interactions in the preferred orientation or by decreasing affinity for the unpreferred orientation. Since all the *para*-substituents, whether polar or hydrophobic, increase the reaction stereoselectivity, a steric factor is most likely involved. This is probably not the only factor involved, however, as each substituent affects the reaction

stereoselectivity to varying degrees independent of the absolute size of the substituent.

Previous efforts to depict an active site topology for P4502B1 using heme alkylation have revealed that two of the heme nitrogens, A and D, can be alkylated (Kunze et al., 1983) or arylated (Tuck and Ortiz de Montellano, 1992), and thus are accessible to solvent. Substrate protection studies indicate that the extent of D ring arylation is decreased in the presence of benzphetamine, aminopyrine and testosterone, suggesting that these substrates bind in a pocket over the D ring of the heme. The fact that P4502B1 only oxidizes large substrates at sterically unencumbered positions at the ends of the molecule (eg, the 16 and 17 positions of testosterone; see Figure 1.14) is consistent with a binding pocket where a majority of the substrate extends beyond the D ring of the heme.

Fitting para-substituted thioanisoles and styrenes into such a model predicts that these small substrates will bind similarly to the larger ones in that the para-substituted phenyl ring would bind over the D ring of the heme (Figure 5.7). Such an orientation would yield the S-sulfoxide of thioanisole and the R-epoxide of styrene, which are the enantiomers preferentially formed by this enzyme (Table 5.3).

The finding that little or no p-hydroxymethyl product is observed with p-methylthioanisole suggests that the SCH_3 group is not sterically hindered from binding near the iron-oxo species, such as is proposed to be the case for $P450_{terp}$. In P4502B1, the A ring of the heme is found to be accessible, unlike it is in $P450_{terp}$, and thus binding of the SCH_3 group over this heme ring imposes fewer restrictions on the availability of the sulfur to the iron-oxo species than does the active site of $P450_{terp}$ (see Figure 5.7).
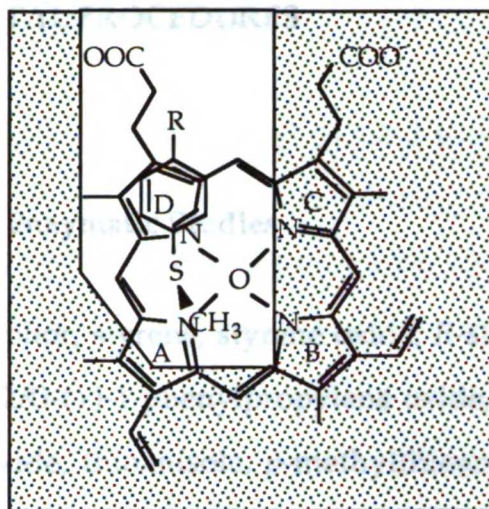
Figure 5.7: *Depiction of the active site of P4502B1 with a para-substituted thioanisole bound in the orientation which would give the S-sulfoxide.*

6.0 EXPERIMENTAL PROCEDURES

6.1 Materials

6.1.1 Reagents for Enzymatic Studies

(1R)-(+)-Camphor, styrene, styrene oxide, R-styrene oxide, trans-β-methylstyrene, (1R,2R)-(+)-1-phenylpropylene oxide, (1S,2S)-(-)-1-phenylpropylene oxide, thioanisole, p-methylthioanisole, p-methoxythioanisole, p-nitrothioanisole, methyl phenyl sulfoxide, p-chlorostyrene, p-methylstyrene, β-pinene oxide, mercuric nitrate, sodium perchlorate and m-chloroperbenzoic acid were purchased from Aldrich Chemical Co. p-Chlorothioanisole and p-cyanothioanisole were obtained from Lancaster Research Chemicals. BSTFA, NADH, NADPH, hydrogen peroxide (30% solution) and catalase were purchased from Sigma. Cis-β-methylstyrene was obtained from K & K Laboratories. ^{18}O-Labeled water was purchased from ICON. Ammonium thiocyanate and ferrous ammonium sulfate were purchased from Fisher. DLPC was from Serdary Research Laboratories (Ontario, Canada). (1R,2S)-(-)-1-Phenylpropylene oxide and (1S,2R)-(+)-1-phenylpropylene oxide, as a 70:30 mixture of the (+) and (-)-enantiomers respectively, were a gift from Dr. Thomas Kodadek (University of Texas, Austin). The 5-exo-hydroxycamphor standard was provided by Dr. Julian A. Peterson (University of Texas Health Sciences Center, Dallas). All chemicals were used without further purification except for the olefins, which were purified by silica gel chromatography with pentane as solvent immediately prior to each experiment.

6.1.2 Enzyme Purification Materials

Whatman DE-52 anion exchange column material was purchased from Fisher. BioGel P-100 size exclusion column material was from BioRad Laboratories. Sephacryl S-200-HR size exclusion column material was from Pharmacia. Buffer reagents--monobasic and dibasic potassium phosphates and MOPS--were obtained from Sigma. β-Mercaptoethanol and glycerol were from BioRad and Aldrich, respectively. DTPA, EDTA and DTT were purchased from Sigma.

6.1.3 Enzymes

Enzymes used in this study whose purifications are not discussed are the $P450_{cam}$ mutants F87A, F87W and Y96F (purified by Dr. Sandra Graham-Lorence or the author following the procedure described for $P450_{cam}$), P4502B1 (purified by Dr. Steven Tuck), P450-NADPH-reductase (purified by Dr. Tuck and the author), $P450_{BM-3}$ and $P450_{terp}$ (purified by Dr. Julian Peterson and coworkers, University of Texas Health Sciences Center, Dallas). The expression of the $P450_{cam}$ mutants was done by Dr. Graham-Lorence (Tuck *et al.*, in press), and $P450_{BM-3}$ and $P450_{terp}$ were expressed by Dr. Peterson and coworkers (Boddupalli *et al.*, 1990; Peterson *et al.*, 1992).

6.2 Instruments

Gas-liquid chromatography was carried out on a Hewlett Packard 5890A gas chromatograph equipped with a flame ionization detector and either a Hewlett Packard 3390A integrator or interfaced to a Hewlett Packard 3365 Chemstation (DOS series). High pressure liquid chromatography was

performed on a system consisting of a Hewlett Packard 9153C controller, a Hewlett Packard diode-array detector, and either two Beckman Model 110A pumps or a Varian 9010 solvent delivery system. Mass spectra were obtained on a VG-70 mass spectrometer equipped with a Hewlett Packard 5890A gas chromatograph. ^{1}H and ^{13}C NMR spectra were obtained using a General Electric GN-300 MHz spectrometer (chemical shift values are reported in parts per million). Measurements of electronic spectra were performed on Hewlett Packard 8450A and 8452A diode array spectrophotometers and on an Aminco DW-2000 UV/vis spectrophotometer. Oxygen consumption was determined using a Gilson 5/6 Oxygraph with a Clark electrode and connected to a Fisher constant temperature bath. Computer graphics pictures were obtained using the MidasPlus Software System at UCSF (Ferrin *et al.*, 1988), and solvent accessible surfaces were calculated using the method of Connolly (Connolly, 1983).

6.3   Protein Purification

P450$_{cam}$, putidaredoxin and Pd reductase have been purified from *P. putida* and as the recombinant enzymes expressed in *E. coli*. The original purification procedure developed in this laboratory, as well as the *P. putida* cell growth and induction by camphor, was adapted from that of Gunsalus and Wagner (1978). Once the recombinant enzymes became available in our laboratory, the procedure was modified to purify these enzymes from the *E. coli* system. The final purification procedure detailed here for the recombinant enzymes is much shorter than the original Gunsalus and Wagner procedure, involving only two columns and ammonium sulfate fractionation to purify each enzyme to relative homogeneity.

The buffers used in the purifications are described in Table 6.1. The Tris and potassium phosphate buffers were prepared from 1 M stocks at pH 7.4 and 7.0, respectively, determined at room temperature. Camphor was added from a saturated solution (~8 mM), DTT was added from a 0.5 M stock solution, and β-mercaptoethanol and glycerol were added neat. Column materials were prepared as described by the manufacturers.

Table 6.1: Buffers used to purify P450$_{cam}$, putidaredoxin and Pd reductase.

Enzyme purified	Buffer name	Buffer contents
P450$_{cam}$	Buffer T	50 mM Tris·Cl, pH 7.4
	Buffer P	20 mM KPi, pH 7.0 100 μM camphor 0.5 mM DTT
	Buffer P-100, P-200, etc.	+ 100 mM KCl, 200 mM, etc.
Putidaredoxin	Buffer T$_{me}$	50 mM Tris·Cl, pH 7.4 10 mM β-mercaptoethanol
	Buffer T$_{me}$-100, -200, etc.	+ 100 mM KCl, 200 mM, etc.
Pd Reductase	Buffer T$_g$	50 mM Tris·Cl, pH 7.4 5% glycerol
	Buffer T$_g$-100, -200, etc.	+ 100 mM KCl, 200 mM, etc.

6.3.1 Cytochrome P450$_{cam}$

Typically three or four liters of *E. coli* cells which express the recombinant protein are grown up at 30 °C for 24-36 hours or until P450 expression is essentially complete. Expression of P450$_{cam}$ is easily detected by

spinning down a small aliquot of the cells and examining the pellet for a pinkish-red color.

The cells are harvested by centrifugation at 6,000 xg for 20 minutes at 4 °C. The pellets, which can be frozen at this point, are resuspended in 200-300 ml of cold Buffer T containing 50 µg RNase, 1 mM PMSF and 1 mM EDTA, then lysed using the Bead Beater apparatus (Biospec Products, Bartlesville, OK) in 3 x 1-minute pulses with one minute rest in between. The cell debris is pelleted by centrifugation at 15,000 xg for 1 hour at 4 °C.

The cell extract is then subjected to ammonium sulfate precipitation in two steps. The clear, reddish supernatant is placed in a beaker on ice, to which 200 g/L $(NH_4)_2SO_4$ (~36% saturation) is slowly added over a 30-minute period. This is allowed to stir for 30 minutes more at 0 °C, and then is centrifuged at 15,000 xg for 30 minutes at 4 °C. The reddish supernatant is poured back into the beaker on ice, and 140 g/L $(NH_4)_2SO_4$ (~60% saturation) is slowly added over a 30-minute period. This is allowed to stir for 30 minutes more at 0 °C and then is centrifuged at 15,000 xg for 30 minutes at 4 °C. The pellet is resuspended in Buffer P and dialyzed overnight at 4 °C against a total of 8 L Buffer P with one buffer change.

The next day the protein is loaded onto a Whatman DE-52 anion exchange column (2.5 x 30 cm) equilibrated in Buffer P and run under gravity (1-2 ml/min) at 4 °C. After loading, the column is washed with Buffer P-100 until the reddish-brown P450 band, initially bound near the top of the column, begins to spread and move down the column (requires ~200 ml of Buffer P-100). At this point, a linear salt gradient is begun starting at 100 mM KCl and finishing at 500 mM KCl (total volume of the gradient is 500 ml). $P450_{cam}$ typically elutes between 200 and 300 mM KCl. A profile of the

column eluant monitored at 280 and 391 nm (the absorbance maxima of the camphor-bound enzyme) is shown in Figure 6.1.

The next day the P450-containing fractions from this column are pooled and concentrated using an Amicon Ultrafiltration cell to less than 20 ml. The deep-red sample is then loaded onto a Sephacryl S-200-HR column (2.5 x 90 cm) equilibrated in Buffer P at 4 °C. The column is developed with the equilibration buffer under gravity (~0.5 ml/min).

The importance of having DTT in the buffers is realized at this step, as without it sometimes a second "P450" peak is observed which elutes just before the main P450 peak. The earlier retention time suggests it runs as a higher molecular weight protein; however, analysis of the protein by SDS PAGE shows no molecular weight bands higher than $P450_{cam}$ (MW 45 kDa). The addition of DTT to the buffers eliminates this problem. An elution profile of this column without DTT present is shown in Figure 6.2.

Generally no more purification is needed after this column. Occasionally a second DE-52 column is needed when the $P450_{cam}$ fractions are not clean by SDS gel. The column used is approximately the same size as the first (2.5 x 26 cm) and is equilibrated in Buffer P at 4 °C. A longer, shallower linear gradient is run from 0 mM KCl to 300 mM KCl (gradient volume is 1000 ml) to elute the proteins. The only time this column was used was when a BioGel P-100 column was run in place of the Sephacryl S-200-HR column. The Sephacryl column is much better at purifying 40-50 kDa proteins than the BioGel P-100, and hence the former column is preferred for purification of $P450_{cam}$ and Pd reductase (MW ~42 kDa). The BioGel P-100 column, on the other hand, works well for putidaredoxin purification (MW ~17 kDa; see Section 6.3.2).

Figure 6.1: *DE-52 column elution profile observed for P450$_{cam}$ monitored at both 280 and 391 nm. Arrows indicate the limits of combined column effluent.*

Figure 6.2: *Sephacryl S-200-HR column elution profile observed for P450$_{cam}$ monitored at both 280 and 391 nm. Arrows indicate the limits of combined column effluent.*

To store the protein, the pure P450$_{cam}$ fractions as judged by SDS PAGE are pooled and the concentration is determined by comparison of the reduced CO-bound protein with the reduced protein ($\varepsilon_{446\text{-}490}$ = 93 mM^{-1} cm^{-1}). The concentration is then adjusted to a suitable stock concentration (generally 20 µM), aliquoted into eppendorf tubes and stored at -70 °C. Typical yields of purified recombinant P450$_{cam}$ from three liters of cells are ~1 µmole, or ~50 mg of protein. A typical spectrum and a gel of the purified, camphor-free protein are shown in Figures 6.3 and 6.10, respectively.

Figure 6.3: Spectrum of purified, camphor-free recombinant P450$_{cam}$.

6.3.2 Putidaredoxin

The basic protocol for putidaredoxin purification is very similar to that for P450$_{cam}$. Typically three or four liters of E. coli cells which express the recombinant protein are grown up at 30 °C for 36 hours or until

putidaredoxin is suitably expressed. Expression is detected by spinning down a small aliquot of the cells and examining the pellet for a dark brown color.

The cells are harvested by centrifugation at 6,000 xg for 20 minutes at 4 °C. The pellets, which can be frozen at this point, are resuspended in 200-300 ml of cold Buffer T_{me} containing 50 µg RNase, 1 mM PMSF and 1 mM EDTA, then lysed using the Bead Beater apparatus in 3 x 1-minute pulses with one minute rest in between. The cell debris is pelleted by centrifugation at 15,000 xg for 1 hour at 4 °C.

The cell extract is then subjected to ammonium sulfate precipitation. The clear, brown supernatant is placed in a beaker on ice, to which 560 g/L $(NH_4)_2SO_4$ (~85% saturation) is slowly added over a 30-minute period. This is allowed to stir for 30 minutes more at 0 °C and then is centrifuged at 15,000 xg for 30 minutes at 4 °C. The pellet is resuspended in Buffer T_{me} and dialyzed overnight at 4 °C against a total of 8 L Buffer T_{me} with one buffer change. Although only one cut was typically performed with success for putidaredoxin, it would be prudent to add an earlier cut (eg, 200 g/L, or ~35% saturation) to effect greater purification and bring down residual RNA and other contaminants.

The next day the protein is loaded onto a Whatman DE-52 anion exchange column (2.5 x 30 cm) equilibrated in Buffer T_{me} and run under gravity (1-2 ml/min) at 4 °C. After loading, the column is washed with Buffer T_{me}-50 until the brown putidaredoxin band, initially bound in a tight band at the top of the column, begins to spread and move down the column (requires ~200 ml of Buffer T_{me}-50). At this point, a linear salt gradient is begun starting at 50 mM KCl and finishing at 500 mM KCl (total volume of the gradient is 500 ml). Putidaredoxin typically elutes very late in the

gradient, at ~400 mM KCl. A profile of the column eluant is shown in Figure 6.4.

The next day the putidaredoxin-containing fractions from this column are pooled and concentrated using an Amicon Ultrafiltration cell to ~10 ml. The deep-brown sample is then loaded onto a BioGel P-100 column (2.5 x 90 cm) equilibrated in Buffer T_{me} at 4 °C. The column is developed with the equilibration buffer under gravity (~0.5 ml/min). An elution profile of this column is shown in Figure 6.5.

To store the protein, the pure putidaredoxin fractions as judged by SDS PAGE are pooled and the concentration is determined spectroscopically from the absorption at 416 nm (ϵ_{416} = 11.1 mM^{-1} cm^{-1}). The concentration is then adjusted to a suitable stock concentration (generally 100 μM), aliquoted into eppendorf tubes and stored at -70 °C. Typical yields of purified recombinant putidaredoxin from three liters of cells are ~1 μmole, or ~20 mg
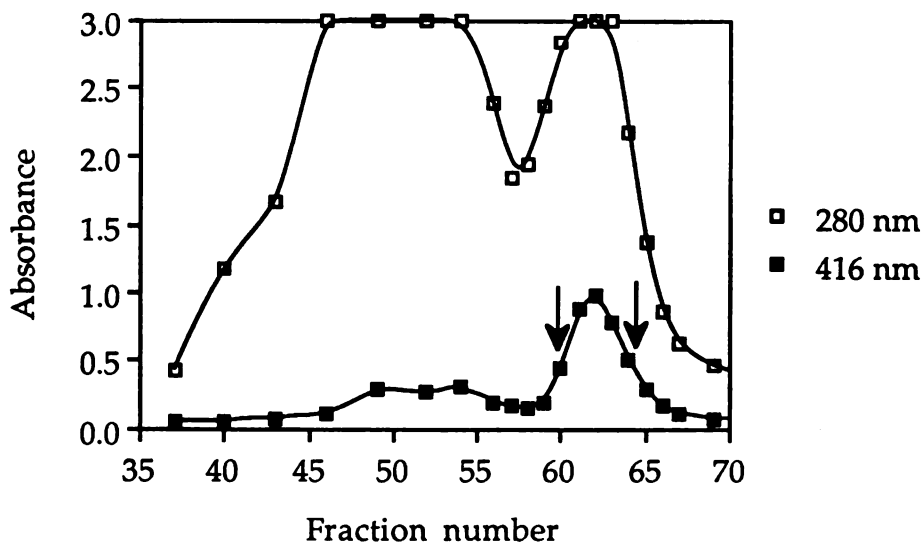
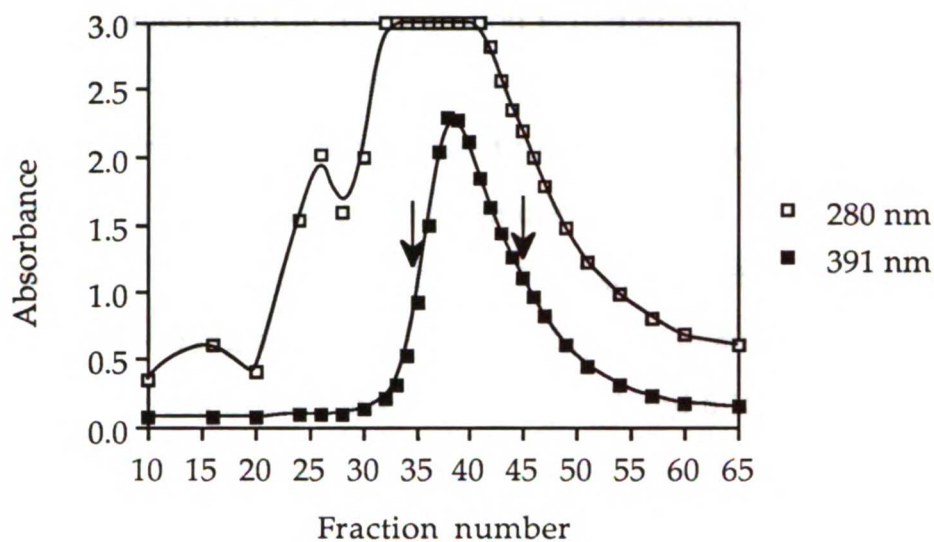*Figure 6.4:* DE-52 column elution profile observed for putidaredoxin monitored at both 280 and 416 nm. Arrows indicate the limits of combined column effluent.
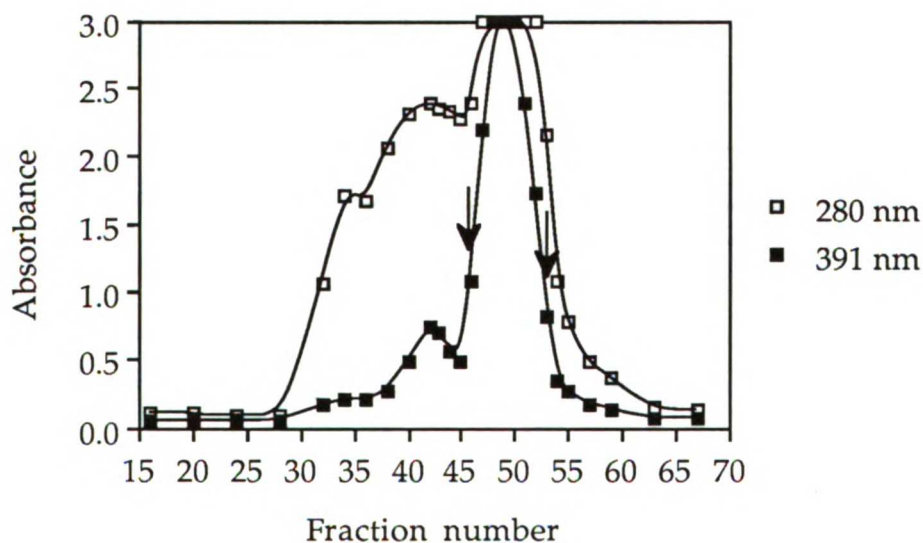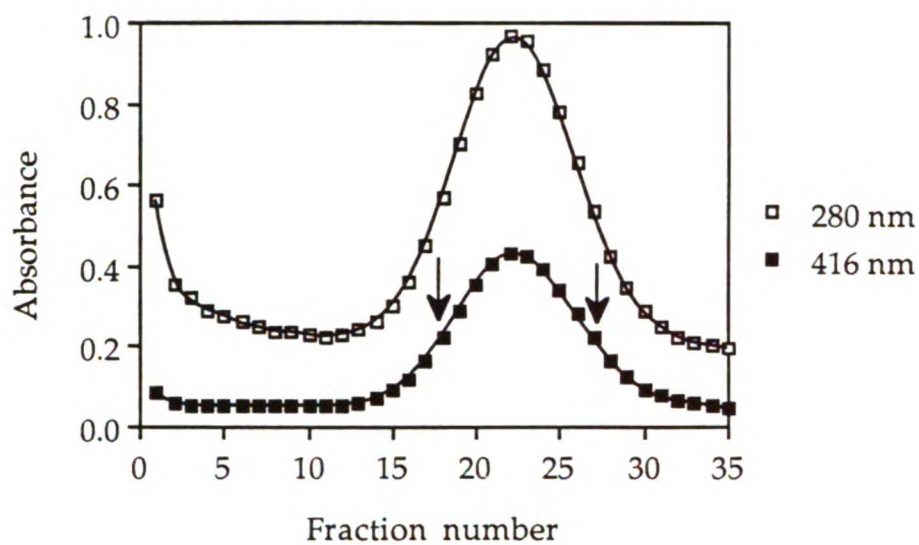
Figure 6.5: *BioGel P-100 column elution profile observed for putidaredoxin monitored at both 280 and 416 nm. Arrows indicate the limits of combined column effluent.*
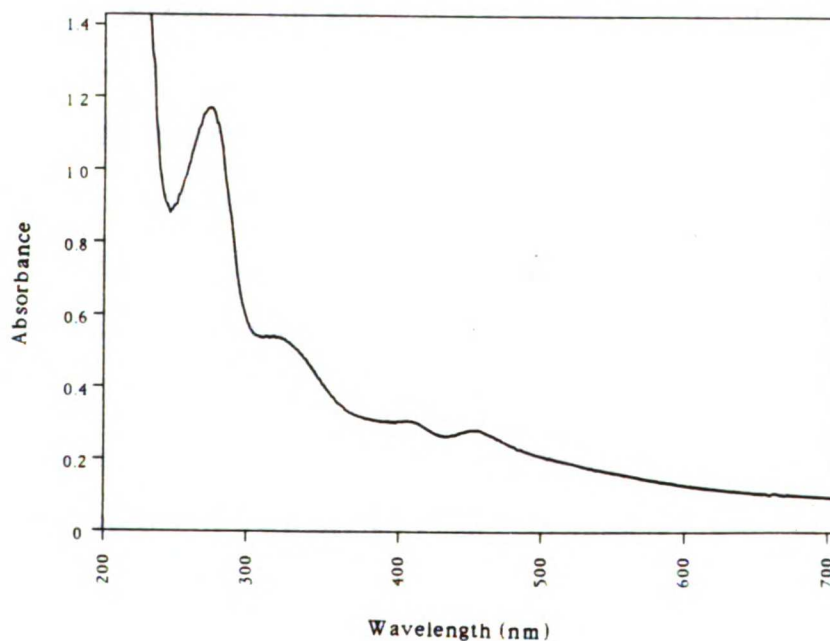
Figure 6.6: *Spectrum of purified recombinant putidaredoxin.*

of protein. A typical spectrum and a gel of the purified protein are shown in Figures 6.6 and 6.10, respectively.

6.3.3 Putidaredoxin Reductase
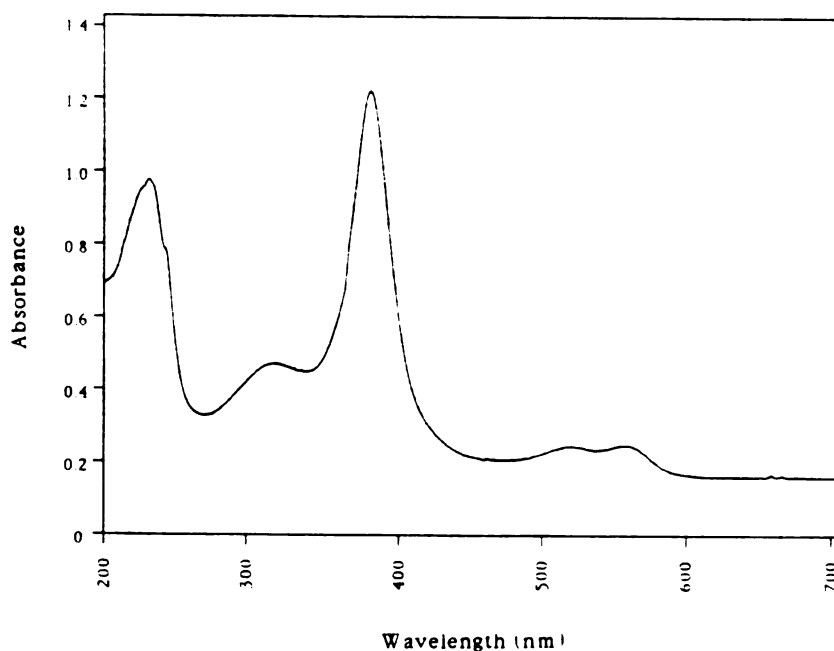
The basic protocol for Pd reductase purification is also very similar to that for P450$_{cam}$. Typically three or four liters of *E. coli* cells which express the recombinant protein are grown up at 30 °C for 24-36 hours. Expression of the reductase is detected by spinning down a small aliquot of the cells and examining the pellet for a slight greenish-yellow color.

The cells are harvested by centrifugation at 6,000 xg for 20 minutes at 4 °C. The pellets, which can be frozen at this point, are resuspended in 200-300 ml of cold Buffer T$_g$ containing 50 µg RNase, 1 mM PMSF and 1 mM EDTA, then lysed using the Bead Beater apparatus in 3 x 1-minute pulses with one minute rest in between. The cell debris is pelleted by centrifugation at 15,000 xg for 1 hour at 4 °C.

The cell extract is then subjected to ammonium sulfate precipitation in two steps. The clear, bright yellow supernatant is placed in a beaker on ice, to which 200 g/L (NH$_4$)$_2$SO$_4$ (~36% saturation) is slowly added over a 30-minute period. This is allowed to stir for 30 minutes more at 0 °C and then is centrifuged at 15,000 xg for 30 minutes at 4 °C. The yellow supernatant is poured back into the beaker on ice, and 300 g/L (NH$_4$)$_2$SO$_4$ (~70% saturation) is slowly added over a 30-minute period. This is allowed to stir for 30 minutes more at 0 °C and then is centrifuged at 15,000 xg for 30 minutes at 4 °C. The pellet is resuspended in Buffer T$_g$ and dialyzed overnight at 4 °C against a total of 8 L Buffer T$_g$ with one buffer change.

The next day the protein is loaded onto a Whatman DE-52 anion exchange column (2.5 x 30 cm) equilibrated in Buffer T_g and run under gravity (1-2 ml/min) at 4 °C. After loading, the column is washed with Buffer T_g-50 until the two yellow bands bound at the top of the column--the top one is greenish-yellow (Pd reductase) and the lower is orangish-yellow-- have separated. At this point, a linear salt gradient is begun starting at 50 mM KCl and finishing at 400 mM KCl (total volume of the gradient is 500 ml). Pd reductase typically elutes between 250 and 350 mM KCl. A profile of the column eluant is shown in Figure 6.7.

The next day the Pd reductase-containing fractions from this column are pooled and concentrated using an Amicon Ultrafiltration cell to less than 20 ml. The bright yellow sample is then loaded onto a Sephacryl S-200-HR column (2.5 x 90 cm) equilibrated in Buffer T_g at 4 °C. The column is developed with the equilibration buffer under gravity (~0.5 ml/min). An elution profile of this column is shown in Figure 6.8.
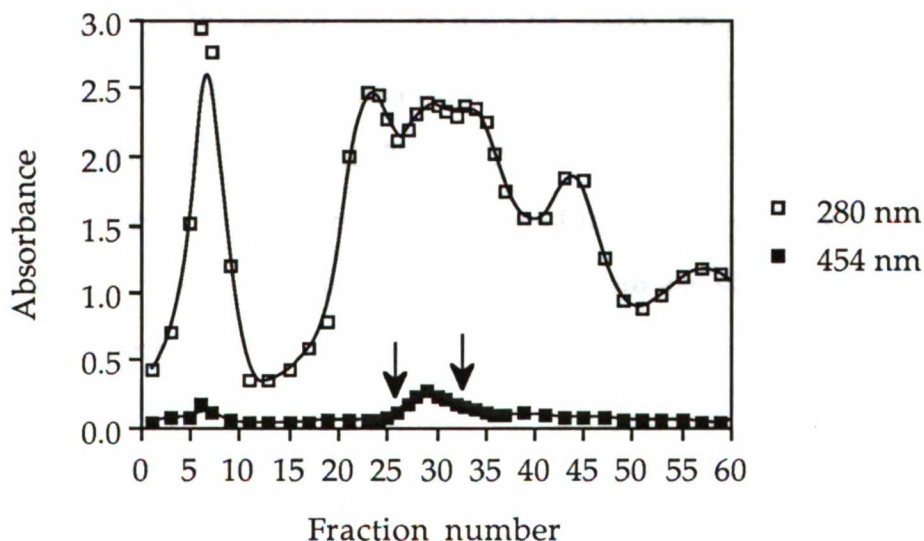
Figure 6.7: *DE-52 column elution profile observed for Pd reductase monitored at both 280 and 454 nm. Arrows indicate the limits of combined column effluent.*

165
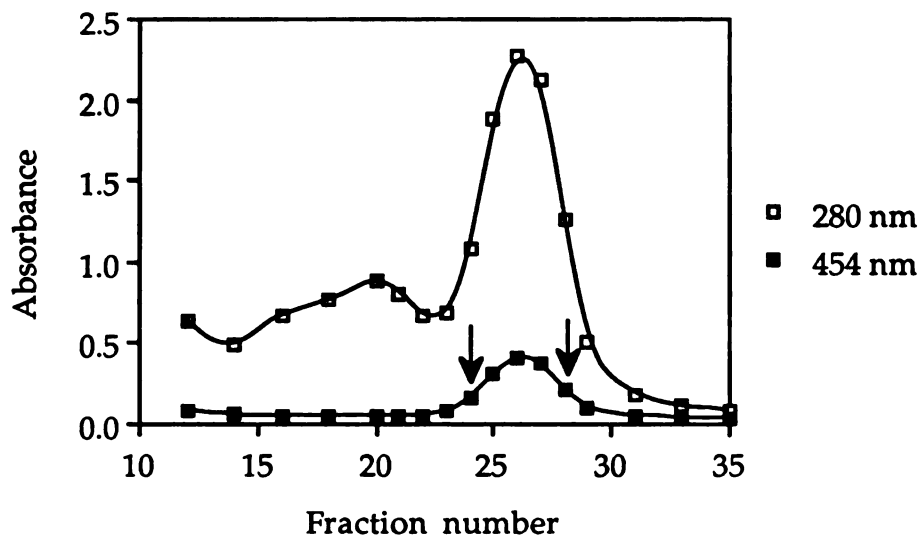
Figure 6.8: *Sephacryl S-200-HR column elution profile observed for Pd reductase monitored at both 280 and 454 nm. Arrows indicate the limits of combined column effluent.*

To store the protein, the pure Pd reductase fractions as judged by SDS PAGE are pooled and the concentration is determined spectroscopically from the absorption at 454 nm (ε_{454} = 10.0 mM^{-1} cm^{-1}). The concentration is then adjusted to a suitable stock concentration (generally 30 μM), aliquoted into eppendorf tubes and stored at -70 °C. Typical yields of purified recombinant Pd reductase from three liters of cells are ~1 μmole, or ~50 mg of protein. A typical spectrum and a gel of the purified protein are shown in Figures 6.9 and 6.10, respectively.

6.4   Enzyme Incubations

In general, 1-ml incubations were run in 10-ml round-bottom test tubes in a shaking water bath kept at a constant temperature. Incubations larger than 2 ml were run in larger test tubes or in 10-ml scintillation vials.

166
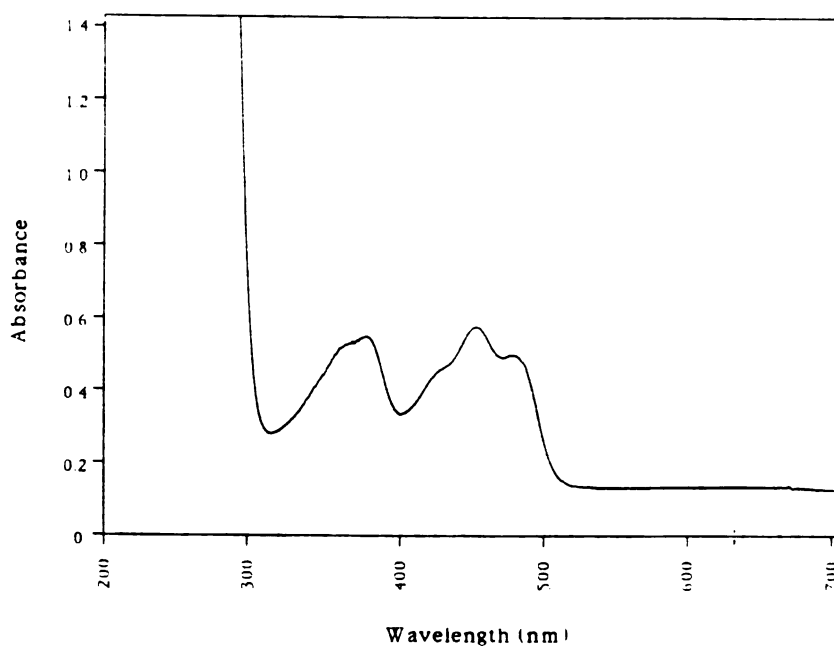
Figure 6.9: Spectrum of purified recombinant Pd reductase.
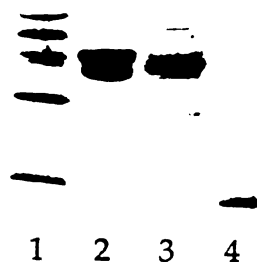
Figure 6.10: SDS PAGE (20 %) of the purified recombinant proteins. The lanes contain the following: (1) molecular weight markers, (2) $P450_{cam}$ (45 kDa), (3) Pd reductase (42 kDa), and (4) putidaredoxin (17 kDa). The lower of the two bands in lane 2 is a contaminating protein which is difficult to remove.

Liquid substrates were added neat, at 0.5 µl/ml, and solid substrates were added as 1 µl/ml of a 20 mM methanolic stock solution. In every case but camphor, the amount of substrate added exceeded the solubility limit of the compound, and thus the actual concentration in the incubation mixture was determined by the solubility of the organic compound in the aqueous phase. The solubility of styrene in water, for example, is 2.8 mM at 25 °C (Hefter, 1989). This concentration is well above the spectroscopic binding constant, K_s, for styrene, measured at 0.64 mM (data not shown).

In order to achieve a saturated solution, the substrate was added first to buffer in a test tube and thoroughly vortexed, then the proteins were added from stock solutions to give the concentrations noted. This procedure minimized protein precipitation due to high localized concentrations of substrate and/or methanol. It should be noted that putidaredoxin and Pd reductase are particularly sensitive to the presence of methanol, and concentrations no higher than 0.1% were used with these proteins.

6.4.1 Cytochrome P450$_{cam}$ (and Mutants)

Prior to incubations of P450$_{cam}$ or any of the active site mutant enzymes with substrates other than camphor, the camphor was removed from the hemoprotein stock solution immediately before use by passing a 0.5-1 ml aliquot over a small Sephadex G-15 column equilibrated with 50 mM potassium phosphate buffer (pH 7.0) and refrigerated at 4 °C. Spectra taken of the protein after the column consistently showed no shoulder at 391 nm, indicating no residual bound camphor.

A typical incubation contained 1 µM P450$_{cam}$ (wild type or mutant), 8 µM putidaredoxin, 2 µM Pd reductase, and 1-3 mM substrate depending on

substrate solubility, in 50 mM potassium phosphate buffer (pH 7.0)

containing 0.8 mM EDTA. Incubations run with *trans*-1-vinylcyclopropane

contained 2- or 3-fold higher protein concentrations. The incubation

mixture was preincubated for 2 minutes at 25 °C in a shaking water bath, and

NADH (1 or 5 mM final concentration) was added from a freshly-prepared

10x stock solution to initiate the reaction. The tubes were then incubated at

25 °C in a shaking water bath.

For incubations containing styrene or *cis*- or *trans*-β-methylstyrene, 1

mM NADH was used; for all the other substrates, 5 mM NADH was used.

Catalase (5-10 μM) was added to incubations containing the thioanisole

analogs to minimize hydrogen peroxide-catalyzed oxidation of the

thioanisoles, and to control incubations for styrene and *trans*-2-phenyl-1-

vinylcyclopropane. Other control incubations include substituting

equivolumes of buffer in place of the NADH stock solution (the "-NADH"

control).

6.4.2 Cytochrome P450$_{BM-3}$

Incubations with P450$_{BM-3}$ contained 1 μM P450$_{BM-3}$ and 1-3 mM

substrate in 50 mM MOPS buffer (pH 7.4). The substrate was added to the

buffer first, thoroughly vortexed, then the protein was added. The mixture

was preincubated at 25 °C for 2 minutes, and 5 mM NADPH was added from

a freshly-prepared 10x stock solution to initiate the reaction. The mixture

was then incubated at 25 °C in a shaking water bath. To the incubations

containing the thioanisole analogs, 5-10 μM catalase was added from a

freshly-prepared stock solution to minimize hydrogen peroxide-catalyzed

oxidation of the thioanisoles. Control incubations contained buffer in place of NADPH stock solution.

6.4.3 Cytochrome P450$_{terp}$

Incubations with P450$_{terp}$ contained 1 μM P450$_{terp}$, 8 μM putidaredoxin, 1 μM Pd reductase, and 1-3 mM substrate in 50 mM MOPS buffer (pH 7.4). The incubation mixture was preincubated for 2 minutes at 25 °C in a shaking water bath, and NADH (5 mM final concentration) was added from a freshly-prepared 10x stock solution to initiate the reaction. The tubes were then incubated at 25 °C in a shaking water bath. To the incubations containing the thioanisole analogs, 5-10 μM catalase was added from a freshly-prepared stock solution to minimize hydrogen peroxide-catalyzed oxidation of the thioanisoles. Control incubations contained buffer in place of NADH stock solution.

6.4.4 Cytochrome P4502B1

Incubations with the microsomal enzyme P4502B1 typically contained 1 μM P4502B1, 2 μM P450-NADPH-reductase, 40 μg/ml DLPC, 1-3 mM substrate and 5 mM NADPH in 100 mM potassium phosphate buffer (pH 7.4) containing 20% glycerol and 1 mM DTPA. The P450, reductase and freshly-sonicated DLPC solution were first combined and allowed to sit at room temperature for 10 minutes. The substrate and enough buffer to bring the volume to 1 ml were added, and the mixture was preincubated at 37 °C for 2 minutes. NADPH was added from a freshly-prepared 10x stock solution to initiate the reaction, and the incubation allowed to go at 37 °C in a shaking water bath. To the incubations containing the thioanisole analogs, 5-10 μM

170

catalase was added from a freshly-prepared stock solution to minimize hydrogen peroxide-catalyzed oxidation of the thioanisoles. Control incubations contained buffer in place of NADPH stock solution.

6.5 Metabolite Assays

The metabolites generated during incubation of the various substrates with P450 enzymes were identified by GLC co-elution of the metabolite with an authentic standard and/or by GLC-mass spectrometric analysis. Although most of the substrate incubations described in this thesis were analyzed in this manner, some were analyzed only by chiral phase HPLC. These incubations include *p*-chloro-, *p*-cyano- and *p*-nitrothioanisoles. The HPLC peaks from a *p*-methoxythioanisole incubation were collected and analyzed by GLC/MS; however, a detailed GLC study was not performed with this substrate.

For GLC analysis, typically a 30- or 60-minute 1-ml enzyme incubation was extracted with 0.5 ml dichloromethane and concentrated under a gentle argon stream. The oven conditions and retention times using a DB-1 fused silica capillary column (0.25 mm id x 30 m) are detailed below for each of the substrates studied. The mass spectrometric data for each of the metabolites are listed in Table 6.2.

Styrene. The column temperature was programmed to hold at 45 °C for 2 minutes then rise by 4 °/min to 140 °C. The retention times are: styrene, 6.8 min; benzaldehyde, 8.9 min; phenylacetaldehyde, 11.3 min; and styrene oxide, 12.7 min.

cis-β-Methylstyrene. The column temperature was programmed to hold at 45 °C for 2 minutes then rise by 4 °/min to 140 °C. The retention

171

times are: *cis*-β-methylstyrene, 10.0 min; *cis*-β-methylstyrene oxide, 14.1 min; phenylacetone, 15.0 min; and *cis*-cinnamyl alcohol (TMS-derivative), 23.5 min.

trans-*β*-Methylstyrene. The column temperature was programmed to hold at 45 °C for 2 minutes then rise by 4 °/min to 140 °C. The retention times are: *trans*-β-methylstyrene, 11.3 min; *trans*-β-methylstyrene oxide, 14.6 min; and *trans*-cinnamyl alcohol (TMS-derivative), 25.8 min.

p-*Methylstyrene*. The oven temperature was programmed to hold at 80 °C for 2 minutes, then increase by 4 °/min to 200 °C. The retention times are: *p*-methylstyrene, 8.7 min; *p*-methylbenzaldehyde, 10.8 min; *p*-methylphenylacetaldehyde, 12.7; *p*-methylstyrene oxide, 13.9 min; and *p*-hydroxymethylstyrene, 17.1 min and 21.2 (TMS derivative).

p-*Chlorostyrene*. The oven temperature was programmed to hold at 60 °C for 2 minutes, then increase by 4 °/min to 185 °C and hold for 5 minutes. The retention times are: *p*-chlorostyrene, 17.5 min; *p*-chlorobenzaldehyde, 19.6 min; and *p*-chlorostyrene oxide, 24.5 min.

Thioanisole. The oven temperature was programmed to hold at 100 °C for 4 minutes, then increase by 10 °/min to 250 °C and hold for 10 minutes. The retention times are: thioanisole, 7.4 min; and methyl phenyl sulfoxide, 11.5 min.

p-*Methylthioanisole*. The oven temperature was programmed to hold at 120 °C for 2 minutes, then increase by 10 °/min to 250 °C and hold for 20 minutes. The retention times are: *p*-methylthioanisole, 11.7 min; methyl *p*-tolyl sulfoxide, 19.5 min; and *p*-hydroxymethylthioanisole (TMS derivative), 22.3 min.

Camphor. The oven temperature was programmed to hold at 130 °C for 2 minutes, then rise by 5 °/min to 200 °C, then rise by 10 °/min to 250 °C.

The retention times of the components are as follows: d-camphor, 8.1 min; and 5-exo-hydroxycamphor (TMS derivative), 13.7 min.

trans-2-*phenyl-1-vinylcyclopropane*. The oven temperature was programmed to hold at 60 °C for 2 minutes, then increase by 4 °/min to 185 °C and hold for 20 minutes. The retention times are: trans-2-phenyl-1-vinylcyclopropane, 18.3 min; (*trans*-2-phenylcyclopropyl)acetaldehyde, 24.4 min; (*trans*-2-phenylcyclopropyl)ethylene oxide, 25.0 and 25.1 min (two diastereomers); *trans*-5-phenylpent-2-en-1-ol, 26.1 min; *trans*-4-phenylpent-2-en-1,5-diol, 32.1 min; and (*trans*-2-phenylcyclopropyl)-1,2-ethanediol, ~32.1 min.

7-*hydroxyterpineol*. The oven temperature was programmed to hold at 60 °C for 2 minutes, then increase by 4 °/min to 185 °C and hold for 3 minutes. The retention times are: α-terpineol, 11.0 min; and 7-hydroxyterpineol, 19.5 min.

Table 6.2: *Summary of the GLC/mass spectrometric data for the metabolites identified in this thesis (m/z values in bold correspond to molecular ions).*

Metabolite	EIMS (m/z)
Benzaldehyde	**106** (100), 105, (100), 77 (90), 51 (40)
Phenylacetaldehyde	**120** (25), 91 (100), 65 (20)
Styrene oxide	**120** (35), 119 (45), 91 (100), 63 (20)
Styrene phenol[a]	**120** (100), 91 (70)
cis-β-Methylstyrene oxide	**134** (50), 117 (20), 105 (55), 90 (100), 77 (25), 63 (20), 51 (20)
trans-β-Methylstyrene oxide	**134** (50), 117 (35), 105 (55), 90 (100), 77 (25), 63 (20), 51 (20)
Phenylacetone	**134** (25), 91 (70), 65 (20), 43 (100)

Table 6.2, continued

Metabolite	EIMS (m/z)
cis-Cinnamyl alcohol	**134** (50), 115 (80), 105 (60), 92 (100), 78 (70)
trans-cinnamyl alcohol	**134** (80), 115 (60), 105 (70), 92 (100), 78 (55)
p-Methylbenzaldehyde	**120** (75), 119 (100), 91 (90)
p-Methylphenylacetaldehyde	**134** (25), 105 (100), 77 (15)
p-Methylstyrene oxide	**134** (35), 119 (25), 105 (100), 91 (20), 77 (25)
p-Hydroxymethylstyrene	**134** (100), 115 (20), 105 (85), 91 (20), 77 (45)
" , TMS-derivative	**206** (50), 191 (55), 161 (20), 117 (100)
p-Chlorostyrene oxide	**154** (20), 125 (75), 119 (40), 89 (100), 63 (60)
p-Chlorobenzaldehyde	**140** (70), 139 (100), 111 (50), 75 (25), 50 (20)
p-Chlorostyrene phenol[a]	**154** (100), 119 (10), 91 (30)
Methyl *p*-tolyl sulfoxide	**154** (55), 139 (100), 123 (15), 91 (60), 77 (20)
p-Hydroxymethylthioanisole, TMS derivative	**226** (30), 211 (15), 179 (15), 137 (100), 122 (15), 73 (25)
(*trans*-2-phenylcyclopropyl)-acetaldehyde	**160** (30), 145 (25), 129 (60), 117 (80), 107 (100), 104 (95), 91 (50), 76 (25)
(*trans*-2-phenylcyclopropyl)-ethylene oxide	**160** (15), 142 (15), 129 (45), 117 (45), 115 (55), 104 (95), 91 (85), 76 (25), 52 (100)
trans-4-phenylpent-2-en-1,5-diol	see Figure 2.11
7-hydroxyterpineol	**170** (not observed), 152 (15), 121 (15), 109 (25), 91 (35), 79 (90), and 59 (100)
" , CI conditions	**170** (30), 153 (50), 135 (100), 121 (10), 109 (12), and 95 (25)

[a] tentative assignments. Location of hydroxyl group on aromatic ring was not determined.

6.6 Epoxide Stereochemistry Assays

To determine the epoxide stereochemistry of the styrene analogs, a 1-ml incubation was extracted with 0.5 ml dichloromethane, carefully concentrated under a gentle argon stream to 10-20 μl, and analyzed using either a 30- or 40-m Chiraldex G-TA capillary column (0.25 mm id, Advanced Separations Technologies, Inc.). For analysis of the styrene and β-methylstyrene oxides, the incubations were extracted with hexane instead of dichloromethane, and the epoxides purified by HPLC prior to analysis by chiral GLC. The isocratic HPLC purification was carried out on an Alltech Partisil Silica 5-μm column eluted with 2.5% THF in hexane at 1 ml/min. The eluant was monitored at 260 nm (rt = 7-8 minutes for the styrene and β-methylstyrene epoxides).

The HPLC step was used to clean up the epoxide sample and thus prolong the GLC column life. However, this step was found to be time-consuming and to give decreased yields of epoxide for the final chiral GLC analysis. Injection of the organic extract directly onto the GLC column did not appear to significantly affect epoxide peak resolution, retention time, nor column life.

Column temperatures and the retention times of the epoxide enantiomers are summarized in Table 6.3.

6.7 Sulfoxide Stereochemistry Assays

To determine the sulfoxide stereochemistry of the thioanisole analogs, a 1-ml incubation was extracted with 0.5 ml dichloromethane, carefully concentrated under a gentle argon stream to ~20 μl and diluted into 0.25 ml

Table 6.3: *Summary of the oven temperatures used with the chiral GLC column and the retention times of the epoxide enantiomers. The conditions listed are those used with the 30-m column.*

Substrate	Column T (°C)[a]	Retention times (min)	
		1S-epoxide	1R-epoxide
Styrene	120	9.8	10.9
cis-β-Methylstyrene	120	9.7	11.9
trans-β-Methylstyrene	120	10.1	11.2
p-Chlorostyrene	100	60.8	61.9

[a] The column temperatures listed are approximate due to problems encountered with the oven temperature controller.

hexane. This was analyzed by HPLC using a Chiracel OB column (4.6 mm id x 25 cm, Daicel Chemical Industries, Ltd.). The column was eluted isocratically at a flow rate of 0.5 ml/min and the eluant was monitored at 254 nm. The proportions of hexane and isopropanol used to separate and elute the sulfoxide enantiomers varied depending on the substrate analyzed, and are as listed in Table 6.4.

6.8 Turnover Number Measurements

6.8.1 Styrene and cis- and trans-β-Methylstyrenes

To quantitate the amounts of epoxide, benzaldehyde and cinnamyl alcohol formed over time in incubations of styrene and cis- and trans-β-methylstyrenes with P450$_{cam}$, 1-ml aliquots were removed from the incubation mixture at designated time points and placed in test tubes kept on ice (for cis- and trans-cinnamyl alcohols, 3-ml aliquots were required for

Table 6.4: Summary of the solvent conditions used with the chiral HPLC column and the retention times of the sulfoxide enantiomers.

Substrate	% hex : % *i*-PrOH	Retention times (min)[a]	
		S-Sulfoxide	R-sulfoxide
Thioanisole	80 : 20	29	47
p-Methylthioanisole	85 : 15	21	46
p-Chlorothioanisole	85 : 15	32	49
p-Methoxythioanisole	75 : 25	29	59
p-Cyanothioanisole	70 : 30	60	80
p-Nitrothioanisole	60 : 40	46	55

[a] The retention times of the sulfoxide enantiomers were found to be dependent on ambient temperature. The values given were obtained at ~20 °C. A shift of up to 20 minutes for the more highly retained sulfoxides (eg, *p*-cyano) was not unusual for a warm day (>25 °C).

accurate quantitation). As rapidly as possible, 5 μl of a 1 mM stock solution of the internal standard in methanol was added to each tube, the solution vortexed, 0.5 ml dichloromethane was added, and the solution again vortexed. The tube was then kept on ice until all the time points were taken.

The biphasic mixture was then centrifuged to minimize the emulsion, and the dichloromethane layer removed and analyzed both with and without BSTFA derivation by GLC on a DB-1 fused silica capillary column (0.25 mm id x 30 m). Derivation with BSTFA, required in order to detect and quantitate the alcohol metabolites, was accomplished by placing 0.1 ml of the dichloromethane extract in a 1-ml Reactivial® and adding ~1 μl BSTFA. This was tightly sealed with a Teflon®-lined cap and heated in a heating block for 20-30 minutes at ~55 °C.

The amount of each metabolite present was quantitated using standard curves with R-styrene oxide as the internal standard for the cis- and trans-β-methylstyrene incubations, and (1S, 2S)-(-)-1-phenylpropylene oxide as the internal standard for the styrene incubations. Each standard curve was prepared by adding appropriate amounts of the metabolite standards to 1-ml solutions containing the complete incubation mixture except for NADH. The presence of the proteins during the extraction procedure was important for obtaining correct turnover values.

6.8.2 Camphor

To quantitate the formation of 5-exo-hydroxycamphor from d-camphor, 0.1-ml aliquots were removed from the incubation mixture at designated time points and added to test tubes kept on ice containing 0.9 ml doubly-distilled water and 4 μl of a 10 mM methanolic stock solution of the internal standard 1-adamantanol. To each tube was immediately added 0.5 ml diethyl ether, and the mixture vortexed and kept on ice until all the time points were taken.

To analyze for the metabolites, 100-200 μl of the ether layer was withdrawn and placed in a 1-ml Reactivial®. The samples were derivatized with BSTFA as described above, and analyzed by gas-liquid chromatography on a DB-1 fused silica capillary column (0.25 mm id x 30 m). The amount of metabolite formed was quantitated using standard curves with 1-adamantanol as the internal standard. In this case it was found extremely important that the proteins were present during the extraction procedure in order to obtain correct turnover values.

6.8.3 Thioanisole and *p*-Methylthioanisole

To quantitate the amounts of sulfoxide formed over time from thioanisole and *p*-methylthioanisole, 0.2 ml aliquots were removed from the incubation mixture at designated time points and placed in test tubes kept on ice. As rapidly as possible, 10 μl of a 1 mM stock solution of the internal standard *p*-chlorothioanisole was added to each tube, the solution vortexed, 0.5 ml dichloromethane was added, and the solution again vortexed. The tubes were kept on ice until all the time points were taken.

The dichloromethane layer was analyzed by GLC on a DB-1 fused silica capillary column (0.25 mm id x 30 m). The amount of sulfoxide was quantitated using a standard curve with *p*-chlorothioanisole as the internal standard. The standard curve was determined with proteins present, as was done for the other turnover measurements.

6.9   NADH Consumption Assays

The rate of NADH utilization by P450$_{cam}$ was determined spectro-photometrically. Aliquots were removed from the incubation mixture at various time points, immediately diluted to 1 ml in a cuvette, the cuvette quickly shaken and the absorbance at 340 nm measured. For the olefin measurements, the aliquot size was 0.2 ml, for the thioanisoles it was 0.075 ml, and for the camphor measurements it was 0.05 ml. The amount of NADH consumed was quantitated using the extinction coefficient $\varepsilon = 6.22$ mM^{-1} cm^{-1}.

179

6.10 Oxygen Consumption Assays

The rate of oxygen consumption by P450$_{cam}$ was measured using a Clark electrode hooked up to a constant temperature bath and a stir plate. The incubation mixture (1.3 or 1.5 ml) was placed inside the cell and allowed to equilibrate at least 5 minutes or until the oxygen level had stabilized. The reaction was initiated by the addition of NADH, and the loss of oxygen monitored until it leveled off. The rate of oxygen consumed was determined as the initial rate over the first 2 or 2.5 minutes, with a full scale deflection corresponding to an oxygen concentration of 232 μM (Lessler and Brierley, 1967). Increasing the volume of the incubation from 1.3 to 1.5 ml (total volume inside cell is ~1.6 ml) had very little effect on the rates.

6.11 Hydrogen Peroxide Formation Assays

The amount of hydrogen peroxide formed by P450$_{cam}$ was measured using an iron(II)-thiocyanate assay (Boltz and Howell, 1978). Accurate measurements using this assay required buffers containing no EDTA or β-mercaptoethanol. The β-mercaptoethanol present in the stock putidaredoxin solutions was removed by passing the enzyme over a small Sephadex G-15 column kept at 4 °C and equilibrated in 50 mM Tris·Cl (pH 7.4) immediately before use.

Aliquots (0.3 ml) were removed from the incubation mixture at various time points and added to 0.2 ml 0.3 N sulfuric acid in a 1.5-ml eppendorf tube kept on ice. After all the time points were taken, the following solutions were added to each tube, in this order: 0.125 ml 6 mM ferrous ammonium sulfate solution, 0.125 ml 6 M ammonium thiocyanate solution, and 0.75 ml doubly-distilled water. The mixture was centrifuged in

a Beckman Microfuge™ at maximum speed for 1 minute to pellet the precipitated protein, and the absorbance at 480 nm measured. The amount of hydrogen peroxide present was calculated from a standard curve made using stock hydrogen peroxide concentrations.

6.12   Identification of α-terpineol metabolite, 7-hydroxyterpineol

The sole product of the reaction of P450$_{terp}$ with α-terpineol was isolated from the crude extract of a one hour incubation sent to us by Julian Peterson at the University of Texas Health Sciences Center in Dallas. TLC analysis of this extract using 40 : 60 ethylacetate : hexane as solvent showed two main spots: one with an R$_f$ value of 0.5 (α-terpineol), and the other with a R$_f$ value of 0.1.

The more polar compound was purified by silica gel chromatography using the TLC solvent system. ^{1}H and ^{13}C NMR spectra (below) and mass spectrometric data (Table 6.2) of the isolated metabolite match those obtained for the 7-hydroxyterpineol synthetic standard. TLC and GLC analyses of the isolated product indicate that it co-elutes with 7-hydroxyterpineol. ^{1}H NMR (300 MHz, CDCL$_3$): δ 1.17, 1.18 (2 x s, 6H, 2 x CH$_3$), 1.22-1.28 (m, 2H, CH-CH$_2$-CH$_2$), 1.51-1.54 (m, 1H, CH), 1.83-2.20 (m, 4H, CH=CH-CH$_2$), 3.96 (s, 2H, CH$_2$OH), and 5.66 (s, 1H, CH=CH$_2$) ppm. ^{13}C NMR (75 MHz, CDCL$_3$): δ 23.4 (C-5), 26.0 (C-6 and C-9), 26.4 (C-3), 27.0 (C-10), 44.9 (C-4), 66.5 (C-7), 72.5 (C-8), 121.9 (C-2), and 137.2 (C-1) ppm.

6.13 Syntheses of metabolite standards

6.13.1 Epoxides

cis-β-Methylstyrene, *p*-methylstyrene and *p*-chlorostyrene oxides were prepared from the corresponding olefins according to the procedure of Amann and coworkers (Amann *et al.*, 1987). To a stirred solution of 5 mmol *m*-chloroperbenzoic acid in 50 ml dichloromethane was added 5 mmol KF. The olefin (5 mmol) in 25 ml dichloromethane was then slowly added, and the reaction allowed to go at room temperature for several hours to overnight until judged complete by TLC. The reaction was quenched by dropwise addition of 10% sodium bisulfite until starch-iodide test was negative. The cloudy white solution was filtered into a separatory funnel, then washed three times with saturated sodium bicarbonate solution, once with water and once with brine. The organic layer was dried over anhydrous sodium sulfate, filtered and the solvent removed by rotary evaporation to yield a clear liquid with a flowery smell.

6.13.2 Sulfoxides

The sulfoxides of *p*-methyl-, *p*-methoxy-, *p*-chloro-, *p*-cyano- and *p*-nitrothioanisoles were prepared from the sulfides according to the procedure of Rettie and coworkers (Rettie *et al.*, 1990). To a solution of 1 mmol sulfide in 10 ml methanol cooled to 0°C in an ice bath was added a solution of 1.25 mmol sodium perchlorate in 2 ml doubly-distilled water. The mixture was allowed to stir for several hours, and the extent of reaction monitored by TLC (50 : 50 ethylacetate : hexane). The reaction was worked up by adding ~30 ml doubly-distilled water, and extracting with dichloromethane. The

organic layer was dried over anhydrous magnesium sulfate, filtered and the solvent removed by rotary evaporation.

6.13.3 7-Hydroxyterpineol

7-Hydroxyterpineol was prepared from β-pinene oxide according to the method of Bluthe and coworkers (Bluthe *et al.*, 1980). β-Pinene oxide (1.5 g) was slowly added to a stirred solution of mercuric nitrate in 1 : 1 THF : water (20 ml). After 5 minutes at room temperature the product was extracted with dichloromethane and purified by silica gel chromatography (40 : 60 ethylacetate : hexane) to a single spot by TLC.

7.0 REFERENCES

Abdel-Monem, M.M. (1975) *J. Med. Chem.* **18**, 427.

Amann, Ourisson, and Luu, (1987) *Synthesis,* 696.

Atkins, W.M. and Sligar, S.G. (1987a) *J. Am. Chem. Soc.* **109**, 3754.

Atkins, W.M. and Sligar, S.G. (1987b) *Biochemistry* **27**, 1610.

Atkins, W.M. and Sligar, S.G. (1988) *J. Biol. Chem.* **263**, 18842.

Atkins, W.M. and Sligar, S.G. (1989) *J. Am. Chem. Soc.* **111**, 2715.

Augusto, O., Beilan, H.S. and Ortiz de Montellano, P.R. (1982) *J. Biol. Chem.* **257**, 11288.

Baldwin, J.M. (1980) *J. Mol. Biol.* **136**, 103.

Bass, M.B., Paulsen, M.D. and Ornstein, R.L. (1992) *Proteins* **13**, 26.

Beckwith, A.L.J. and Moad, G. (1980) *J. Chem. Soc., Perkins Trans.* **2**, 1473.

Berg, A., Ingelman-Sundberg, M. and Gustafsson, J. (1979) *J. Biol. Chem.* **254**, 5264.

Bernhardt, R., Dao, N.T.N., Stiel, H., Schwarze, W., Friedrich, J., Janig, G. and Ruckpaul, K. (1983) *Biochim. Biophys. Acta* **745**, 140.

Black, S.D. and Coon, M.J. (1986) in *Cytochrome P450 Structure, Mechanism and Biochemistry* (Ortiz de Montellano, P.R., ed) pp. 161-216, Plenum Publishing Corp., New York.

Blake II, R.C. and Coon, M.J. (1979) *J. Biol. Chem.* **255**, 4100.

Blake II, R.C. and Coon, M.J. (1989) *J. Biol. Chem.* **264**, 3694.

Bluthe, N., Ecoto, J., Retizon, M. and Lazare, S. (1980) *J. Chem. Soc., Perkin Trans. I*, 1747.

Boddupalli, S.S., Estabrook, R.W. and Peterson, J.A. (1990) *J. Biol. Chem.* **265**, 4233.

Boddupalli S.S., Pramanik, B.C., Slaughter, C.A., Estabrook, R.W. and Peterson, J.A. (1992) *Arch. Biochem. Biophys.* **292**, 20.

Boltz, D.F. and Howell, J.A., eds. (1978) in *Colorimetric Determination of Nonmetals* (Boltz, D.F. and Howell, J.A., eds.) pp. 301-316, John Wiley and Sons, New York.

Bowry, V.W., Lusztyk, J. and Ingold, K.U. (1989) *J. Am. Chem. Soc.* **111**, 1927.

Bowry, V.W. and Ingold, K.U. (1991) *J. Am. Chem. Soc.* **113**, 5699.

Bradshaw, W.H., Conrad, H.E., Corey, E.J., Gunsalus, I.C. and Lednicer, D. (1959) *J. Am. Chem. Soc.* **81**, 5007.

Brinigar, W.S., Chang, C.K., Geibel, J. and Traylor, T.G. (1974) *J. Am. Chem. Soc.* **96**, 5597.

Brown, C.A. and Black, S.D. (1989) *J. Biol. Chem.* **264**, 4442.

CaJacob, C.A., Chan, W.K., Shephard, E. and Ortiz de Montellano, P.R. (1988) *J. Biol. Chem.* **263**, 18640.

Carlsson, D.J. and Ingold, K.U. (1968) *J. Am. Chem. Soc.* **90**, 7047.

Carman, R.M., Greenfield, K.L. and Robinson, W.R. (1986) *Aust. J. Chem.* **39**, 21.

Champion, P.M., Lipscomb, J.D., Munck, E., Debrunner, P. and Gunsalus, I.C. (1975) *Biochemistry* **14**, 4152.

Champion, P.M., Stallard, B.R., Wagner, G.C. and Gunsalus, I.C. (1982) *J. Am. Chem. Soc.* **104**, 5469.

Chance, B., Powers, L., Ching, Y., Poulos, T., Schonbaum, G.R., Yamazaki, I. and Paul, K. (1984) *Arch. Biochem. Biophys.* **235**, 596.

Collins, J.R. and Loew, G.H. (1988) *J. Biol. Chem.* **263**, 3164.

Collman, J.P., Brauman, J.I., Halbert, T.R. and Suslick, K.S. (1976) *Proc. Natl. Acad. Sci. U.S.A.* **73**, 3333.

Conney, A.H. (1986) *Life Sci.* **39**, 2493.

Connolly, M.L. (1983) *Science* **221**, 709.

Cramer, S.P., Dawson, J.H., Hodgson, K.O. and Hager, L.P. (1978) *J. Am. Chem. Soc.* **100**, 7282.

Cushman, D.W., Tasi, R.L. and Gunsalus, I.C. (1967) *Biochem. Biophys. Res. Commun.* **26**, 577.

Davies, M.D. Qin, L., Beck, J.L., Suslick, K.S., Koga, H., Horiuchi, T. and Sligar, S.G. (1990) *J. Am. Chem. Soc.* **112**, 7396.

Dawson, J.H., Kelm, R.H., Trudell, J.R., Barth, G., Linder, R. E., Bunnenberg, E., Djerassi, C. and Tang, S.C. (1976) *J. Am Chem. Soc.* **98**, 3707.

Dawson, J.H., Andersson, L.A. and Sono, M. (1982) *J. Biol. Chem.* **257**, 3606.

De Lemos-Chiarandini, C., Frey, A.B., Sabatini, D.D. and Kreibich, G. (1987) *J. Cell. Biol.* **104**, 209.

De Meester, C., Poncelet, F., Roberfroid, M., Rondelet, J. and Mercier, M. (1977) *Mutat. Res.* **56**, 147.

DePierre, J.W. and Ernster, L. (1977) *Annu. Rev. Biochem.* **46**, 201.

Eble, K.S. and Dawson, J.H. (1984) *J. Biol. Chem.* **259**, 14389.

Edwards, R.J., Murray, B.P., Boobis, A.R. and Davies, D.S. (1989) *Biochemistry* **28**, 3762.

Ellin, A. and Orrenius, S. (1975) *FEBS Lett.* **50**, 378.

Ferrin, T.E., Huang, C.C., Jarvis, L.E. and Langridge, R. (1988) *J. Mol. Graphics* **6**, 13.

Fisher, M.T. and Sligar, S.G. (1985) *J. Am. Chem. Soc.* **107**, 5018.

Fruetel, J.A., Collins, J.R., Camper, D.L., Loew, G.H. and Ortiz de Montellano, P.R. (1992) *J. Am. Chem. Soc.* **114**, 6987.

Fruetel, J.A., Chang, Y.-T., Collins, J.R., Loew, G.H. and Ortiz de Montellano, P.R. (1992), *J. Am. Chem. Soc.*, submitted.

Fu, H., Look, G.C., Zhang, W., Jacobsen, E.N. and Wong, C.-H. (1991) *J. Org. Chem.* **56**, 6497.

Furuya, H., Shimizu, T., Hatano, M. and Fujii-Kuriyama, Y. (1989a) *Biochem. Biophys. Res. Commun.* **160**, 669.

Furuya, H., Shimizu, T., Hirano, K., Hatano, M., Fujii-Kuriyama, Y., Raag, R. and Poulos, T.L. (1989a) *Biochemistry* **28**, 6848.

Garfinkel, D. (1958) *Arch. Biochem. Biophys.* **77**,493.

Gelb, M.H., Heimbrook, D.C., Malkonen, P. and Sligar, S.G. (1982a) *Biochemistry* **21**, 370.

Gelb, M.H., Malkonen, P. and Sligar, S.G. (1982b) *Biochem. Biophys. Res. Commun.* **3**, 853.

Gibson, G.G. and Tamburini, P.P. (1984) *Xenobiotica* **14**, 27.

Gotoh, O., Tagashira, Y., Iizuka, T. and Fujii-Kuriyama, T. (1983) *J. Biochem.* **93**,807.

Gould, P.V., Gelb, M.H. and Sligar, S.G. (1981) *J. Biol. Chem.* **256**, 6686.

Graham-Lorence, S., Khalil, M.W., Lorence, M.C., Mendelson, C.R. and Simpson, E.R. (1991) *J. Biol. Chem.* **266**, 11939.

Griffin, B.W. and Peterson, J.A. (1975) *J. Biol. Chem.* **250**, 6445.

Groves, J.T., McClusky, G.A., White, R.E. and Coon, M.J. (1978) *Biochem. Biophys. Res. Commun.* **81**, 154.

Groves, J.T. and Myers, R.S. (1983) *J. Am. Chem. Soc.* **105**, 5791.

Groves, J.T. and Nemo, T.E. (1983) *J. Am. Chem. Soc.* **105**, 5786.

Groves, J.T. and Subramanian, D.V. (1984) *J. Am. Chem. Soc.* **106**, 2177.

Groves, J.T. and Watanabe, Y. (1986) *J. Am. Chem. Soc.* **108**, 507.

Groves, J.T., Avaria-Neisser, G.E., Fish, K.M., Imachi, M. and Kuczkowshi, R.L. (1986) *J. Am. Chem. Soc.* **108**, 3837.

Gunsalus, I.C. and Wagner, G.C. (1978) *Methods Enzymol.* **52**, 166.

Gustafsson, J., Rondahl, L. and Bergman, J. (1979) *Biochemistry* **18**, 865.

Hanzlik, R.P. and Tullman, R.H. (1982) *J. Am. Chem. Soc.* **104**, 2048.

He, G.-X. and Bruice, T.C. (1991) *J. Am. Chem. Soc.* **113**, 2747.

Hedegaard, J. and Gunsalus, I.C. (1965) *J. Biol. Chem.* **240**, 4038.

Hefter, G.T. (1986) in *Hydrocarbons with Water and Seawater; Part II: Hydrocarbons C8-C36* (Kertes, A.S., ed) vol. 38, pp. 1-8, Pergamon Press, Oxford.

Heimbrook, D.C. and Sligar, S.G. (1981) *Biochem. Biophys. Res. Commun.* **99**, 530.

Henschler, D., Hoos, W.R., Fetz, H., Dallmeier, E. and Metzler, M. (1979) *Biochem. Pharmacol.* **28**, 543.

Holland, H.L. (1988) *Chem. Rev.* **88**, 473.

Hrycay, E.G., Gustafsson, J.-Å., Ingelman-Sundberg, M. and Ernster, L. (1975) *Biochem. Biophys. Res. Commun.* **66**, 209.

Huff, J.E. (1984) *Prog. Clin. Biol. Res.* **141**, 227.

Hui Bon Hoa, G. and Marden, M. (1982) *Eur. J. Biochem.* **124**, 311.

Imai, M., Shimada, H., Watanage, Y., Matsushima-Hibiya, Y., Makino, R., Koga, H., Horiuchi, T. and Ishimura, Y. (1989) *Proc. Natl. Acad. Sci. USA* **86**, 7823.

Ingelman-Sundberg, M. (1986) in *Cytochrome P450 Structure, Mechanism and Biochemistry* (Ortiz de Montellano, P.R., ed) pp. 119-160, Plenum Publishing Corp., New York.

Iwasaki, M., Juvonen, R., Lindberg, R. and Negishi, M. (1991) *J. Biol. Chem.* **266**, 3380.

Jerina, D.M., Michaud, D.P., Feldmann, R.J., Armstrong, R.N., Vyas, K.P., Thakker, D.R., Yagi, H., Thomas, P.E., Ryan, D.E. and Levin, W. (1982) in *Microsomes, Drug Oxidations and Drug Toxicity* (R. Sato and R. Kato, eds.) pp. 195-201, Japan Scientific Societies Press, Tokyo.

Kadlubar, F.F., Morton, K.C. and Ziegler, D.M. (1973) *Biochem. Biophys. Res. Commun.* **54**, 1255.

Katagiri, M., Ganguli, B.N. and Gunsalus, I.C. (1968) *J. Biol. Chem.* **243**, 3543.

Klingenberg, M. (1958) *Arch. Biochem. Biophys.* **76**, 376.

Kunze, K.L., Mangold, B.L.K., Wheeler, C., Beilan, H.S. and Ortiz de Montellano, P.R. (1983) *J. Biol. Chem.* **258**, 4202.

Kuthan, H., Tsuji, H., Graf, H., Ullrich, V., Werringloer, J. and Estabrook, R.W. (1978) *FEBS Lett.* **91**, 343.

Lessler, M.A. and Brierley, G.P. (1967) in *Methods of Biochemical Analysis,* vol. 17, p. 19.

Liebler, D.C. and Guengerich, F.P. (1983) *Biochemistry* **22**, 5482.

Leibman, K.C. and Ortiz, E. (1969) *Biochem. Pharmacol.* **18**, 552.

Light, D.R., Waxman, D.J. and Walsh, C. (1982) *Biochemistry* **21**, 2493.

Lindberg, R.L.P. and Negishi, M. (1989) *Nature* **339**, 632.

Macdonald, T.L., Burka, L.T., Wright, S.T. and Guengerich, F.P. (1982a) *Biochem. Biophys. Res. Commun.* **104**, 620.

Macdonald, T.L., Zirvi, K., Burka, L.T., Peyman, P. and Guengerich, F.P. (1982b) *J. Am. Chem. Soc.* **104**, 2050.

Mansuy, D., Leclaire, J., Fontecave, M. and Momenteau, M. (1984) *Biochem. Biophys. Res. Commun.* **119**, 319.

Marnett, L.J., Weller, P. and Battista, J.R. (1986) in *Cytochrome P450 Structure, Mechanism and Biochemistry* (Ortiz de Montellano, P.R., ed) pp. 29-76, Plenum Publishing Corp., New York.

Martinis, S.A., Atkins, W.A., Stayton, P.S. and Sligar, S.G. (1989) *J. Am. Chem. Soc.* **111**, 9252.

Matsunaga, E., Zeugin, T., Zanger, U.M., Aoyama, T., Meyer, U.A. and Gonzalez, F.J. (1990) *J. Biol. Chem.* **265**, 17197.

McMurry, T.J. and Groves, J.T. (1986) in *Cytochrome P450 Structure, Mechanism and Biochemistry* (Ortiz de Montellano, P.R., ed) pp. 1-28, Plenum Publishing Corp., New York.

Miller, R.E. and Guengerich, F.P. (1982) *Biochemistry* **21**, 1090.

Miller, V.P., Fruetel, J.A. and Ortiz de Montellano, P.R. (1992) *Arch. Biochem. Biophys.* **298**, 697.

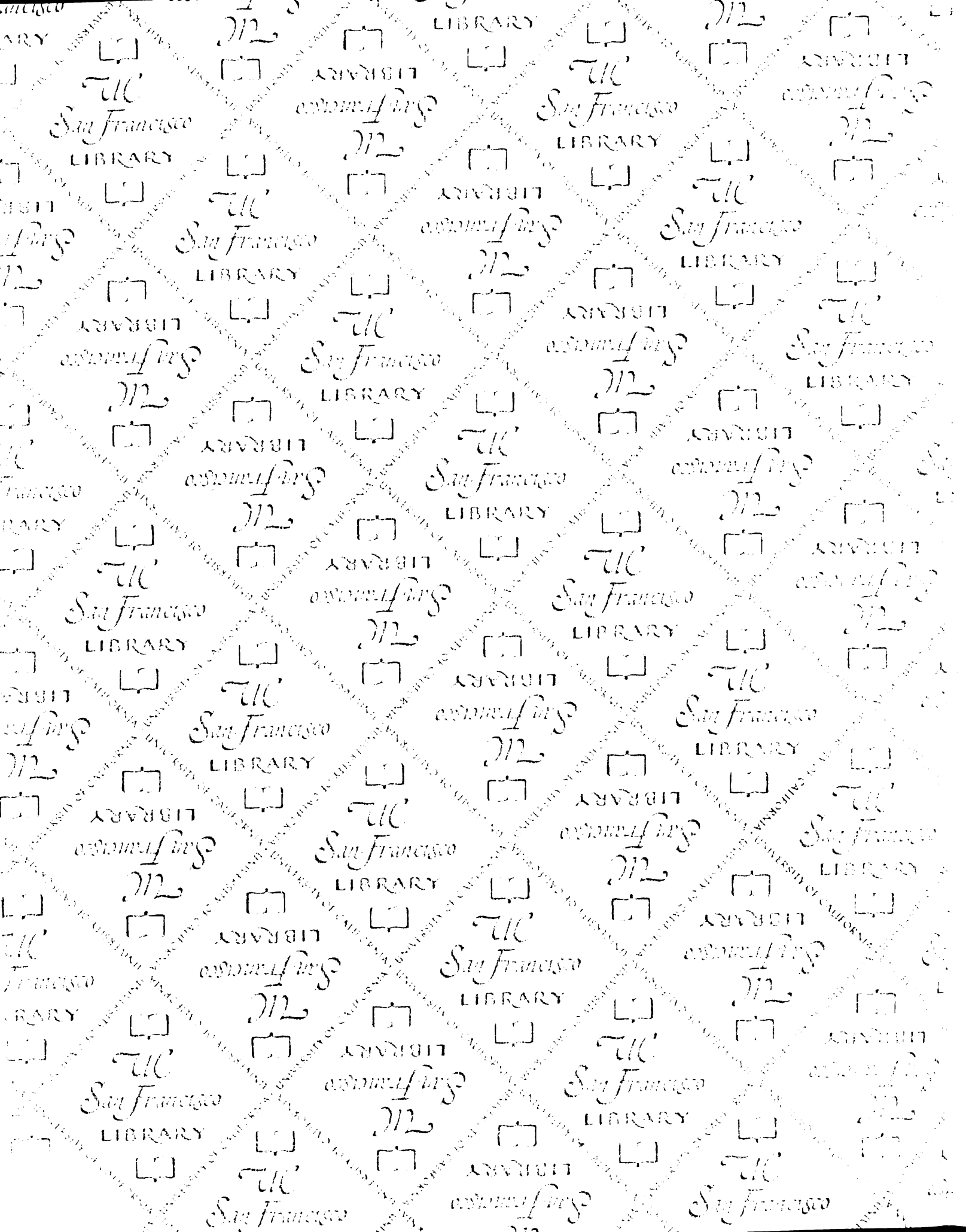Miwa, G.T., Garland, W.A., Hodshon, B.J., Lu, A.Y.H. and Northrop, D.B. (1980) *J. Biol. Chem.* **255**, 6049.

189

Miwa, G.T., Walsh, J.S., Kedderis, G.L. and Hollenberg, P.F. (1983) *J. Biol. Chem.* **258**, 14445.

Miwa, G.T., Walsh, J.S. and Lu, A.Y.H. (1984) *J. Biol. Chem.* **259**, 3000.

Monier, S., Van Luc, P., Kreibich, G., Sabatini, D.D. and Adesnik, M. (1988) *J. Cell. Biol.* **107**, 457.

Narhi, L.O. and Fulco, A.J. (1986) *J. Biol. Chem.* **261**, 7160.

Nebert, D.W., Nelson, D.R., Coon, M.J., Estabrook, R.W., Feyereisen, R., Fujii-Kuriyama, Y., Gonzalez, F.J., Guengerich, F.P., Gunsalus, I.C., Johnson, E.F., Loper, J.C., Sato, R., Waterman, M.R. and Waxman, D.J. (1991) *DNA and Cell Biology*, **10**, 1.

Nelson, D.R. and Strobel, H.W. (1987) *Mol. Biol. Evol.* **4**, 572.

Nelson, D.R. and Strobel, H.W. (1988) *J. Biol. Chem.* **263**, 6038.

Nelson, D.R. and Strobel, H.W. (1989) *Biochemistry* **28**, 656.

Newcomb, M. and Manek, M.B. (1990) *J. Am. Chem. Soc.* **112**, 9662.

Nordblom, G.D. and Coon, M.J. (1977) *Arch. Biochem. Biophys.* **180**, 343.

O'Malley, S. and Kodadek, T. (1989) *J. Am. Chem. Soc.* **111**, 9116.

Omura, T. and Sato, R. (1964) *J. Biol. Chem.* **239**, 2370.

Ortiz de Montellano, P.R., Kunze, K.L., Beilan, H.S. and Wheeler, C. (1982) *Biochemistry* **21**, 1331.

Ortiz de Montellano, P.R., Mangold, B.L.K., Wheeler, C., Kunze, K.L. and Reich N.O. (1983) *J. Biol. Chem.* **258**, 4208.

Ortiz de Montellano, P.R. (1985) in *Bioactivation of Foreign Compounds* (Anders, M.W., ed) pp. 121-155, Academic, New York.

Ortiz de Montellano, P.R. (1986) in *Cytochrome P450 Structure, Mechanism and Biochemistry* (Ortiz de Montellano, P.R., ed) pp. 217-271, Plenum Publishing Corp., New York.

Ortiz de Montellano, P.R. and Stearns, R.A. (1987) *J. Am. Chem. Soc.* **109**, 3415.

Ortiz de Montellano, P.R., Fruetel, J.A., Collins, J.R., Camper, D.L. and Loew, G.H. (1991) *J. Am. Chem. Soc.* **113**, 3195.

Ostovic, D. and Bruice, T.C. (1989) *J. Am. Chem. Soc.* **111**, 6511.

Paulsen, M.D. and Ornstein, R.L. (1990) Abstract 283, *8th International Symposium on Microsomes and Drug Oxidations*, Stockholm, Sweden, June 25.

Peng, S.M. and Ibers, J.A. (1976) *J. Am. Chem. Soc.* **98**, 8032.

Peterson, J. (1971) *Arch. Biochem. Biophys.* **144**, 678.

Peterson, J.A. and Prough, R.A. (1986) in *Cytochrome P450 Structure, Mechanism and Biochemistry* (Ortiz de Montellano, P.R., ed) pp. 89-117, Plenum Publishing Corp., New York.

Peterson, J.A., Lorence, M.C. and Amarneh, B (1990) *J. Biol. Chem.* **265**, 6066.

Peterson, J.A., Lu, J.-Y., Geisselsoder, J., Graham-Lorence, S., Carmona, C., Witney, F. and Lorence, M.C. (1992) *J. Biol. Chem.* **267**, 14193.

Philson, S.B., Debrunner, P.G., Schmidt, P.G. and Gunsalus, I.C. (1979) *J. Biol. Chem.* **254**, 10173.

Pochapsky, T.C. and Ye, X.M. (1991) *Biochemistry* **30**, 3850.

Ponomarkov, V., Cabral, J.R.P., Wahrendorf, J. and Galendo, D. (1984) *Cancer Lett.* **24**, 95.

Poulos, T.L. and Kraut, J. (1980) *J. Biol. Chem.* **255**, 8199.

Poulos, T.L., Finzel, B.C., Gunsalus, I.C., Wagner, G.C. and Kraut, J. (1985) *J. Biol. Chem.* **260**, 16122.

Poulos, T.L., Finzel, B.C. and Howard, A.J. (1986) *Biochemistry* **25**, 5314.

Poulos, T.L., Finzel, B.C. and Howard, A.J. (1987) *J. Mol. Biol.* **195**, 687.

Poulos, T.L. and Howard, A.J. (1987) *Biochemistry* **26**, 8165.

Poulos, T.L. and Raag, R. (1992) *FASEB J.* **6**, 674.

Raag, R. and Poulos, T.L. (1989a) *Biochemistry* **28**, 917.

Raag, R. and Poulos, T.L. (1989b) *Biochemistry* **28**, 7586.

Raag, R., Swanson, B.A., Poulos, T.L. and Ortiz de Montellano, P.R. (1990) *Biochemistry* **29**, 8119.

Raag, R., Martinis, S.A., Sligar, S.G. and Poulos, T.L. (1991) *Biochemistry* **30**, 11420.

Rahimtula, A.D. and O'Brien, P.J. (1974) *Biochem. Biophys. Res. Commun.* **60**, 440.

Rahimtula, A.D. and O'Brien, P.J. (1975) *Biochem. Biophys. Res. Commun.* **62**, 268.

Rheinwald, J.G., Chakrabarty, A.M. and Gunsalus, I.C. (1973) *Proc. Natl. Acad. Sci USA* **70**, 885.

Richey, H. (1972) in *Carbonium Ions* (Olah, G. and Schleyer, P.v.R., eds) vol. 3, pp. 1201-1294, Wiley, New York.

Ritchie, C.D. and Sager, W.F. (1964) *Prog. Phys. Org. Chem.* **2**, 323.

Ruettinger, R.T., Wen, L.-P. and Fulco, A.J. (1989) *J. Biol. Chem.* **264**, 10987.

Sakaguchi, M., Mihara, K. and Sato, R. (1987) *EMBO J.* **6**, 2425.

Shaanan, B. (1983) *J. Mol. Biol.* **171**, 31.

Sharrock, M., Munck, E., Debrunner, P.G., Marshall, V., Lipscomb, J.D. and Gunsalus, I.C. (1973) *Biochemistry* **12**, 258.

Sharrock, M., Debrunner, P.G., Shulz, D., Lipscomb, J.D., Marshall, V. and Gunsalus, I.C. (1976) *Biochem. Biophys. Acta* **420**, 8.

Shimizu, T., Hirano, K., Takahashi, M., Hatano, M. and Fujii-Kuriyama, Y. (1988) *Biochemistry* **27**, 4138.

Sligar, S.G., Lipscomb, J.D., Debrunner, P.G. and Gunsalus, I.C. (1974) *Biochem. Biophys. Res. Commun.* **61**, 290.

Sligar, S.G. and Gunsalus, I.C. (1976) *Proc. Natl. Acad. Sci. U.S.A.* **73**, 1078.

Sligar, S.G. and Gunsalus, I.C. (1979) *Biochemistry* **18**, 2290.

Sligar, S.G. and Murray, R.I. (1986) in *Cytochrome P450 Structure, Mechanism and Biochemistry* (Ortiz de Montellano, P.R., ed) pp. 429-503, Plenum Publishing Corp., New York.

Sligar, S.G., Filipovic, D. and Stayton, P.S. (1991)*Methods Enzymol.* **206,** 31.

Stayton, P.S., Fisher, M.T. and Sligar, S.G. (1988) *J. Biol. Chem.* **263,** 13544.

Stayton, P.S., Poulos, T.L. and Sligar, S.G. (1989) *Biochemistry* **28,** 8201.

Stayton, P.S. and Sligar, S.G. (1990) *Biochemistry* **29,** 7381.

Stayton, P.S. and Sligar, S.G. (1991) *Biochemistry* **30,** 1845.

Swanson, B.A., Dutton, D.R., Lunetta, J.M., Yang, C.S. and Ortiz de
Montellano, P.R. (1991) *J. Biol. Chem.* **266,** 19258.

Swanson, B.A., Halpert, J.R., Bornheim, L.M. and Ortiz de Montellano, P.R.
(1992) *Arch. Biochem. Biophys.* **292, 42.**

Swinney, D.C., Ryan, D.E., Thomas, P.E. and Levin, W. (1987) *Biochemistry*
26, 7073.

Tanaka, K., Kurihara, N. and Nakajima, M. (1979) *Pestic. Biochem. Physiol.*
10, 79.

Tarr, G.E., Black, S.D., Fujita, V.S. and Coon, M.J. (1983) *Proc. Natl. Acad. Sci.
USA* **80,** 6552.

Traylor, T.G. and Mitsztal, A.R. (1989) *J. Am. Chem. Soc.* **111,** 7443.

Traylor, T.G., Nakano, T., Dunlap, B.E., Traylor, P.S. and Dolphin, D. (1986) *J.
Am. Chem. Soc.* **108,** 2782.

Tretiakov, V.E., Degtyarenko, K.N., Uvarov, V.Y. and Archakov, A.I. (1989)
Arch. Biochem. Biophys. **275,** 429.

Tsai, R.L., Yu, C.-A., Gunsalus, I.C., Peisach, J., Blumberg, W., Orme-Johnson,
W.H. and Beinert, H. (1970) *Proc. Natl. Acad. Sci. U.S.A.* **66,** 1157.

Tuck, S.F., Peterson, J.A. and Ortiz de Montellano, P.R. (1992) *J. Biol. Chem.*
267, 5614.

Tuck, S.F. and Ortiz de Montellano, P.R. (1992) *Biochemistry* **31,** 6911.

Tuck, S.F., Graham-Lorence, S., Peterson, J.A. and Ortiz de Montellano, P.R.
J. Biol. Chem., in press.

Tullman, R.H., Walsh, J.S. and Miwa, G.T. (1984) *Fed. Proc.* **43,** 346.

Unger, B.P., Gunsalus, I.C. and Sligar, S.B. (1986) *J. Biol. Chem.* **261**, 1158.

Vergeres, G., Winterhalter, K.H. and Richter, C. (1989) *Biochemistry* **28**, 3650.

Watabe, T., Ueno, Y. and Imazumi, J. (1971) *Biochem. Pharmacol.* **20**, 912.

Watabe, T. and Akamatsu, K. (1974) *Biochem. Pharmacol.* **23**, 1079.

Waxman, D.J., Light, D.R. and Walsh, C. (1982) *Biochemistry* **21**, 2499.

White, R.E. and McCarthy, M.-B. (1984) *J. Am. Chem. Soc.* **106**, 4922.

Ye, X.M., Pochapsky, T.C. and Pochapsky, S.S. (1992) *Biochemistry* **31**, 1961.

Yu, C.A., Gunsalus, I.C., Katagiri, M., Suhara, K. and Takemori, S. (1974) *J. Biol. Chem.* **249**, 94.

Zhou, D., Korzekwa, K.R., Poulos, T. and Chen, S. (1992) *J. Biol. Chem.* **267**, 762.